RESPONSE OF LARGE MARINE ECOSYSTEMS TO CLIMATE VARIABILITY: PATTERNS, PROCESSES, CONCEPTS, AND METHODS

A Dissertation

Presented to the Faculty of the Graduate School

of Cornell University

in Partial Fulfillment of the Requirements for the Degree of

Doctor of Philosophy

by

Andrew John Pershing

May 2001

RESPONSE OF LARGE MARINE ECOSYSTEMS TO CLIMATE VARIABILITY: PATTERNS, PROCESSES, CONCEPTS, AND METHODS

Andrew John Pershing, Ph.D.

Cornell University 2001

Based on a review of the response of populations in the Northeast Atlantic to the North Atlantic Oscillation (NAO), a hierarchy of effects that climate can have on populations is developed. The hierarchy consists of three classes sorted by their ecological complexity. The first class, called *translations*, recognizes that climate-induced circulation changes can move populations from one area to another, and these are often the strongest effects of climate variability on marine populations Although the hierarchy was developed for marine systems, it also applies on land. On land, spatial transformations are less common, but translations in time can be important.

The Gulf of Maine ecosystem provides an opportunity to apply the hierarchy developed in Chapter 1. An analysis of time series of temperature and the NAO Index suggests that the region operates as a "Coupled Slope Water System" that becomes colder during negative NAO conditions, warmer during positive conditions. The changes in temperature are positively correlated to the abundance of *Calanus*

finmarchicus. Several mechanisms are proposed that might account for the correlation.

A substantial portion of temperature variability in the temperate ocean can be traced to the movements and properties of intermediate water masses. A simple model of phytoplankton dynamics coupled to a 1D mixing model was used to investigate the potential impact that interannual temperature differences could have on the spring bloom. Even a change in temperature of only a few degrees can have a significant influence one the development of spring stratification and the ensuing phytoplankton bloom. This mechanism, called *nonlinear stratification* could be an important source of variability in the spring bloom, especially on interdecadal scales.

Studying the response of marine populations to climate variability will require detailed simulations of ocean circulation on large spatial and temporal scales. To decrease the time required for these simulations and allow for larger domains, a parallel implementation of a finite-element circulation model was developed. The implementation of this model provides an example of how to parallelize finite difference and finite element models and how to achieve good performance on clusters of workstations.

Biographical Sketch

Like most lives, Andy's began with his birth in Lincoln, NE on June 10, 1973. Soon after, his father John, a member of the Army's elite corps of dentists, was assigned to Fort Devens in Massachusetts (it is now just Devens, but Andy had nothing to do with that), and the small Pershing clan–John, Cathy, and little Andy, moved east. A few months later, the population of Pershings increased by one with the birth of Andy's brother Matt.

After John's discharge from the Army, the four Pershings returned back to Lincoln so John could attend orthodontics school at the University of Nebraska. For the most part, the early part of Andy's life contained little more than the usual events of learning English, cutting teeth (a momentous event in a family full of dentists), and avoiding a little brother's rapidly developing teeth. However, in the summer of '76, Andy experienced his first life-changing experience. Despite the best intentions of the Motion Picture Association of America's ratings committee, John and Cathy thought a family trip to the local drive-in to see "Jaws" would be appropriate entertainment for toddlers. Matt and Andy spent most of the time between shark feedings snacking in the back, drinking iced tea (which Matt spilled). The morning after, Cathy asked Andy the fateful question "Did you like the movie?" Not knowing where this would lead, Andy remarked that he "liked the big fish." As

good parents, John and Cathy felt it was their duty to encourage Andy's blossoming interest and purchased a plastic shark and several books on marine life. When John graduated in 1978, the family moved further west (120 miles further from the ocean) to Hastings, and John went into practice with Cathy's father, Robert Butz.

After 6 years of corrective shoes and 5 years of braces (only two were actually required, the final three were "experimental"), Andy started high school. By this time, he had amassed a collection of marine oriented books larger than the one at the local library. Andy also had other interests, including the saxophone and golf. Although Hastings Senior High was the academic pinnacle of south central Nebraska, Andy was restless for new experiences. Inspired by Lars Magnussen, the exchange student who refused to leave, Andy spent his junior year in Kristiansund, Norway. Although he didn't know it at the time, the three months of never ending rain was Andy's first direct contact with the North Atlantic Oscillation. After a year, Andy returned to the plains as a wiser, thinner version of his former self. He completed high school and prepared to attend Brown University.

Andy claims that his decision to attend Brown was based on its reputation for academic excellence and the fact that it offers a major in aquatic biology. However, exclusive interviews have revealed that he went to Brown because the high-class, eastern women were "prettier than girls at Carelton." Andy's desire for knowledge (among other things), lead to the second life-changing experience of his life. After two weeks at Brown, Andy was excited for his first opportunity to do serious science on his BIO19a "Life of Birds" field trip. After observing the elusive hammer ducks found only at the pond in front of the Stanley tool factory, Andy decided his scientific interests would be enhanced by borrowing the class binoculars that were entrusted to the TA, Emily Constable. This was Andy's first contact with a high-class, eastern

woman, and he enjoyed the experience. After a week of cautious advances (dating the TA is never easy), Andy and Emily dated, a pairing that has persisted to this day.

Between classes and Emily, Andy's scientific interests blossomed. He volunteered his freshman year to work on a project investigating the larval ecology of barnacles in Narragansett Bay. From barnacles, Andy graduated to larger crustaceans, spending the next two summers working for Rick Wahle studying the ecology and behavior of juvenile lobsters in Maine. This work eventually lead to an honors thesis, which entailed Andy's first attempt at ecological modeling. Although lobsters are interesting, they are rare in upstate New York where Emily planned to attend veterinary school. After his junior year, Andy took a break from marine ecology and took a job as a summer intern at Oneida Lake, working for Nelson Hairston and Carla Caceres on the ecology of diapausing crustaceans. The job introduced Andy to the beauty of copepods (at least they don't pinch like lobsters) and brought him in contact with Chuck Greene. Chuck provided Andy with exactly what he was looking for: an opportunity to do oceanography in Ithaca. Andy finished his senior year at Brown, moved to Ithaca, and married Emily.

Andy worked hard as a graduate student (although his definition of hard is a bit liberal). Following a cherished family tradition, Andy developed an interest in his father-in-law's profession, in this case, computer science. For a time, it seemed like Andy might abandon his childhood dream of becoming a marine biologist in favor of a job at some dot-com; however, he eventually hit on a way to mix his new interest in computation with his old interest in oceanography. During the last half of Andy's graduate tenure, he pursued three main projects: studying interannual variability in the Gulf of Maine ecosystem, parallelizing a circulation model, and

increasing his own fitness. The third project bore the most fruit: Harry who was born on December 16, 1997 and Gregory who was born on October 24, 1999. These two boys are the proudest accomplishment of Andy's graduate career, far greater and much more interesting than the results that follow.

To Emily who has been a constant source of support and inspiration.

Acknowledgements

The work presented in this dissertation would never have occurred with out the help and support of many people. First, I would like to thank my family for providing much needed love and support. My parents have always encouraged me to pursue my interests, no matter how strange (like wanting to study marine biology from the center of the continent), and generously provided me with many opportunities that I would never have experienced on my own. My wife Emily inspires me every day with her intelligence and her patience. I'm not sure where I'd be if she hadn't encouraged me to take the research job in Maine so many years ago. She has provided enormous moral support over these last years, and she was instrumental making this dissertation readable. I could never have completed this without her. My father-in-law Robert Constable has also provided invaluable advice on academic and scientific matters. His enthusiasm for science and life in general is an inspiration.

On a professional level, I have received tremendous support from the small oceanography community at Cornell. My advisor, Charles Greene, has been an invaluable source of advice and ideas, and I have learned an amazing amount from him, about oceanography and how to get research done in a university setting. He has provided me with many opportunities and all of the resources my work required, and has been very supportive of my ideas no matter how anomalous they were. I

have greatly enjoyed collaborating with him during this time. The other members of our lab have been very helpful, and I would especially like to thank Bruce Monger, Jennifer Whiteis, Karen Fisher, Andrew Barton, and the many undergraduates who have worked with us over the years. I would also like to thank Shonali Chandy and Gideon Gal for providing lots of help and advice to a naive graduate student, and for softening-up Chuck.

I have had many beneficial interactions with people both at and beyond Cornell. I would especially like to thank Peter Wiebe for demonstrating an infectious enthusiasm for oceanography and for introducing me to Matlab at the start of all of this. Dan Lynch, Chris Naimie, Cisco Werner, Charles Hannah, and the rest of the Quoddy community have provided lots of encouragement and have been instrumental in helping me learn the black art of ocean modeling and finite elements. Data was generously provided by Jack Jossi at the National Marine Fisheries Service and by the Brian Petrie and others at the Bedford Institute of Oceanography. The consultants at the Cornell Theory Center have been very helpful and have answered many stupid questions. My committee members, Nelson Hairston Jr. and Steve Vavasis, have provided many helpful comments on this manuscript.

Finally, before I started as a graduate student, I thought science was a pristine activity removed from many of the details inherent in more traditional professions. As I soon discovered, navigating the bureaucracy of a major research university (especially one as schizophrenic as Cornell), is even harder than learning finite elements. The administrative staff at Snee, especially Lynda Keister and Cathy Lopez, have been extremely helpful, guiding me through the tangles of Cornell (and getting my paycheck on time).

Table of Contents

1 The Climate Variability Response Hierarchy: A General Approach for Understanding the Ecology of Climate **1**
1.1 Introduction . . . 1
1.2 Interdecadal Climate Variability: the NAO . . . 2
1.3 Response of North Atlantic Ecosystems to the NAO . . . 7
1.3.1 Zooplankton . . . 8
1.3.2 Phytoplankton . . . 10
1.3.3 Fish . . . 11
1.4 Interpretation: A Hierarchy of Mechanisms . . . 12
1.4.1 Marine Ecosystems . . . 15
1.4.2 Terrestrial Ecosystems . . . 17
1.4.3 Lakes . . . 20
1.5 Conclusion . . . 21
1.6 References . . . 23

2 Climate Variability and the Gulf of Maine Ecosystem: *Calanus*, Slope Water, and the NAO **27**
2.1 Introduction . . . 27
2.2 Methods . . . 29
2.2.1 Physical Oceanography . . . 30
2.2.2 Biological Oceanography . . . 31
2.2.3 Cross-correlation Analysis . . . 34
2.3 Results . . . 35
2.3.1 Temperature Time Series . . . 35
2.3.2 CPR Seasonal Cycles . . . 37
2.3.3 Intercomparison of the Time Series . . . 38
2.4 Discussion . . . 42
2.4.1 Physical Oceanography–a "Coupled Slope Water System" . . . 43
2.4.2 Biological Oceanography–response to CSWS . . . 48
2.5 Conclusion . . . 51
2.6 References . . . 52

3 Nonlinear Stratification: Spring Bloom Variability Forced by Winter Hydrography **56**
3.1 Introduction . . . 56
3.2 Methods . . . 60
3.2.1 The Physical Model: NubbleTS . . . 61
3.2.2 The Biological Model . . . 63
3.2.3 Initialization . . . 64
3.2.4 The Simulations . . . 65
3.2.5 Biology Simulations . . . 70
3.3 Results . . . 71
3.3.1 Physics Simulations . . . 74
3.4 Discussion . . . 79
3.4.1 Modelling Issues . . . 81
3.4.2 Nonlinear Stratification and Real Ecosystems . . . 83
3.5 Conclusion . . . 85
3.6 References . . . 87

4 Computing Ocean Circulation on Clusters of Workstations **89**
4.1 Introduction . . . 89
4.2 Ideas, Methods, and Model Development . . . 91
4.2.1 The Basic Model . . . 93
4.2.2 Parallel Programming Considerations . . . 94
4.2.3 Parallelization: Domain decomposition . . . 95
4.2.4 Modifications to Quoddy . . . 100
4.2.5 Performance Experiments . . . 103
4.3 Results . . . 105
4.4 Discussion . . . 110
4.4.1 Future Improvements . . . 112
4.5 Conclusion . . . 114
4.6 References . . . 115

List of Tables

1.1 The Climate Variability Response Hierarchy. 14

3.1 Summary of the treatments in the two sets of simulations. 70
3.2 Mean reduction in post-bloom growth rates relative to the 5° run ($R\%$) 76
3.3 Mean reduction in post-bloom growth rates relative to the 5° run ($R\%$). 79
3.4 Mean reduction in post-bloom growth rates for the treatments using Wind 2-4 from the Physics Simulations. 83
3.5 Percent of the growth-rate reduction from Table 3.4 due to the temperature change. 84

4.1 Definition of the sets to which the nodes are assigned. 99
4.2 Condition numbers for the matrices from the three meshes. 113

List of Figures

1.1 Hurrell's winter NAO Index . . . 3
1.2 Atmospheric conditions over the North Atlantic associated with the NAO . . . 4
1.3 Oceanographic changes in the North Atlantic associated with the NAO 6
1.4 Spatial and temporal scales for physical processes and biological groups on land and in the ocean . . . 17

2.1 The major circulation features of the Northwest Atlantic . . . 28
2.2 Location of data used in this study . . . 30
2.3 Temperature anomaly time series for the Northwest Atlantic shelf. . 35
2.4 The first two principal component vectors for the analysis of the temperature time series . . . 37
2.5 The observations and mean seasonal cycles for both *Calanus* and the color index . . . 38
2.6 The time series of the winter NAO, regional temperature, *Calanus*, and the color index. . . . 39
2.7 Cross-correlations among the time series in Figure 2.6 . . . 40
2.8 The significant relationships between NAO and temperature and temperature and *Calanus* . . . 43
2.9 The significant or most likely relationships between temperature and the color index and between color and *Calanus* . . . 44
2.10 The distribution of Labrador Subarctic Slope Water (LSSW) and Atlantic Temperate Slope Water (ATSW) during the states of the CSWS. . . . 46

3.1 The density of sea water as a function of temperature . . . 59
3.2 Vertical distribution of velocity and eddy diffusivity (κ) after the initialization period. . . . 64
3.3 Forcing functions for heat flux and surface irradiance. . . . 66
3.4 Time series of wind stress . . . 68
3.5 Contours of temperature relative to the initial temperature for the 0, 2, 4, and 5° C runs in a Physics treatment . . . 71
3.6 Distribution of the Brunt-Väisälä frequency . . . 72
3.7 The development of populations in the the Physics Simulations. . . . 73

3.8 The growth rates of the populations for the Physics Simulations expressed as a percent of the maximum (5°) rate. 74
3.9 The development of populations for the Biology Simulations. 77
3.10 The growth rates of the populations for the Biology Simulations expressed as a percent of the maximum (5°) rate. 78

4.1 A simple unstructured mesh composed of two triangular elements. . 92
4.2 A small horizontal mesh showing the vertical projections used by QUODDY. 94
4.3 A mesh divided into two submeshes by a single partition. 96
4.4 A mesh divided into four submeshes showing the communication patterns. 100
4.5 The three meshes used in the timing experiments. 104
4.6 Performance of MPQUODDY on the BANK150 mesh measured as time for a complete iteration and parallel efficiency. 106
4.7 The percent of the time spent in the six timing sections during the G2S runs. 108
4.8 The efficiency of subroutines `Elevation` and `Vertical` during the G2S runs. 109
4.9 The percent of time spent in subroutines `Elevation` and `Vertical` during the NCHIRES runs. 110
4.10 The efficiency of subroutines `Elevation` and `Vertical` during the NCHIRES runs. 111
4.11 The efficiency of runs using the G2S and NCHIRES meshes with processors assigned by `Machine_Divide`. 112

Chapter 1

The Climate Variability Response Hierarchy: A General Approach for Understanding the Ecology of Climate

1.1 Introduction

Considerable attention has been focused in recent years on how ecosystems respond to natural climate variability, with the understanding that this knowledge will be useful for managing natural resources in the face of anthropogenic climate change. This work has shown that climate variability influences the ecology of many species and can play an important role in ecosystem dynamics (McGowan et al., 1998; Ottersen et al., 2001). Beyond simply improving our knowledge about a single ecosystem, studying the response of ecosystems to climate variability offers a unique opportunity to study the dynamics of ecosystems on large scales. In theory, if one can identify a specific, quantifiable climate phenomenon, it could be viewed as a

series of natural experiments at the scale of the phenomenon. This approach should make it possible to develop general ideas of how ecosystems are structured and how they respond to climate variability.

The North Atlantic Oscillation (NAO) is a quantifiable climate phenomenon that can be used to develop this approach. A large portion of the variability in the climate of the North Atlantic is determined by the NAO, and several indices have been created to quantify this variability (Hurrell, 1995; Rogers, 1984; Jones et al., 1997). There are few existing ecological time series of sufficient length to detect the influence of the NAO. Because of the economic importance of North Atlantic fish stocks, there is a long history of research to understand the variability in the fisheries and ecosystems in this region (Mills, 1989), and the time series from this research provide a unique opportunity to study population responses to the NAO. Although the results from the North Atlantic involve many species and ecosystems, the processes linking the populations to climate fall into three general categories: translations, transformations, and indirect effects. Applying this hierarchy of effects to results from regions beyond the North Atlantic provides a unique insight into population responses to climate.

1.2 Interdecadal Climate Variability: the NAO

The strongest and most well known mode of climate variability is the El Niño-Southern Oscillation (ENSO), a phenomenon originating in the tropical Pacific Ocean but impacting weather patterns and ecosystems around the world (McPhaden,

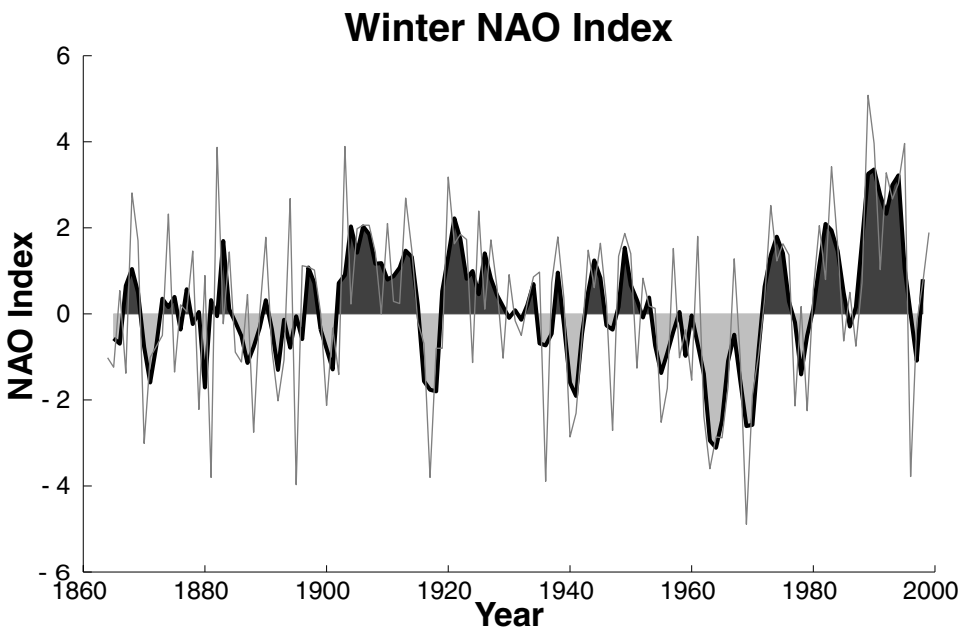

Figure 1.1: The winter NAO Index (Hurrell, 1995). The dark line and shading are a three-year running mean of the yearly data (light line).

1999). Although the North Atlantic lacks an interannual mode of climate variability comparable in intensity to ENSO, it does exhibit an interdecadal mode, the North Atlantic Oscillation (NAO; van Loon and Rodgers, 1978; Rogers, 1984; Hurrell, 1995).

Several indices have been developed to quantify the state of the NAO. All of the various NAO indices are based on the average atmospheric pressure difference between the Azores High and the Subpolar Low during winter. A positive phase of the NAO corresponds to a period of enhanced pressure differences; a negative phase corresponds to a period of reduced pressure differences. The most widely used index, Hurrell's NAO Index (Hurrell, 1995), computes the pressure difference based on measurements from Lisbon, Portugal and Stykkisholmur, Iceland. The

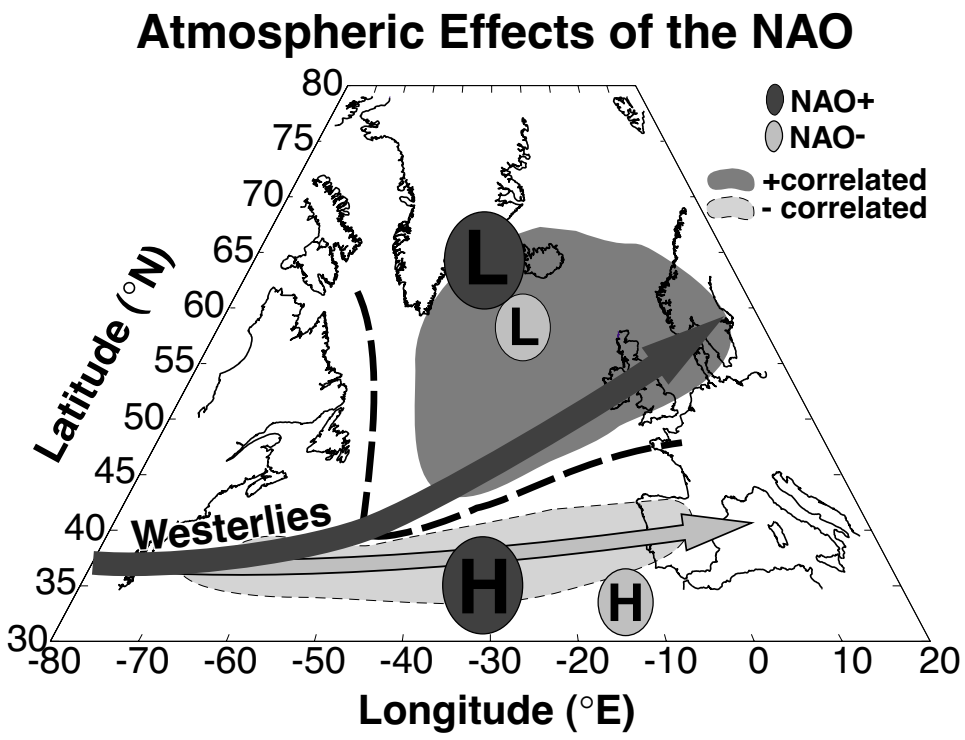

Figure 1.2: Atmospheric conditions over the North Atlantic associated with the NAO. During the NAO's positive phase (indicated by dark gray), the Icelandic Low and Azores High are intensified, producing strong westerlies (dark gray arrow) that are shifted to the north. When the NAO is in the negative phase (light gray), the difference between the pressure centers is diminished and both shift to the east. The westerlies are weakened and shift to the south (light gray arrow). The scalar wind speeds in areas northeast of the dashed line are positively correlated with the NAO (windy during positive phases—dark region), while wind speeds south are negatively correlated (light region)

NAO Index has fluctuated considerably during the 20th century (Figure 1.1), but three general trends can be identified. The NAO Index was predominantly positive before 1935, negative from the late 1950s to the early 1970s, and positive from the early 1970s to the mid 1990s.

The NAO was originally described as a "seesaw" pattern with opposite temperature anomalies occurring on the eastern and western sides of the Atlantic (van Loon and Rodgers, 1978). During positive phases of the NAO, westerly winds intensify

and shift to the north (Figure 1.2). The changes in the westerlies lead to colder, stormier conditions in the Northwest Atlantic and Greenland and warmer, milder conditions in the Northeast Atlantic and northern Europe (Hurrell, 1995; Dickson et al., 1996). In contrast, during negative phases of the NAO, westerly winds diminish in intensity and shift south. This leads to warmer, milder conditions in the Northwest Atlantic and Greenland and colder, drier conditions in northern Europe (Hurrell, 1995; Dickson et al., 1996). The influence of the NAO on the wind is not restricted to the narrow band of westerlies. Reid and Planque (1999) found that during positive NAO conditions, the wind speed during winter increases over a broad area in the Northeast Atlantic, while areas to the south experience increased winds during negative NAO conditions (Figure 1.2).

The atmospheric shifts associated with the NAO cause changes in the location of deepwater formation as well as changes in the circulation of the Atlantic (Figure 1.3). When the NAO Index is positive, the cold, stormy conditions over the Labrador Sea produce a layer of dense Labrador Sea Water (LSW) which spreads throughout the Atlantic (Figure 1.3). When the NAO reverses, LSW production decreases and the production of very dense Greenland Sea Deep Water (GSDW) increases as the cold conditions shift to the eastern Atlantic (Figure 1.3). The general circulation of the Atlantic also responds to the NAO, although the changes are not immediate. Under negative NAO conditions, the Labrador Current intensifies and extends around the Tail of the Grand Bank, bringing cold water past Cape Cod 1-2 years after the NAO (Petrie and Drinkwater, 1993; Dickson et al., 1996; Rossby and Benway, 2000;

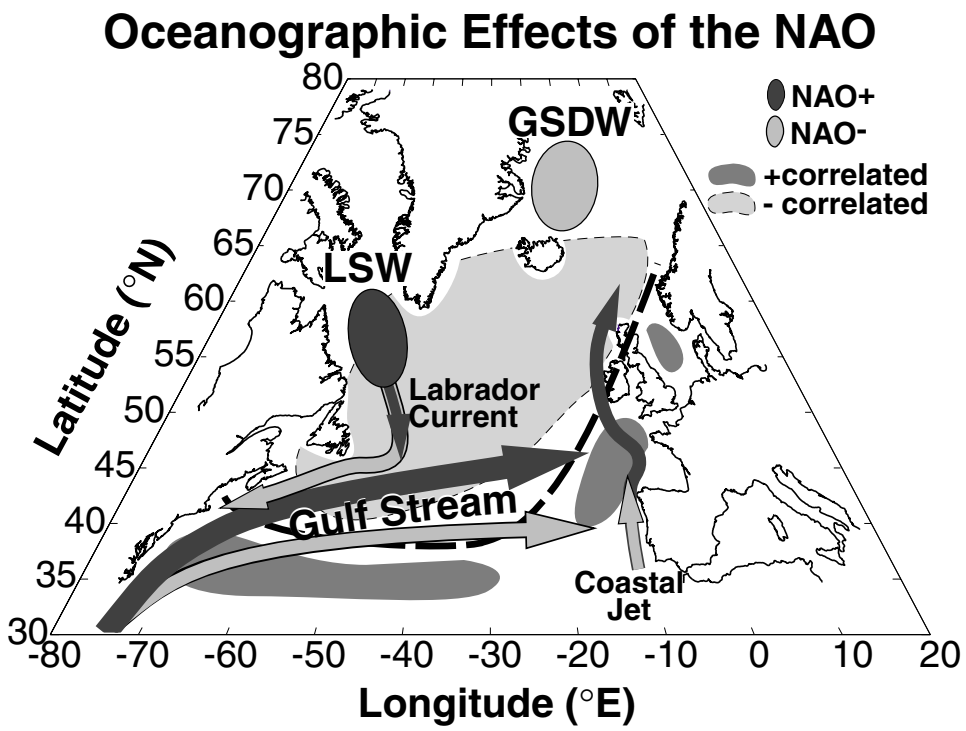

Figure 1.3: Oceanographic changes in the North Atlantic associated with the NAO. During positive phases, the convection in the Labrador Sea increases and Labrador Sea Water (LSW—dark circle) production is enhanced. The coastal jet on the European Shelf intensifies and the Gulf Stream is shifted to the north (dark arrows). During negative phases, convection in the Greenland Sea intensifies and the production of Greenland Sea Deep Water (GSDW—light circle) increases. The transport in the Labrador Current also increases and the Gulf Stream shifts to the south (light arrows). The sea surface temperature south and east of the dashed line is positively correlated with the NAO (cold during positive phases—dark region), while temperatures north and east are negatively correlated (light region).

Drinkwater et al., 2000). The changes in the Labrador Current are accompanied by a southward shift in the Gulf Stream (Taylor and Stephens, 1998). In the eastern Atlantic, Reid and Planque (1999) and Reid et al. (2001) describe a northward-flowing coastal jet that extended further north following several years of strongly positive NAO conditions during the mid-1980's.

The atmospheric and circulation changes associated with the NAO are further

reflected in the correlations between winter sea surface temperature and the NAO (Reid and Planque, 1999). When the NAO is positive, a large area in the center of the North Atlantic is cooler, and areas to the south and east are warmer. Sea surface temperature in the North Sea is positively correlated with the NAO. The correlation is similar to that for air temperature over the North Sea, but is also related to NAO-associated changes in the water flowing into the North Sea from the Atlantic. When the NAO is negative, the inflow increases in the eastern section, bringing cool water from the Norwegian Sea (Stephens et al., 1998). When the NAO is positive, the inflow is restricted to a small section off the Scottish coast, and the water entering is warmer, especially in years when the coastal jet is intensified.

1.3 Response of North Atlantic Ecosystems to the NAO

The Continuous Plankton Recorder (CPR) surveys conducted by the Sir Alister Hardy Foundation for Ocean Science (SAHFOS) provide a detailed picture of long-term variability in the ecosystems of the North Atlantic, particularly the eastern Atlantic (Gamble, 1994). The SAHFOS surveys, which began in the late 1940's, rely on commercial ships traveling on their usual routes. The CPR sieves plankton on to a silk gauze that is periodically advanced to expose a fresh section of gauze, providing a quantitative record of the abundance of zooplankton and large phytoplankton in discrete segments along the ship's path. The SAHFOS surveys are complemented

by traditional oceanographic surveys throughout the Northeast Atlantic, especially those by Norwegian researchers in the Norwegian and Barents Seas (Skjoldal et al., 1992; Helle and Pennington, 1999; Ottersen et al., 2001). Recently, Ottersen et al. (2001) reviewed the effect of the NAO on ecosystems in and around the North Atlantic, including several of the results from the SAHFOS surveys. Rather than duplicate that review, I will summarize some of the dominant patterns from the plankton records.

1.3.1 Zooplankton

Of all the species in the North Atlantic, few have received more attention than the calanoid copepod, *Calanus finmarchicus*. This species is abundant throughout the North Atlantic, especially during the spring and early summer (Marshall and Orr, 1955; Planque et al., 1997). *C. finmarchicus* in the Northeast Atlantic, together with its cogener *Calanus helgolandicus*, were the first zooplankton species whose fluctuations in abundance were directly correlated with the NAO (Fromentin and Planque, 1996). During positive NAO conditions, the abundance of *C. finmarchicus* in the North Sea decreases, while the abundance of most other zooplankton, including *C. helgolandicus*, increases. The situation reverses during negative NAO years.

Several hypotheses have been advanced to explain the NAO-associated fluctuations in the North Sea between populations of these two copepods. Fromentin and Planque (1996) proposed that changes in temperature associated with the NAO (warmer during positive years, colder during negative; Figure 1.3) drive the species

shifts, with *C. helgolandicus*, which is typically found in warmer waters, flourishing during warmer conditions and *C. finmarchicus*, which is typically found in cold waters, flourishing during colder conditions. Stephens et al. (1998) suggest that increased flow from the north and west during negative NAO conditions advects large numbers of *C. finmarchicus* to the shelf region from their principle overwintering habitat in the deeper waters. If the temperature changes in the North Sea are determined by the water mass movements, then these two hypotheses may be related. Specifically, increased flow from the Norwegian Sea during negative NAO conditions would cool the North Sea and bring *C. finmarchicus* on to the shelf while displacing *C. helgolandicus* to the south.

The abundance of *C. finmarchicus* is also related to the NAO in regions beyond the North Sea. In the Barents Sea, the abundance of *C. finmarchicus* is closely tied to the supply of warm Atlantic Water flowing from the Norwegian Sea (Skjoldal et al., 1992; Helle and Pennington, 1999). When the flow increases, it advects *C. finmarchicus* and other Norwegian Sea zooplankton into the Barents. Although the abundance of *C. finmarchicus* in the Barents has not been formally correlated with the NAO, the transport of Norwegian Sea water is associated with positive NAO conditions (Dickson et al., 2000). *C. finmarchicus*' abundance in the Gulf of Maine is also related to the NAO (Conversi et al., 2001; Greene and Pershing, 2001). At this time, no clear mechanism has been identified; however, a circulation-recruitment mechanism analogous to Stephens et al. (1998) seems likely (Head et al., 1999; Greene and Pershing, 2001).

1.3.2 Phytoplankton

The climate over the North Atlantic also influences phytoplankton standing stocks, although the exact mechanisms are unclear. Working with the CPR data prior to 1980, Dickson et al. (1988) proposed that variations in the North Sea phytoplankton community were related to the strength of the spring winds. Increased vertical mixing by strong winds causes phytoplankton to spend a significant amount of time below the compensation depth—the depth at which a phytoplankter's photosynthetic rate equals its respiration rate. The overall reduction in photosynthesis caused by strong winds delays the development of the spring phytoplankton bloom. The data analyzed by Dickson et al. (1988) showed a general decline in phytoplankton stocks between 1960 and 1980 that was associated with increased winds. During this same period, the NAO increased (Figure 1.1), suggesting a negative correlation between phytoplankton and the NAO.

An analysis by Reid et al. (1998) of an extended data set (1948-1995) suggests an association between phytoplankton and the NAO that is different than the one implied by Dickson et al. (1988). The expanded data set reveals a trend towards increased phytoplankton in the North Sea and longer growing seasons (earlier spring blooms, extended fall blooms), especially since the late 1980's (Reid et al., 1998). This newer analysis suggests a positive association with the NAO, since the trend in the NAO was also positive over this time; however, the correlation is weak (Reid and Planque, 1999). The extension of the coastal jet (Figure 1.3) reported by Reid and Planque (1999) and Reid et al. (2001) may help reconcile for the contradictory as-

sociation between North Sea phytoplankton and the NAO. Prior to the mid-1980's, variations in spring wind speeds may have been responsible for the phytoplankton fluctuations through the mechanism suggested by Dickson et al. (1988). During the mid-1980's, the coastal jet extended farther up the shelf and brought warm water into the North Sea. The warm water caused increased vertical density gradients which reduced the effect of wind mixing; thus, even though the winds remained strong during the late 1980's and early 1990's, the phytoplankton stocks were high. In 1988, phytoplankton standing stocks increased dramatically as did populations of several zooplankton and fish species (Reid et al., 2001), suggesting that the switch from wind-controlled to advection-controlled blooms occurred in that year. However, the increase in phytoplankton started a few years before this time, which may indicate that the effects of warm water began before 1988.

1.3.3 Fish

The abundance of several fish species in the North Sea have been linked to the changes described above (Ottersen et al., 2001). However, the response of fish stocks is not necessarily linked to climate through changes in plankton populations. In the Barents Sea, the distribution of cod larvae is associated with the same water masses as *C. finmarchicus* (Helle and Pennington, 1999), and years with large influxes of warm Atlantic water (positive NAO years) are typically good years for cod. Although increased zooplankton abundance is certainly a factor (Skjoldal et al., 1992), Ottersen et al. (2001) argue that some of the effect is due to the direct influ-

ence of temperature on cod growth.

1.4 Interpretation: A Hierarchy of Mechanisms

The main goal of classifying population responses to climate variability is to simplify the complexity inherent in both ecological and climate studies. Synthesizing many observations of how populations are influenced by climate into a few general categories makes it possible to focus research on understanding general principles rather than explaining specific examples. Thus, an important criterion for judging the merits of a classification should be how well it reflects the underlying principles. In their review, Ottersen et al. (2001) propose a three-way classification for the effects of the NAO on populations. They categorize the effects as direct, indirect, and integrated. Direct effects result from physical changes such as the relationship between temperature and cod growth in the Barents Sea. Indirect effects are population changes that result from ecological interactions with a species that is directly influenced by climate. Integrated effects occur in populations that exhibit a detectable response only after several years in a particular climate state, or when the physical process affecting a population increases with the amount of time in a particular state.

Although the classification scheme proposed by Ottersen et al. (2001) is both general and comprehensive, it does not consistently reflect the important dynamics underlying climate-population interactions. Climate variability implies changes in the physical environment; thus, a natural classification of the response of populations

to climate should distinguish between effects due to physical forcing and effects due to biological changes. Although the direct and indirect classes in the Ottersen et al. (2001) system distinguish between some physical and biological effects, effects in their integrated class may result from physical or biological processes. Furthermore, their class of direct effects lumps two distinct ways that physical processes can affect populations, specifically, *translations* and *transformations*.

In the Northeast Atlantic, some of the largest climate-induced fluctuations in populations are associated with displacements of water masses. Examples of this mechanism are the link between *C. finmarchicus* populations in the Barents and North Seas and the water mass movement from the Norwegian Sea. In both cases, the circulation changes associated with the NAO moved populations between regions, but the circulation changes did not alter the populations in any other way. In geometry, moving an object without changing its shape or orientation is known as translation. Borrowing this terminology, the portion of a population's variability due to climate-induced circulation changes will be called "translations."

Translational effects are caused by entirely physical mechanisms; however, biological processes are also important. Climate variability and climate change are most commonly associated with changes in temperature. Increasing or decreasing temperature can alter an organism's vital rates as demonstrated by the link between temperature and cod larvae in the Barents Sea. Pursuing the geometric analogy further, the temperature changes associated with the NAO *transform* the cod larvae by altering their feeding and growth rates; thus, this category of effects will be re-

Table 1.1: The Climate Variability Response Hierarchy.

I. Translations	Climate variability causes shifts in the distribution of physical properties. These shifts can cause species to move.
II. Transformations	Climate variability can directly alter properties of a population such as its growth and feeding rates. Because these changes involve the inherent biological properties of the organisms, they are known as transformations.
III. Indirect Effects	Even if they are not directly influenced by physical changes associated with climate variability, species or ecosystem properties can be affected by climate through their interaction with species that are directly influenced.

ferred to as "transformations." The variations in cod populations in the Barents Sea may also be linked to climate-induced fluctuations in zooplankton abundance. This portion of the variability in the cod population is related to climate only through a translational effect on the zooplankton. Following the classification of Ottersen et al. (2001), changes in a population that are linked to climate only through its effect on another population (either through a translation or transformation) will be called indirect effects.

The new classification of the effects of climate variability on populations, called the "Climate Variability Response Hierarchy" (Table 1.1) has many of the desirable properties discussed above. Since the hierarchy is based on the three classes described by Ottersen et al. (2001), it is equally comprehensive. The main difference between the two systems is that the response hierarchy does not separate integrated

effects from the others. Integrated effects are certainly interesting and important; however, they are special subclasses of the main categories. The key advantage of the response hierarchy is that it is arranged according to the ecological complexity of the effects. Translations are the least complex, involving only physical processes. Transformations occur at the interface between physics and biology, and indirect effects are due solely to ecological interactions. As demonstrated by the response of cod populations in the Barents Sea, a specific population's response to climate variability may not fall exactly into one of these categories, but can be a weighted combination of the three. The hierarchy's combinatorial nature allows it to describe a wide variety of climate-population interactions.

Transformations and indirect effects have been recognized in many ecosystems and by many authors, although the terminology used may differ. The unique feature of the Climate Variability Response Hierarchy is its class of translational effects. Although the translation class was developed based on results from the Northeast Atlantic, translations are a general feature of the response of marine populations to climate. Furthermore, translational effects are also present in continental ecosystems, although in an altered form.

1.4.1 Marine Ecosystems

The hierarchy proposed above is sorted by ecological complexity, and an important consequence of this arrangement is that the classes often coincide with the magnitude of the climate response. The most dramatic changes in ocean ecosystems are

associated with large scale changes in water mass distributions and fronts. After an ENSO event, warm tropical waters extend north to California, bringing with them many tropical species such as pelagic red crabs (*Pleuroncodes planipus*), tuna, and other warm water fish (McGowan, 1985). The changes associated with ENSO are an example of an extreme translational event involving the movements of a whole community, not just a few populations. The population changes in the Northeast Atlantic associated with the extension of the coastal jet may be another example of a broad community translation on par with the ENSO changes in California, but one that persists for many years. As with the ENSO changes in California, the circulation changes on the European Shelf lead to range extensions of many warm-water species to the north (Reid et al., 2001).

Translations associated with frontal shifts have an especially strong effect on species with distributions tied to a specific geographic feature, provided the shift passes over the feature. The nesting grounds of marine birds and breeding grounds of seals are limited to a few locations. During frontal shifts such as those occurring during ENSO in the Pacific, these species are often the hardest hit (Graybill and Hodder, 1985). Many commercially important fish species have similar restrictions, spawning only at a few locations, principally submarine banks (Mann and Lazier, 1996). The dramatic nature of these indirect effects results from the species sampling their environment from a fixed point. Shelf ecosystems are similarly fixed relative to adjacent circulation features; thus, they should be particularly sensitive to changes in circulation. This may explain the strong response of shelf populations such as

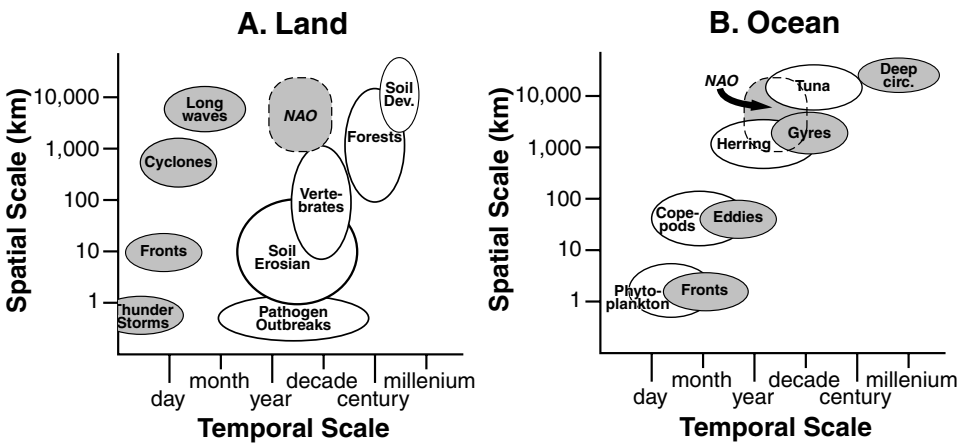

Figure 1.4: Spatial and temporal scales for physical processes and biological groups on land and in the ocean (A and B, respectively; Steele and Henderson, 1994). The space-time boundaries for the NAO have been added.

those in the North Sea to climate variability, and the predominance of translational effects linking climate variability to population changes in the ocean.

1.4.2 Terrestrial Ecosystems

The response hierarchy was developed to explain the variability seen in marine ecosystems; however, the ideas are applicable outside the oceans and provide a interesting contrast between terrestrial and oceanic domains. Traditionally, comparisons between marine and terrestrial ecosystems have characterized marine ecosystems as dominated by physical processes, while terrestrial ecosystems are dominated by density-dependent processes (Steele, 1991; Steele and Henderson, 1994). This view is supported by the correspondence between the physical and biological processes in the ocean with respect to their characteristic temporal and spatial scales, and a lack of correspondence on land (Figure 1.4; Steele and Henderson, 1994). Although

the paper by Steele and Henderson (1994) is only seven years old, there were only two examples at that time linking population changes to the NAO (Ottersen et al., 2001). However, Steele and Henderson (1994) proposed that physical forcing on interannual or longer time scales should be an important process in both marine and terrestrial ecosystems. Climate variations like the NAO and ENSO occur on long temporal and large spatial scales, closer to the scale of biological processes on land than the other atmospheric processes.

Translation is the only element in the hierarchy that is not readily transferrable to terrestrial ecosystems. In general, terrestrial ecosystems lack organisms comparable to plankton whose movements are controlled primarily by physical processes. For this reason, large-scale species translations are less common on land. For example, primary producers on land are sessile, making it impossible for these populations to be translated in space. However, it should be noted that some plants produce seeds that can be transported by the wind, so shifts in wind patterns associated with climate variability could lead to translational effects in some primary producers. At higher trophic levels, some insects also may be affected by wind shifts. Even large species that can not be carried by the wind may still exhibit a translational response if they actively follow a particular environmental condition. Climate phenomena like the NAO, cause translations of environmental conditions on the scale of the continents, far larger than the movement patterns of most terrestrial animals. However, in mountainous areas, climate fluctuations create shifts in the vertical distributions of important environmental features, such as the snow line, and these changes occur

on scales that can be tracked by many species (Mysterud et al., 2000). Unlike the movements of plankton, this kind of translation requires the active participation of the animal; however, the animal is not changed significantly by the movement (it is not transformed).

Although most species are unable to shift their spatial distribution to follow interannual climate fluctuations, many species exhibit temporal shifts in their distributions or some aspect of their life history. In Europe, especially Norway, positive NAO conditions are associated with warmer springs. Warmer springs allow for earlier flowering (Post et al., 1999) which could lead to an increase in seed number and size (Ottersen et al., 2001). These shifts in the timing of major ecological events possess many of the same characteristics as translational effects. First, the populations move without being altered, only the movement is to an earlier time rather than to a different location. Furthermore, the changes are due entirely to physical processes such as the timing of the spring thaw.

Temporal shifts are a common response to climate variability. European birds and amphibians also exhibit a temporal shift, reproducing earlier in warm years (Forchhammer et al., 1998; McCleery and Perrins, 1998). The cause for the shift in the timing of vertebrate reproduction is unclear; however, it could be a response to the plants (an indirect effect) or to the same physical processes as the plants (a temporal shift). Temporal shifts are not restricted to the continents: the changes in the timing of the spring phytoplankton bloom such as those proposed by Dickson et al. (1988) are another example.

1.4.3 Lakes

Lakes provide an interesting contrast with marine systems. Although the taxonomic composition in lakes is similar to that in the ocean, lake ecosystems should respond to climate variability more like terrestrial systems because standard spatial translations are more difficult. In a study of Lake Constance in southern Germany, Straille (2000) described the effect of the NAO on the physical and biological conditions in the lake. The warmer winters associated with positive NAO years cause the surface waters of the lake to stratify and warm earlier. The warm conditions enhance the growth rates of the *Daphnia* population, a transformation similar to the response of cod to temperature in the Barents Sea. Increased grazing by the *Daphnia* cause an indirect effect on the phytoplankton community, reducing its abundance and leading to an earlier and extended clear-water phase. Thus, the main effect of the NAO on Lake Constance is a shift in the timing of seasonal events such as the clear-water phase. A similar response has also been observed in another European lake with very different physical characteristics (Straille and Adrian, 2000). Although these responses have many of the same characteristics as temporal shifts, they are actually transformations and result from biological rather than physical processes.

Despite the predominance of transformations and indirect effects, lakes and ponds might exhibit spatial translations mediated by stocks of diapausing eggs. Many zooplankton species produce resting eggs as a means of surviving adverse conditions (Hairston and Cáceres, 1996), the most dramatic condition being the complete drying of a pond (Hutchinson, 1967). These eggs can remain viable for

many years (Marcus et al., 1994; Hairston et al., 1995; Cáceres, 1998), providing an "egg bank" (De Stasio, 1989). If a species has diapausing eggs in lakes distributed over a wide area, then it is possible that the distribution of that species could follow large spatial changes in climate conditions. Translations produced by this mechanism could be particularly important for small ponds that may only be filled under specific climate conditions, and could also apply to plants with long-lived seed banks.

1.5 Conclusion

The Climate Variability Response Hierarchy's separation of physical effects into translational and transformational is the key difference between this classification and the one proposed by Ottersen et al. (2001). Translation of ecosystem properties in space is a characteristic feature of the response of marine ecosystems to climate, and many indirect effects can be traced to these movements. On land, translations are present primarily as shifts in the timing of seasonal events, and these temporal shifts have the potential to alter other ecosystem properties. Recognizing the importance of spatial and temporal translations associated with climate variability has the potential to enhance our understanding of climate-ecosystem interactions.

Compared with our understanding of ecosystem dynamics, our ability to simulate and even predict climate phenomenon is quite good. Given our knowledge of physical changes, recognizing spatial and temporal translations should be simpler than detecting the effects in the other classes. Recognizing translational effects will reveal features of ecosystems that are governed by transformations or indirect

effects. Transformations and indirect effects are based on the biology of specific organisms and their interactions with others; thus, these responses will depend on the details of each ecosystem and are likely to change from one ecosystem to another. If a translation is found in one population, the same translation will likely affect others in the region. For this reason, spatial translations and temporal shifts, should be general features of adjacent ecosystems, and focusing on these changes would provide a good first approximation towards understanding ecosystem-climate links on large scales.

1.6 References

Cáceres, C. E. (1998). Interspecific variation in the abundance, production, and emergence of *Daphnia* diapausing eggs. *Ecology*, 79:1699–1710.

Conversi, A., Piontkovski, S., and Hameed, S. (2001). Seasonal and interannual dynamics of *Calanus finmarchicus* in the Gulf of Maine (Northeastern US shelf) with reference to the North Atlantic Oscillation. *Deep-Sea Research II*, 48:519–520.

De Stasio, Jr., B. T. (1989). The seed bank of a freshwater crustacean: copepodology for the plant ecologist. *Ecology*, 70:1377–1389.

Dickson, R., Lazier, J., Meincke, J., Rhines, P., and Swift, J. (1996). Long-term coordinated changes in the convective activity of the North Atlantic. *Progress in Oceanography*, 38:241–295.

Dickson, R. R., Kelly, P. M., Colebrook, J. M., Wooster, W. S., and Cushing, D. H. (1988). North winds and production in the eastern North Atlantic. *Journal of Plankton Research*, 10:151–169.

Dickson, R. R., Osborn, T. J., Hurrell, J. W., Meincke, J., Blindheim, J., Adlandsvik, B., Vinje, T., Alekseev, G., and Maslowski, W. (2000). The Arctic Ocean response to the North Atlantic Oscillation. *Journal of Climate*, 13:2671–2696.

Drinkwater, K. F., Mountain, D. B., and Herman, A. (2000). Variability in the slope water properties off eastern North America and their effects on the adjacent seas. *Journal of Geophysical Research*, In press.

Forchhammer, M. C., Post, E., and Stenseth, N. C. (1998). Breeding phenology and climate. *Nature*, 391:29–30.

Fromentin, J. and Planque, B. (1996). *Calanus* and the environment in the eastern North Atlantic. II. Influence of the North Atlantic Oscillation on *C. finmarchicus* and *C. helgolandicus*. *Marine Ecology Progress Series*, 134:111–118.

Gamble, J. C. (1994). Long-term planktonic time series as monitors of marine environmental change. In Leigh, R. A. and Johnston, A. E., editors, *Long-term Experiments in Agriculture and Ecological Sciences: Proceedings of a Conference to Celebrate the 150th Anniversary of Rothamsted Experimental Station, held at Rothamsted, 14-17 July, 1993*, pages 365–386. CAB International, Wallingford, U. K.

Graybill, M. R. and Hodder, J. (1985). Effects of the 1982-83 El Niño on reproduction of six species of seabirds in Oregon. In Wooster, W. S. and Fluharty, D. L., editors, *El Niño North: El Niño Effects in the Eastern Subarctic Pacific Ocean*, pages 205–210. Univeristy of Washington, Seattle.

Greene, C. H. and Pershing, A. J. (2001). The response of *Calanus finmarchicus* populations to climate variability in the Northwest Atlantic: Basin-scale forcing associated with the North Atlantic Oscillation. *ICES Journal of Marine Science*, in press.

Hairston, Jr., N. G., Brunt, R. A. V., Kearns, C. M., and Engstrom, D. R. (1995). Age and survivorship of diapausing eggs in a sediment egg bank. *Ecology*, 76:1706–1711.

Hairston, Jr., N. G. and Cáceres, C. E. (1996). Distribution of crustacean diapuase: micro- and macroevolutionary pattern and process. *Hydrobiologia*, 320:27–44.

Head, E. J. H., Harris, L. R., and Petrie, B. (1999). Distribution of *Calanus* spp. on and around the Nova Scotia Shelf in April–evidence for an offshore source of *Calanus finmarchicus* to the mid- and western regions. *Canadian Journal of Fisheries and Aquatic Science*, 56:2463–2476.

Helle, K. and Pennington, M. (1999). The relation of the spatial distribution of early juvenile cod (*Gadus morha L.*) in the Barents Sea to zooplankton density and water flux during the period 1978-1984. *ICES Journal of Marine Science*, 56.

Hurrell, J. (1995). Decadal trends in the North Atlantic Oscillation: regional temperatures and precipitation. *Science*, 269:676–679.

Hutchinson, G. E. (1967). *A Treatise on Limnology. Volume 2. Introduction to Lake Biology and the Limnoplankton.* Wiley, New York, New York.

Jones, P. D., Jonsson, T., and Wheeler, D. (1997). Extension to the North Atlantic Oscillation using early intsrumental pressure observations from Gibralter and south-west Iceland. *International Journal of Climatology*, 17:1433–1450.

Mann, K. H. and Lazier, J. R. N. (1996). *Dynamics of Marine Ecosystems: Biological-Physical Interactions in the Oceans.* Blackwell Science, Cambridge, MA.

Marcus, N. H., Lutz, R., Burnett, W., and Cable, P. (1994). Age, viability, and vertical distribution of zooplankton resting eggs from an anoxic basin: evidence of an egg bank. *Limnology and Oceanography*, 39:154–158.

Marshall, S. M. and Orr, A. P. (1955). *The Biology of a Marine Copepod.* Oliver and Boyd, Edinburgh.

McCleery, R. H. and Perrins, C. M. (1998). Temperature and egg-laying trends. *Nature*, 391:30–31.

McGowan, J. A. (1985). El Niño 1983 in the southern California Bight. In Wooster, W. S. and Fluharty, D. L., editors, *El Niño North: El Niño Effects in the Eastern Subarctic Pacific Ocean*, pages 166–184. Univeristy of Washington, Seattle.

McGowan, J. A., Cayan, D. R., and Dorman, L. M. (1998). Climate-ocean variability and ecosystem response in the Northeast Pacific. *Science*, 281:210–217.

McPhaden, M. J. (1999). Genesis and evolution of the 1997-98 El Nino. *Science*, 283:950–954.

Mills, E. L. (1989). *Biological Oceanography. An Early History, 1870-1960*. Cornell University Press, Ithaca, NY.

Mysterud, A., Yoccoz, N. G., Stenseth, N. C., and Langvatn, R. (2000). Relationships between sex ratio, climate and density in red deer: the importance of spatial scale. *Journal of Animal Ecology*, 69:959–974.

Ottersen, G., Planque, B., Belgrano, A., Post, E., Reid, P. C., and Stenseth, N. C. (2001). Ecological effects of the North Atlantic Oscillation. *Oecologia*, in press.

Petrie, B. D. and Drinkwater, K. (1993). Temperature and salinity variability on the Scotian Shelf and in the Gulf of Maine, 1945-1990. *Journal of Geophysical Research*, 98:20,079–20,089.

Planque, B., Hays, G. C., Ibanez, F., and Gamble, J. C. (1997). Large scale spatial variations in the seasonal abundance of *Calanus finmarchicus*. *Deep-Sea Research I*, 44:315–326.

Post, E., Forchhammer, M. C., and Stenseth, N. C. (1999). Population ecology and the North Atlantic Oscillation. *Ecological Bulletins*, 47:117–125.

Reid, P. C., de Fatima Borges, M., and Svendsen, E. (2001). A regime shift in the North Sea circa 1988 linked to changes in the North Sea fishery. *Fisheries Review*, in press.

Reid, P. C., Edwards, M., Hunt, H. G., and Warner, A. J. (1998). Phytoplankton change in the North Atlantic. *Nature*, 391:546.

Reid, P. C. and Planque, B. (1999). Long-term planktonic variations and the climate of the North Atlantic. In Mills, D., editor, *The Life of the Atlantic Salmon*, pages 153–169. Blackwell Science, Oxford.

Rogers, J. C. (1984). The association between the North Atlantic Oscillation and the Southern Oscillation. *Monthly Weather Review*, 112:1999–2015.

Rossby, T. and Benway, R. L. (2000). Slow variations in mean path of the Gulf Stream east of Cape Hatteras. *Geophysical Research Letters*, 27:117–120.

Skjoldal, H. R., Gjøsæter, H., and Loeng, H. (1992). The Barents Sea ecosystem in the 1980s: ocean climate, plankton, and capelin growth. *ICES Marine Science Symposia*, 195:278–290.

Steele, J. H. (1991). Can ecological theory cross the land-sea boundary? *Journal of Theoretical Biology*, 153:425–436.

Steele, J. H. and Henderson, E. W. (1994). Coupling between physical and biological scales. *Proceedings of the Royal Society of London B*, 343:5–9.

Stephens, J. A., Jordan, M. B., Taylor, A. H., and Proctor, R. (1998). The effects of fluctuations in North Sea flows on zooplankton abundance. *Journal of Plankton Research*, 20:943–956.

Straille, D. (2000). Meteorological forcing of plankton dynamics in a large and deep continental European lake. *Oecologia*, 122:44–50.

Straille, D. and Adrian, R. (2000). The North Atlantic Oscillation and plankton dynamics in two European lakes—two variations on a general theme. *Global Change Biology*, 6:663–670.

Taylor, A. H. and Stephens, J. A. (1998). The North Atlantic Oscillation and the latitude of the Gulf Stream. *Tellus*, 50:134–142.

van Loon, H. and Rodgers, J. C. (1978). The seasaw in winter temperatures between Greenland and northern Europe. Part 1: General description. *Monthly Weather Review*, 106:296–210.

Chapter 2

Climate Variability and the Gulf of Maine Ecosystem: *Calanus*, Slope Water, and the NAO

2.1 Introduction

A major thread through climate studies of the last decade has been an appreciation for the range of variability inherent in the Earth's climate system. Typically, these studies identify a characteristic mode or oscillation in the state of the atmosphere over a particular region. Over the North Atlantic Basin, the dominant climate mode is the North Atlantic Oscillation (NAO), and as with the El Niño-Southern Oscillation (ENSO), the atmospheric and oceanographic changes associated with the NAO have an impact on ecosystems around the North Atlantic (Chapter 1; Ottersen et al., 2001).

Most of the results linking the NAO to variability in marine ecosystems come from studies in the Northeast Atlantic. Starting with Fromentin and Planque

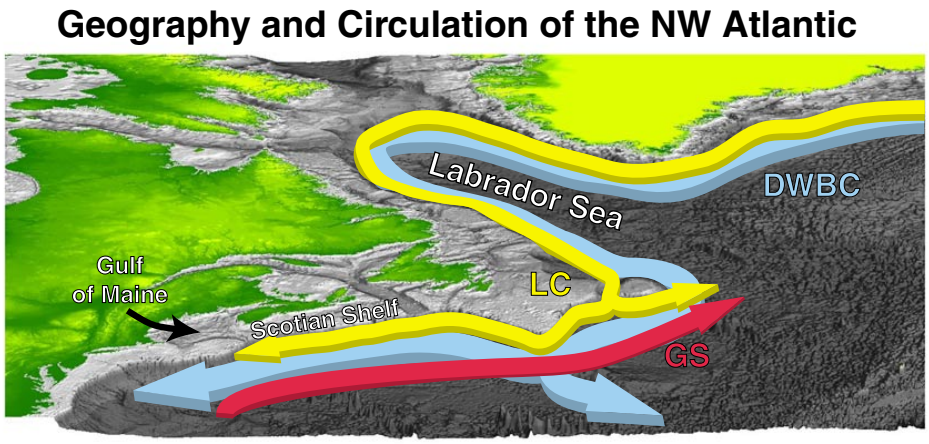

Figure 2.1: The major circulation features of the Northwest Atlantic. LC = Labrador Current, GS = Gulf Stream, DWBC = Deep Western Boundary Current. Land is indicated by shades of green, and the sea floor is indicated by shades of gray (light gray on the continental shelf, dark gray in deeper areas).

(1996) who related variability in the North Sea populations of the copepod *Calanus finmarchicus* in the North Sea to the NAO, researchers have documented NAO-associated changes in marine ecosystems throughout the region (Chapter 1; Ottersen et al., 2001). However, the importance of the NAO in the eastern Atlantic should not be surprising, given the strong influence the NAO has on European weather.

The relationship between the NAO and the weather over the Northwest Atlantic Shelf is less clear than in the North Sea. In maps of the correlation between the NAO and atmospheric properties such as wind speed or sea-level pressure, the Gulf of Maine/Scotian Shelf region appears as an area of low or zero correlation. However, the Northwest Atlantic Shelf is located at the meeting point of the subtropical and subpolar gyres represented by the Gulf Stream and Labrador Current, respectively (Figure 2.1), both of which are influenced by the NAO (Dickson et al., 1996; Taylor

and Stephens, 1998). Thus, any effects the NAO has on the ecosystems of the NW Atlantic Shelf are likely to be mediated by oceanographic processes.

Initial work on long-term changes in the Gulf of Maine ecosystem have supported this view. Conversi et al. (2001) and Greene and Pershing (2001) both noted a positive association between the NAO and the abundance of the copepod *Calanus finmarchicus*. Both studies found that the population changes were preceded by changes in the physical environment, specifically sea surface temperature (Conversi et al., 2001) and the temperature in the deep basins on the continental shelf (Greene and Pershing, 2001). The goal of this study is to extend this work and characterize in more detail the physical and biological changes in the ecosystems surrounding the Gulf of Maine.

2.2 Methods

Time series of a variety of physical and biological variables were used to quantify interannual variability in the Gulf of Maine ecosystem. Subsurface temperature data were acquired from the Bedford Institute of Oceanography's database (e. g. Petrie et al., 1996). A time series of the abundance of *Calanus finmarchicus* in the Gulf of Maine was constructed with data from Continuous Plankton Recorder (CPR) surveys conducted by the National Marine Fisheries Service. The CPR data were also used to construct a time series of relative phytoplankton abundance based on the CPR color index. The North Atlantic Oscillation (NAO) Index time series (Hurrell, 1995) was used to represent winter climate of the North Atlantic. The

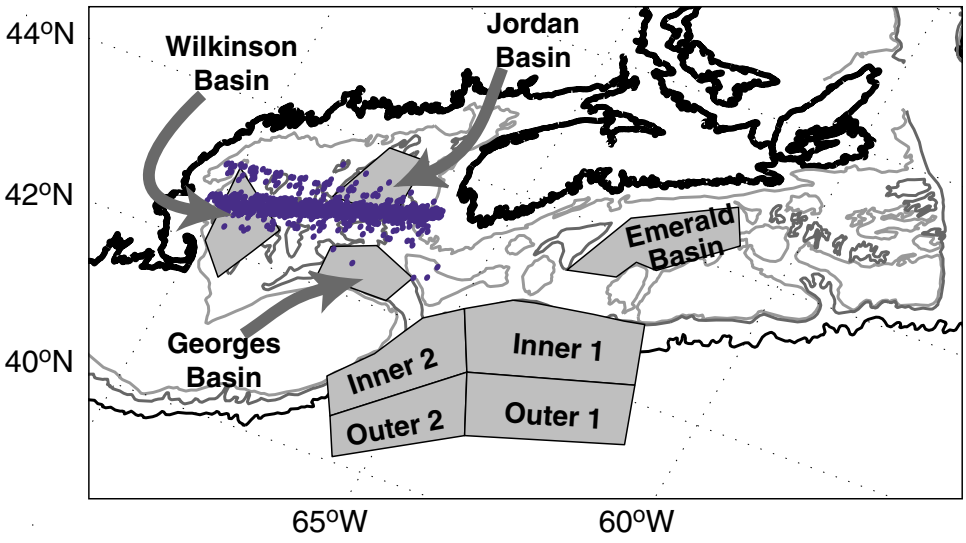

Figure 2.2: Location of data used in this study. Each circle represents a CPR observation included in the analysis. The polygons are the regions for the temperature analysis.

relationships between the time series were explored using cross-correlations.

2.2.1 Physical Oceanography

Temperature observations were obtained from a database of hydrographic measurements maintained by the Bedford Institute of Oceanography. All of the temperature observations from depths between 150 and 250 m in 8 predefined regions were collected (Figure 2.2). The 8 regions included three deep basins in the Gulf of Maine, Emerald Basin on the Scotian Shelf, and four regions over the continental slope adjacent to the Gulf of Maine and Scotian Shelf. The mean temperature of this layer for each region and each year was computed. The relatively deep water was chosen since this layer exhibits the strongest interannual patterns and significantly influences temperature near the surface (Petrie and Drinkwater, 1993).

Despite the large geographic extent and range of atmospheric forcing in the study region, similar patterns of interannual variability have been found throughout the area (Petrie and Drinkwater, 1993; Drinkwater et al., 2000). For this reason, a principal component analysis of the 8 temperature time-series was performed. The dominant mode from this analysis was used to represent the coupled variability of the hydrography in the whole region.

2.2.2 Biological Oceanography

All biological data used in this study come from surveys using the Continuous Plankton Recorder (CPR), originally designed by Sir Alister Hardy (Hardy, 1939). The Sir Alister Hardy Foundation for Ocean Science (SAHFOS) has conducted CPR surveys for over 50 years using merchant ships passing through the North Atlantic (Gamble, 1994). The instrument is towed at a shallow depth ($\sim$10m) and sieves plankton from the surrounding waters with a silk gauze. The instrument provides spatial information by periodically advancing the gauze to expose a fresh section. The zooplankton and large phytoplankton retained on the gauze are counted, and the discoloration of the gauze from algal pigments is evaluated and assigned a qualitative phytoplankton color value (Colebrook, 1979). After the samples are processed, the CPR data set includes spatially indexed counts of hundreds of different zooplankton taxa, counts of several of the largest phytoplankton taxa; and qualitative values for the phytoplankton color index.

The CPR survey in the Gulf of Maine is conducted by the U. S. National Ma-

rine Fisheries Service in Narragansett, RI according to the methods used by the SAHFOS surveys (Jossi and Goulet, 1993). The Gulf of Maine survey consists of a transect between Boston, MA USA and Yarmouth, NS Canada (Figure 2.2). The survey samples a relatively small area, but the data extend, with occasional gaps, back to 1961. We focused our analysis on two data sets: the abundance of the copepod *Calanus finmarchicus* (hereafter, *Calanus*) and the phytoplankton color index. *Calanus* was selected because it is the dominant zooplankton species during the spring and early summer in this region, providing an important link between the primary productivity occurring in the spring bloom and higher trophic levels (Bigelow, 1926; Davis, 1987; Meise and O'Reilly, 1996). Although qualitative, the color index is strongly correlated with primary productivity in the North Atlantic (Reid et al., 1998). Our analysis used only data from the central Gulf of Maine since previous studies suggest the populations near the end of the surveys (Massachusetts Bay and the Scotian Shelf) have different dynamics than the central section (Jossi and Goulet, 1993).

Calanus has a strong seasonal cycle with a range of over an order of magnitude (Meise and O'Reilly, 1996). Computing simple yearly means of these data would bias the time series towards years that were sampled more intensively during the weeks of peak abundance. For this reason, a filtering procedure was developed to correct the CPR observations for the seasonal pattern. First, the climatological seasonal cycle was estimated by fitting a "hat" function to the log-transformed data using Matlab's `nonlinfit` function. The hat function assumes that a peak in abundance

occurs at a specific time and that the population increases and declines linearly about the peak. Outside the period when the population is growing or declining, the abundance is assumed to be constant, although the levels before and after the peak are not required to be the same. Mathematically, the function is defined by 6 parameters: the abundance before the population begins to increase, the time when the population begins to increase, the peak abundance, the time when the peak occurs, the time when the population ceases to decline, and the abundance after this time. The *Calanus* data were converted into anomalies by subtracting the expected abundance (based on the best-fit hat function) from the observed values. The mean of the abundance anomalies for each year was then computed. Two years (1963 and 1977) were excluded from the analysis because the sampling did not resolve the abundance peak.

The color index is a qualitative measure of phytoplankton concentration. Each section of CPR gauze is assigned a value of 0, 1, 2, or 6.5 based on its color when compared to a set of standards. A procedure similar to that used for *Calanus* was used to create a time series of CPR color index values. The color index cycle was dominated by the spring bloom period (Julian days 66-125); thus, yearly means were computed based only on the mean anomaly during this period. The variance of the anomalies increased during the bloom period; thus, yearly means of these data will be sensitive to year-to-year differences in the sampling dates. To minimize the effect of sampling time, years were excluded if the mean sampling date in the bloom period was more than 3 standard errors away from the mean sampling date

in all springs.

2.2.3 Cross-correlation Analysis

Cross-correlation analysis is a powerful way of examining the relationship between two time series. The procedure computes the correlation between two time series as the two series are shifted in time relative to each other. However, the time series must be processed with care to avoid spurious correlations (Box and Jenkins, 1976; Chatfield, 1984). Specifically, the series should be filtered, a process known as *pre-whitening*, to remove autocorrelations in each series. The four time series examined are all significantly autocorrelated at 1 year, that is, the value of a given year depends on the value from the previous year. Therefore, the lag-1 autocorrelation was removed by first solving for a and b in the equation:

$$X_{n+1} = aX_n + b \tag{2.1}$$

where X_n is the value of the series at year n. Using this equation, the pre-whitened series is constructed by subtracting the observed value at $n + 1$ from the value predicted by Equation 2.1. For an appropriately filtered time-series, correlation values significantly different from zero will fall outside the interval $\pm 2N^{-1/2}$ where N is the number of data pairs used to compute the correlation (Chatfield, 1984). The main disadvantage to this filtering procedure is that Equation 2.1 can not be computed for data points occurring after a gap, and these points must be discarded.

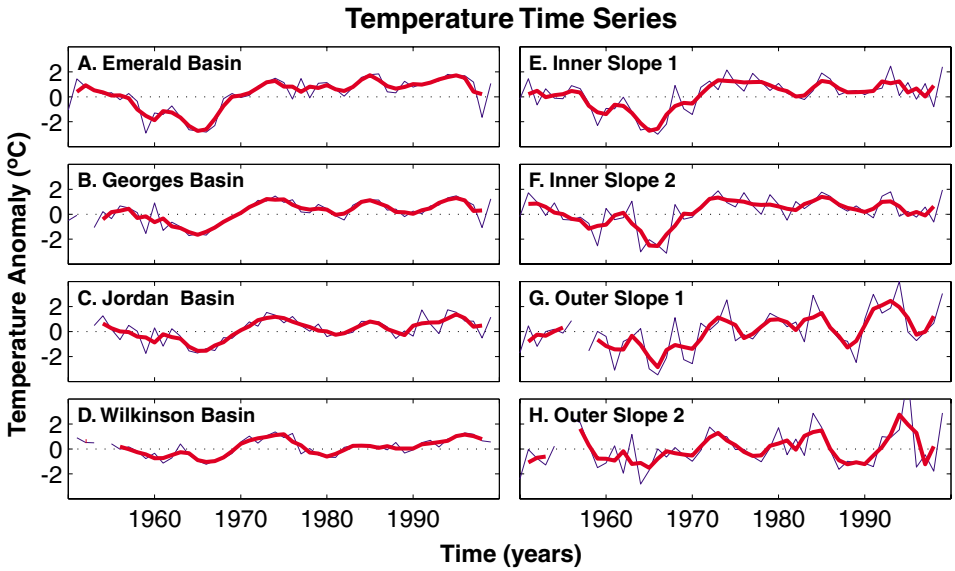

Figure 2.3: Temperature anomaly time series for the Northwest Atlantic shelf. The regions are plotted with the easternmost (upstream) regions near the top and the shelf basins on the left. The polygons defining the regions are in Figure 2.2. The heavy line is the three-year running mean.

2.3 Results

2.3.1 Temperature Time Series

Over the last 50 years, the temperature between 150-250 m in each of the regions exhibited fluctuations with amplitudes ranging from 2° in Wilkinson Basin (Figure 2.3 D) to nearly 8° C in the outer slope regions (Figure 2.3 G-H). The highest variability was found in the outer slope regions, while the lowest variability was found in the shelf basins. Among the shelf basins, the variability decreased in the downstream (east-to-west) direction. Computing the three-year running means of the time series (Figure 2.3, heavy lines) smooths out the year-to-year variability, revealing the lower frequency patterns. The running mean and yearly time series are

almost indistinguishable in the deep basins. This suggests that the variability in the basins was strongest at lower frequencies, while the offshore regions had more pronounced variability at higher frequencies. A feature present in most of the regions was the temperature minimum that occurred between 1964 and 1966. The mid-60's minimum dominated the variability in many of the time series, especially the shelf basins and inner slope regions. The temperatures in these regions were warmer and relatively constant after the 60's event; however, low amplitude oscillations with periods of 5-10 years were present. Although present in all areas, the amplitudes of these oscillations were greater in the offshore regions with maxima around 1973, 1985, and 1994.

In summary, the inner slope regions and shelf basins had similar time series, and the patterns in the outer slope regions were similar but had greater variability. The principal components analysis supports this impression. The first principal component explained 64.8% of the variability of the whole region (Figure 2.4 A). This vector corresponds to a weighted average of the entire region, with the most variable regions (those to the east and offshore) receiving the largest weights. The largest values in the second component occur for the two outer-slope regions, and the values are of opposite sign (Figure 2.4 B). It is generally difficult to construct physical interpretations of higher components; however, in this case, they explained only a small fraction of the variability (12.7% for the second component, less than 22.5% for the remaining 6 components).

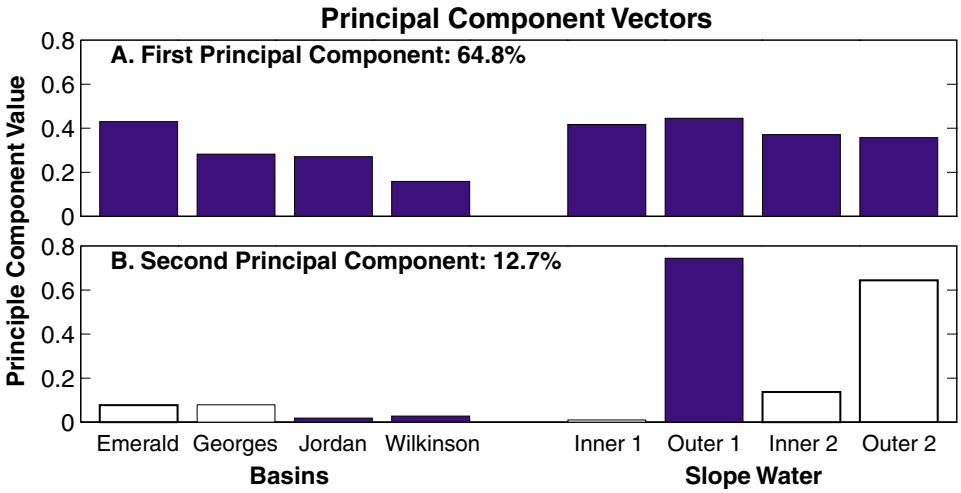

Figure 2.4: The first two principal component vectors for the analysis of the temperature time series. The height of the bars indicates the magnitude of the vector component associated with each region. The color of the bar indicates the sign of the component: dark=positive, white=negative. The percent of the total variance explained by each vector is listed above it.

2.3.2 CPR Seasonal Cycles

There was considerable interannual variation in the abundance of *Calanus* and the CPR color index (Figure 2.5). On average, the seasonal cycle in *Calanus* abundance determined from the CPR exhibited the same patterns as previous studies (Meise and O'Reilly, 1996); the *Calanus* population in the Gulf of Maine reached its peak abundance during May and June and the amplitude of the mean seasonal cycle was approximately an order of magnitude. However, there was considerable variability about the mean cycle. The spring phytoplankton bloom is the dominant feature in the plot of seasonal color index values (Figure 2.5 B).

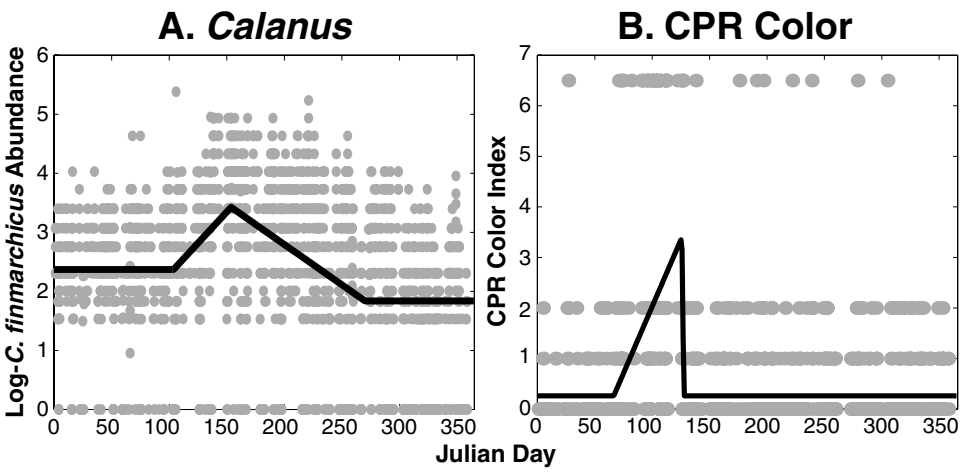

Figure 2.5: The observations and mean seasonal cycles for both A. *Calanus* and B. color index.

2.3.3 Intercomparison of the Time Series

The time series assembled for this study reveal considerable variability in the climate of the North Atlantic (Figure 2.6 A), the physical conditions in the Northwest Atlantic (Figure 2.6 B), and in the abundance patterns at two different trophic levels in the Gulf of Maine (Figure 2.6 C). Both the NAO Index and the first principal component of the temperature analysis (hereafter, the temperature index) possess similar features. The low temperature values prior to 1972 occurred during a period of predominantly negative NAO years. After 1971, both the NAO and temperature indices were predominantly positive. Furthermore, the NAO Index oscillated with a period of 7-10 years and these features were generally followed a few years later by similar changes in the temperature index.

The general patterns in both the *Calanus* and color index series (Figure 2.6 C) follow the temperature index. After periods such as the 1960's and early 1990's

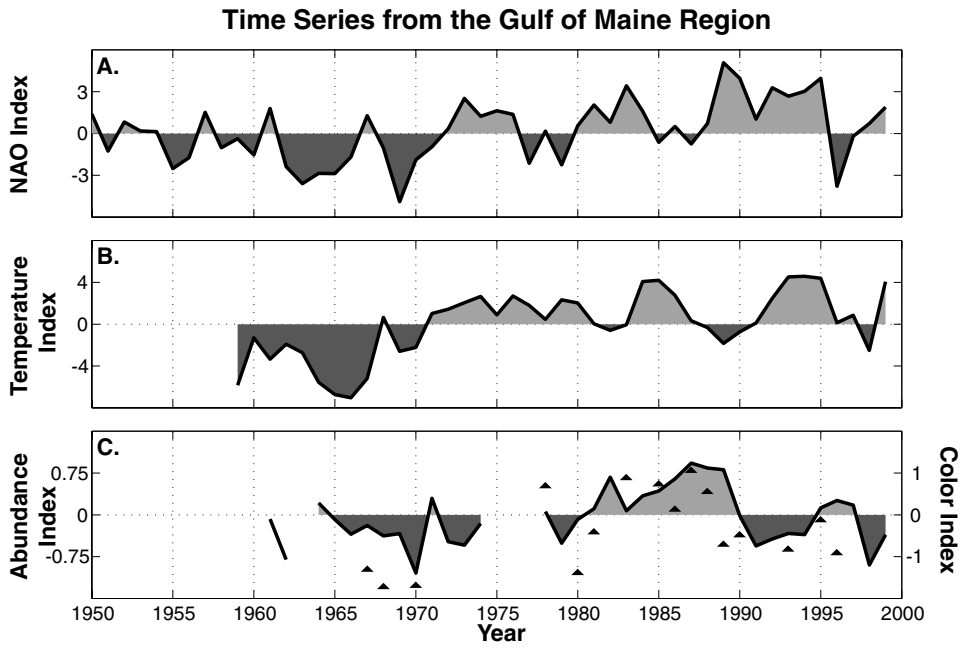

Figure 2.6: The three time series analyzed: A. The winter NAO time series, B. The first principal component of the regional temperature, C. *Calanus* abundance index (line and the color index (triangles). The shading underneath the curve indicates whether the anomalies are positive (light) or negative (dark).

when the temperature index was negative or near zero, *Calanus* was less abundant and lower color index values were observed. The highest color index and *Calanus* levels occurred in the mid-1980's following a period of warm temperatures.

The cross-correlation analysis reveals many of the same patterns described above (Figure 2.7). For each cross-correlation, one time-series was assumed to force the other. The plots in Figure 2.7 are organized so that each column of plots uses the same "forcing" series, and each row uses the same "response" series. The heavy lines are the functions using the raw time series, the light lines use the pre-whitened series. The color index series could not be pre-whitened because of the numerous gaps; therefore, no light lines or confidence intervals are reported for these cross-

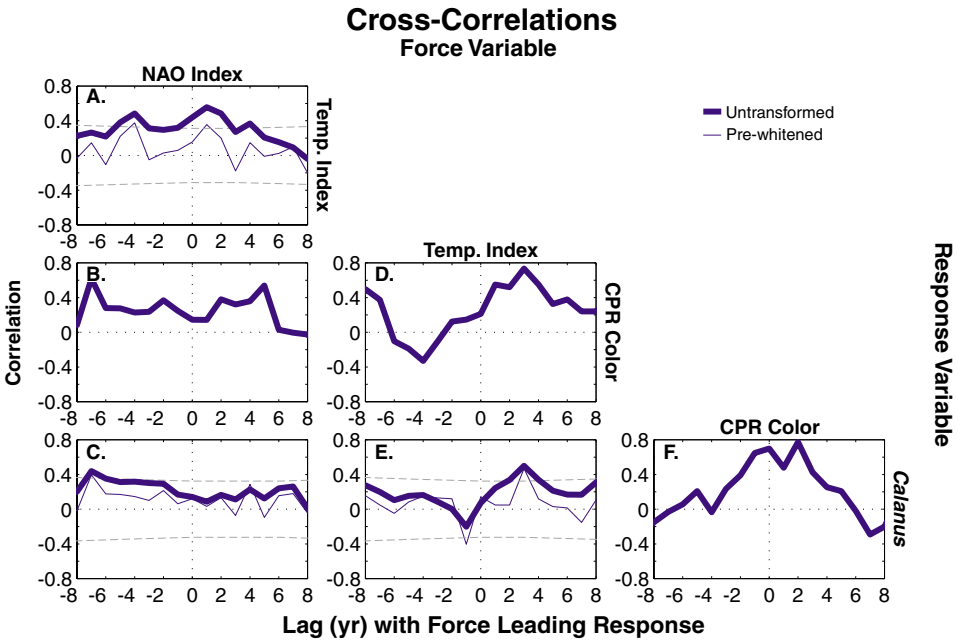

Figure 2.7: Cross-correlations among the time series in Figure 2.6. The plots are organized as a table with the same "forcing" series used in each column and the same "response" series used in each row. The heavy lines are the cross-correlation functions using the raw data; the light lines are the functions using the pre-whitened data. Peaks in the functions for the pre-whitened data indicate a significant correlation at that lag at the 95% confidence value. Because the color index data could not be pre-whitened, only the cross-correlation using the raw data is displayed.

correlations. Peaks of the pre-whitened cross-correlations above the upper dashed line are significant at the 95% level. Although a few significant correlations were found at negative lags, only the correlations at positive lags are interpreted as these are more likely to reflect the underlying mechanisms. Furthermore, the peaks at negative lags most likely reflect the periodicities in the data rather than the relationship sought. The highest correlations between the NAO and temperature indices occurred at lags of 0-2 years (Figure 2.7 A). The maximum correlation at a lag of 1 year (i.e. the changes in temperature follow one year after the NAO) was significant based on the cross-correlation using the pre-whitened series. No significant correlations were found between the NAO and the biological data (Figure 2.7 B-C). The analysis suggests that high color index values and large numbers of *Calanus* should occur 2-3 years after high temperature index values (Figure 2.7 D-E); the correlation with *Calanus* at 3 years is significant. Adding the lag of the maximum correlation between the CPR data and temperature to the lag from the correlation between temperature and the NAO suggests that the cross correlation functions of *Calanus* and the color index versus the NAO should have peaks near 4 years. This is indeed the case, especially for the color index; however, the actual correlations are weak. *Calanus* and the color index were strongly correlated with a time lag between -1 and 2 years (Figure 2.7 F).

2.4 Discussion

From the cross-correlation analysis, a plausible set of relationships among the time series can be indentified, suggesting a chain of events that frequently starts with the NAO. A simple linear relationship with the NAO explains 31% of the variance in the temperature index series (Figure 2.8 A); thus, on average, one year following a winter with positive NAO conditions, the temperature in the Gulf of Maine region will be warmer than average. According to the cross-correlation analysis, three years after warm conditions in the region, higher populations of *Calanus* and higher standing stocks of phytoplankton should be observed in the Gulf of Maine. This scenario accounts for 25% of the variance in the *Calanus* population (Figure 2.8 B) and a large fraction of the variance in the color index series (Figure 2.9 A). The relationship between temperature and *Calanus* would be higher if the *Calanus* data from 1998 (or the temperature from 1995) were excluded. 1995 was one of the warmest years in the record, yet the abundance of *Calanus* in 1998 was the second lowest in the record. This outlier suggests that the lag between temperature and *Calanus* may be variable, since a shorter lag would align the *Calanus* observation with cooler temperatures in 1996 or 1997. The relationship between the color index and temperature is determined by three observations of low color values (1967, 1968, and 1970) following cold years (1964, 1965, and 1967). This analysis suggests that the changes in the color index are driven by the large differences between the 1960s and 1980-1990; however, the numerous gaps in the color index data make any interpretation uncertain. However, the correlation between temperature and the

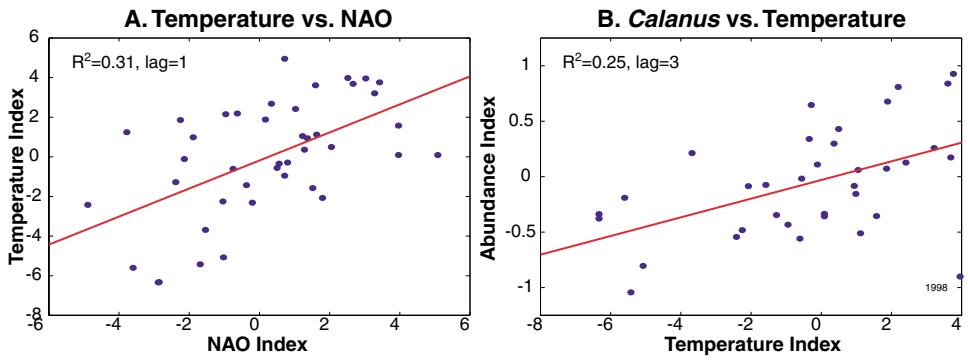

Figure 2.8: The significant relationships between NAO and temperature (A) and temperature and *Calanus* (B) identified by the cross-correlation analysis. All of the best-fit lines have slopes significantly different from zero.

color index at a lag of 3 years was signficant based on the Spearman rank correlation, a better technique for data that are non-normal. Despite the problems with the color index data, its variability is closely tied with that of *Calanus* (Figure 2.9 B).

2.4.1 Physical Oceanography–a "Coupled Slope Water System"

The common patterns in the temperature data suggest that the region responds to the NAO in a coupled fashion. At the most basic level, this system appears to oscillate between two states: a cold state following negative NAO conditions and a warm state following positive NAO conditions. During the cold state, exemplified by 1965, the waters in the deep basins and the slope water region are composed of relatively cold and fresh water referred to as Labrador Slope Water by Gatien (1976), but renamed Labrador Subarctic Slope Water (LSSW) by Greene and Pershing (2001). These authors renamed this water mass to better reflect its origin and to

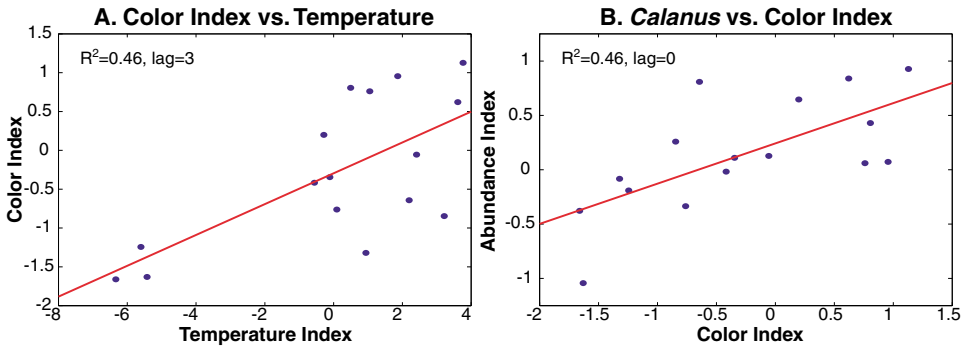

Figure 2.9: The significant or most likely relationships between temperature and the color index (A) and between color and *Calanus* (B) identified by the cross-correlation analysis. All of the best-fit lines have slopes significantly different from zero. Both relationships are also significant based on a Spearman rank correlation (R_s^2=0.40 and 0.50, respectively).

avoid confusion with Labrador Sea Water. During the warm state, exemplified by 1985, the dominant water mass is relatively warm, salty Atlantic Temperate Slope Water (ATSW). The shift between these two states occurs when the front separating the two water masses moves north and east towards the Tail of the Grand Bank during the warm phase and south and west towards the Mid-Atlantic Bight during the cold phase (Figure 2.10; Drinkwater et al., 2000).

In a previous analysis of the hydrography of the NW Atlantic Shelf, Petrie and Drinkwater (1993) related much of the variability in the temperature time series to variability in the volume of water transported around the Tail of the Grand Banks by the Labrador Current. The southwestward flow over the continental slope adjacent to the Scotian Shelf is a direct extension of the Labrador Current, which extends back around the Labrador Sea and beyond to the eastern side of Greenland (Figure 2.1). Their work suggests that the cold state of the temperature index occurs when the transport of the Labrador Current increases, bringing LSSW into

the region and moving the ATSW/LSSW front to the south. When the transport decreases, ATSW returns.

Atmospheric conditions over the Labrador Sea are closely tied to the state of the NAO (Hurrell, 1995; Dickson et al., 1996; Dickson, 1997). Recent observations following the dramatic drop in the NAO during 1996 have provided an insight into the connection between NAO-related conditions in the Labrador Sea and circulation changes along the Northwest Atlantic Shelf (Drinkwater et al., 2000). Following the negative NAO event in the winter of 1996, the transport in the Labrador Current increased, and LSSW spread rapidly along the continental slope, displacing ATSW away from the shelf (Drinkwater et al., 2000). By fall of 1997, the cold water extended past the middle of the continental shelf, reaching the Mid-Atlantic Bight by spring of 1998. This event is visible in the temperature time series and temperature index in 1998 (Figures 2.3 and 2.6). Although the cross-correlation analysis indicates a 1 year lag between changes in the NAO Index and the response of the temperature index, the movement of the LSSW following the 1996 NAO event suggests a lag approaching 2 years. The cross-correlation function using the unfiltered data (Figure 2.7 A) shows a peak centered at 1 year, but with high values at 0 and 2 years. Although not significant, the correlations at 0 and 2 years together with the observations by Drinkwater et al. (2000) suggest that the response of the temperature index to the NAO exhibits a variable time lag ranging from 0-2 years.

The ATSW/LSSW transitions in the NW Atlantic are associated with changes in the distribution and characteristics of water masses and currents throughout the

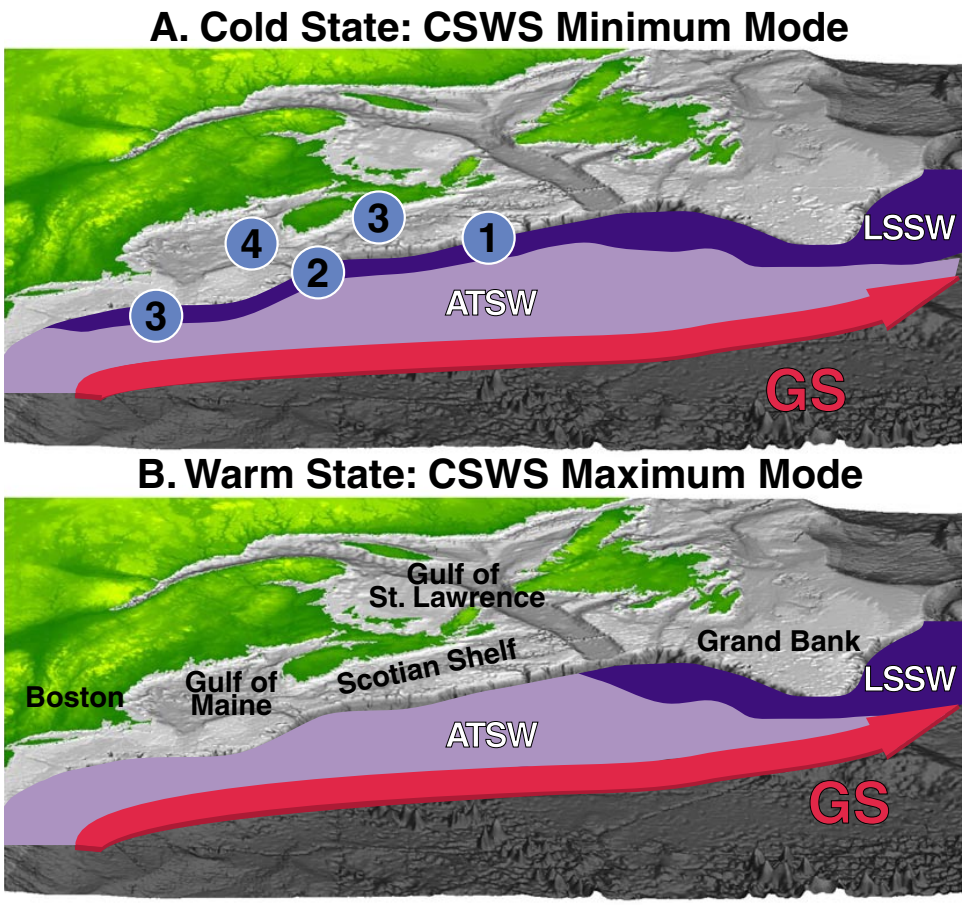

Figure 2.10: The distribution of Labrador Subarctic Slope Water (LSSW), Atlantic Temperate Slope Water (ATSW), and the position of the Gulf Stream (GS) during the cold (A) and warm (B) states of the CSWS. The numbers in (A) show the first observations of LSSW following the 1996 drop in the NAO: ①= September 1997, ② = January 1998, ③= February 1998, ④= August 1998 (Drinkwater et al., 2000). Land is indicated by shades of green, and the sea floor is indicated by shades of gray (light gray on the continental shelf, dark gray in deeper areas). Several geographic locations are also marked in B.

Northwest Atlantic (Taylor and Stephens, 1998; Keigwin and Pickart, 1999; Pickart et al., 1999; Rossby and Benway, 2000). Pickart et al. (1999) suggest that the region exhibits two characteristic modes. Their minimum mode corresponds to the cold-water phase described above with increased transport in the Labrador Current. Along with the changes in the slope waters, the layer of deep Labrador Sea Water becomes less prominent and the transport in the Deep Western Boundary Current decreases. The changes are reversed during the positive mode.

The conclusions of Pickart et al. (1999) and Drinkwater et al. (2000) suggest that the changes in the Gulf of Maine region presented above are part of a larger *Coupled Slope Water System* (CSWS) extending from the Grand Banks to the Mid-Atlantic Bight. Further support for this concept comes from observations of the seasonal and interannual movements of the Gulf Stream's North Wall (Taylor and Stephens, 1998; Rossby, 1999; Rossby and Benway, 2000). The position of the North Wall is correlated with the NAO Index at a two-year lag such that the Gulf Stream shifts south two years following negative NAO conditions (Taylor and Stephens, 1998). Taylor and Stephens (1998) hypothesize that the Gulf Stream shifts are driven by the changes in the position of the westerly winds associated with the NAO. This mechanism implies that the intrusion of LSSW around the Tail of the Grand Banks may be caused by the southward shift of the Gulf Stream. Rossby and Benway (2000) turn this implication around and propose that the southward shifts in the Gulf Stream following negative NAO years are caused by increased transport of LSSW around the Tail of the Grand Bank. At this point, both of these hypotheses

are plausible, and both suggest that the dynamics of the Northwest Atlantic Shelf region are closely tied with the basin-scale circulation of the North Atlantic.

2.4.2 Biological Oceanography–response to CSWS

Given the dramatic physical changes that occur when the CSWS shifts from one mode to another, it is not surprising that there are equally dramatic changes in the populations inhabiting the Northwest Atlantic Shelf. Much of the variability in sea surface temperature in this region is determined by the temperature of slope water (Petrie and Drinkwater, 1993); thus, the link between *Calanus* and the temperature index is consistent with previous results connecting *Calanus* abundance to sea surface temperature (Conversi et al., 2001).

The Climate Variability Response Hierarchy developed in Chapter 1 provides a useful framework for identifying the mechanisms that might drive the CSWS-*Calanus* association. The hierarchy sorts the effects of climate on populations according to the ecological complexity of the effect. The simplest effects are due to the movements of populations associated circulation changes. These effects, termed translations, are responsible for the dramatic ecological changes associated with ENSO (Graybill and Hodder, 1985; McGowan, 1985; McGowan et al., 1998) and in the North Sea (Fromentin and Planque, 1996; Reid and Planque, 1999; Reid et al., 2001). The circulation differences between the two states of the CSWS raise the possibility that the *Calanus* fluctuations in the Gulf of Maine could be another example of a translational effect (Chapter 1).

The dynamics of *Calanus* populations on shelf regions such as the Gulf of Maine and North Sea are complicated by this species' life-history and behavior. During the fall and early winter, *Calanus* is rare in the surface waters. Instead, large numbers of late-stage (C5-C6) copepodites are found at depth in diapause (Marshall and Orr, 1955; Hirche, 1996). The animals remain in this state of low metabolic activity until late winter when they swim to the surface waters and begin feeding and reproducing. This overwintering strategy limits the distribution of *Calanus* in winter to deep water beyond the continental shelf break and to the few deep basins on the shelf. Despite this restriction, *Calanus* is an important component of shelf ecosystems around the North Atlantic, including the Gulf of Maine. However, these shelf populations are not likely to be self sustaining and consist of expatriates from nearby deep water populations (Longhurst, 1998; Head et al., 1999). Because shelf populations of *Calanus* require periodic restocking, Greene and Pershing (2001) propose that these populations should be particularly sensitive to advective changes associated with climate variability.

Calanus can enter the Gulf of Maine via two main pathways: the Northeast Channel which connects the Slope Water to Georges Basin, or from the Scotian Shelf (Hannah et al., 1998; Lynch et al., 1998; Miller et al., 1998). During the cold state of the CSWS, there is an increased density contrast across the front separating ATSW from LSSW (Pickart et al., 1999). The amount of exchange across a front is inversely proportional to the density contrast (Rossby, 1999); thus, the strengthened front may provide a barrier that reduces the supply of *Calanus* to the Gulf of Maine

and Scotian Shelf. Observations of *Calanus* on the Scotian Shelf support this idea. Head et al. (1999) found that *Calanus* was more abundant on the Scotian Shelf when there was evidence of intrusions of ATSW on to the shelf. This hypothesis requires that the concentrations of *Calanus* in ATSW are higher than LSSW; however, a field study testing this condition has not been conducted.

Another transport-based hypothesis involves the deep changes in the CSWS. The Labrador Sea is the center of distribution of *Calanus* in the Northwest Atlantic (Planque et al., 1997). During the warm state of the CSWS, the transport of Labrador Sea Water in the Deep Western Boundary Current (DWBC) increases. It is possible that the DWBC brings large numbers of diapausing *Calanus* into the region. This mechanism could interact positively with the hypothesis above, providing a source of *Calanus* for the ATSW.

Increased population growth rates during the warm state may also account for the association between *Calanus* and temperature. The best evidence for this hypothesis is the correlation between *Calanus* and the color index. There is evidence that the concentrations of nitrate are higher in the ATSW which might allow for higher standing stocks of chlorophyll during the warm state (Petrie and Yeats, 2000). Modeling studies also suggest that warm slope waters might increase stratification during the spring, allowing for a larger spring bloom (see Chapter 3).

2.5 Conclusion

This examination of physical and biological time series from the NW Atlantic has documented dramatic changes in the environment of the region. The configuration of the waters on and adjacent to the NW Atlantic Shelf alternates between two characteristic modes or states, suggesting that the region operates as a Coupled Slope Water System. The variability in the CSWS is closely tied to the winter atmospheric conditions over the North Atlantic as represented by the NAO Index. Furthermore, the variability in the CSWS impacts the abundance of the copepod *Calanus*, an important species in the ecosystems of the region. Although the exact mechanisms linking the biological, physical, and climatic conditions in the Gulf of Maine are not yet known, the significant correlations among them provide a means to forecast changes in the Gulf of Maine ecosystem.

2.6 References

Bigelow, H. B. (1926). Plankton of the offshore waters of the Gulf of Maine. *Bulletin of the United States Bureau of Fisheries*, 40:1–509.

Box, G. E. P. and Jenkins, G. M. (1976). *Time Series Analysis: Forecasting and Control*. Holden-Day, San Francisco.

Chatfield, C. (1984). *The Analysis of Time Series: An Introduction*. Chapman and Hall, New York.

Colebrook, J. M. (1979). Continuous plankton records: seasonal cycles of phytoplankton and copepods in the North Atlantic and North Sea, 1948-1975. *Marine Biology*, 51:23–32.

Conversi, A., Piontkovski, S., and Hameed, S. (2001). Seasonal and interannual dynamics of *Calanus finmarchicus* in the Gulf of Maine (Northeastern US shelf) with reference to the North Atlantic Oscillation. *Deep-Sea Research II*, 48:519–520.

Davis, C. S. (1987). Zooplankton life cycles. In Backus, R. H., editor, *Georges Bank*, pages 256–267. MIT Press, Cambridge, Massachusetts.

Dickson, R. (1997). From the Labrador Sea to global change. *Nature*, 386:649–650.

Dickson, R., Lazier, J., Meincke, J., Rhines, P., and Swift, J. (1996). Long-term coordinated changes in the convective activity of the North Atlantic. *Progress in Oceanography*, 38:241–295.

Drinkwater, K. F., Mountain, D. B., and Herman, A. (2000). Variability in the slope water properties off eastern North America and their effects on the adjacent seas. *Journal of Geophysical Research*, In press.

Fromentin, J. and Planque, B. (1996). *Calanus* and the environment in the eastern North Atlantic. II. Influence of the North Atlantic Oscillation on *C. finmarchicus* and *C. helgolandicus*. *Marine Ecology Progress Series*, 134:111–118.

Gamble, J. C. (1994). Long-term planktonic time series as monitors of marine environmental change. In Leigh, R. A. and Johnston, A. E., editors, *Long-term Experiments in Agriculture and Ecological Sciences: Proceedings of a Conference to Celebrate the 150th Anniversary of Rothamsted Experimental Station, held at Rothamsted, 14-17 July, 1993*, pages 365–386. CAB International, Wallingford, U. K.

Gatien, M. (1976). A study in the slope water region south of Halifax. *Journal of the Fisheries Research Board of Canada*, 33:2213–2217.

Graybill, M. R. and Hodder, J. (1985). Effects of the 1982-83 El Niño on reproduction of six species of seabirds in Oregon. In Wooster, W. S. and Fluharty, D. L., editors, *El Niño North: El Niño Effects in the Eastern Subarctic Pacific Ocean*, pages 205–210. Univeristy of Washington, Seattle.

Greene, C. H. and Pershing, A. J. (2001). The response of *Calanus finmarchicus* populations to climate variability in the Northwest Atlantic: Basin-scale forcing associated with the North Atlantic Oscillation. *ICES Journal of Marine Science*, in press.

Hannah, C. G., Naimie, C. E., Loder, J. W., and Werner, F. E. (1998). Upper ocean transport mechanisms from the Gulf of Maine to Georges Bank, with implications for Calanus supply. *Continental Shelf Research*, 17:1887–1911.

Hardy, A. C. (1939). Ecological investigations with the continuous plankton recorder, object, plan, and methods. *Hull Bulletins of Marine Ecology*, 1:1–57.

Head, E. J. H., Harris, L. R., and Petrie, B. (1999). Distribution of *Calanus* spp. on and around the Nova Scotia Shelf in April–evidence for an offshore source of *Calanus finmarchicus* to the mid- and western regions. *Canadian Journal of Fisheries and Aquatic Science*, 56:2463–2476.

Hirche, H.-J. (1996). The reproductive biology of the marine copepod *Calanus finmarchicus*—a review. *Ophelia*, 44:111–128.

Hurrell, J. (1995). Decadal trends in the North Atlantic Oscillation: regional temperatures and precipitation. *Science*, 269:676–679.

Jossi, J. and Goulet, J. (1993). Zooplankton trends: US north-east shelf ecosystem and adjacent regions differ from north-east Atlantic and North Sea. *ICES Journal of Marine Science*, 50:303–313.

Keigwin, L. and Pickart, R. (1999). Slope water current over the Laurentian Fan on interannual to millenial time scales (vol 285, pg 520, 1999). *Science*, 286:1479–1479.

Longhurst, A. (1998). *Ecological Geography of the Sea*. Academic Press, San Diego, CA.

Lynch, D. R., Gentleman, W. C., McGillicuddy, D. J., and Davis, C. S. (1998). Biological/physical simulations of *Calanus finmarchicus* population dynamics in the Gulf of Maine. *Marine Ecology Progress Series*, 169:189–210.

Marshall, S. M. and Orr, A. P. (1955). *The Biology of a Marine Copepod*. Oliver and Boyd, Edinburgh.

McGowan, J. A. (1985). El Niño 1983 in the southern California Bight. In Wooster, W. S. and Fluharty, D. L., editors, *El Niño North: El Niño Effects in the Eastern Subarctic Pacific Ocean*, pages 166–184. Univeristy of Washington, Seattle.

McGowan, J. A., Cayan, D. R., and Dorman, L. M. (1998). Climate-ocean variability and ecosystem response in the Northeast Pacific. *Science*, 281:210–217.

Meise, C. J. and O'Reilly, J. E. (1996). Spatial and seasonal patterns in abundance and age-composition of *Calanus finmarchicus* in the Gulf of Maine and on Georges Bank. *Deep-Sea Research II*, 43:1473–1501.

Miller, C. B., Lynch, D. R., Carlotti, F., Gentleman, W. C., and Lewis, C. (1998). Coupling of an individual-based population dynamical model for stocks of *Calanus finmarchicus* with a circulation model for the Georges Bank region. *Fisheries Oceanography*.

Ottersen, G., Planque, B., Belgrano, A., Post, E., Reid, P. C., and Stenseth, N. C. (2001). Ecological effects of the North Atlantic Oscillation. *Oecologia*, in press.

Petrie, B., Drinkwater, K., Gregory, D., Pettipas, R., and Sandstr om, A. (1996). Temperature and salinity atlas for the Scotian Shelf and Gulf of Maine. *Canadian Technical Report of Hydrography and Ocean Sciences*, 171.

Petrie, B. and Yeats, P. (2000). Annual and interannual variability of nutrients and their estimated fuxes in the Scotian Shelf-Gulf of Maine region. *Canadian Journal of Fisheries and Aquatic Science*, in press.

Petrie, B. D. and Drinkwater, K. (1993). Temperature and salinity variability on the Scotian Shelf and in the Gulf of Maine, 1945-1990. *Journal of Geophysical Research*, 98:20,079–20,089.

Pickart, R., McKee, T., Torres, D., and Harrington, S. (1999). Mean structure and interannual variability of the slopewater system south of Newfoundland. *Journal of Physical Oceanography*, 29:2541–2558.

Planque, B., Hays, G. C., Ibanez, F., and Gamble, J. C. (1997). Large scale spatial variations in the seasonal abundance of *Calanus finmarchicus*. *Deep-Sea Research I*, 44:315–326.

Reid, P. C., de Fatima Borges, M., and Svendsen, E. (2001). A regime shift in the North Sea circa 1988 linked to changes in the North Sea fishery. *Fisheries Review*, in press.

Reid, P. C., Edwards, M., Hunt, H. G., and Warner, A. J. (1998). Phytoplankton change in the North Atlantic. *Nature*, 391:546.

Reid, P. C. and Planque, B. (1999). Long-term planktonic variations and the climate of the North Atlantic. In Mills, D., editor, *The Life of the Atlantic Salmon*, pages 153–169. Blackwell Science, Oxford.

Rossby, T. (1999). On gyre interactions. *Deep-Sea Research II*, 46:139–164.

Rossby, T. and Benway, R. L. (2000). Slow variations in mean path of the Gulf Stream east of Cape Hatteras. *Geophysical Research Letters*, 27:117–120.

Taylor, A. H. and Stephens, J. A. (1998). The North Atlantic Oscillation and the latitude of the Gulf Stream. *Tellus*, 50:134–142.

Chapter 3

Nonlinear Stratification: Spring Bloom Variability Forced by Winter Hydrography

3.1 Introduction

The temperate ocean's ability to retain properties of winter conditions is a unique feature of the Earth's climate system (Dickson, 1997; McCartney, 1997; Curry et al., 1998). During winter, cold continental air masses move over the ocean. The contrast in temperature between air and water causes a net flux of heat from the sea surface in the form of infrared (long-wave) radiation and through conduction. The loss of heat causes the surface waters to cool and become more dense, and creates an unstable situation with dense water on top of light water. Gravity causes the cooler water to sink, mixing it with the less dense waters below. Strong winds from winter storms create additional turbulence and contribute to the mixing. Over time, winter cooling and wind mixing homogenizes the surface layer of the ocean down many

tens of meters and below 1000 m in major deepwater formation centers such as the Labrador and Greenland Seas (Dickson et al., 1996). During late winter and early spring, the amount of heat added to the water over a day increases as the days lengthen. The temperature of the ocean rises primarily due to shortwave radiation which can penetrate many meters below the surface. Heating water decreases its density, creating a stable situation with warm water overlying cool water. The density contrast between the warm waters at the surface and cool waters below provides a barrier to vertical mixing; thus, incoming heat tends to stay near the surface. Once stratification begins, it proceeds rapidly as the density contrast traps incoming heat near the surface, further increasing the stratification.

Cooling creates instabilities and tends to homogenize the surface waters, while heating tends to stabilize the water column. This asymmetry between heating and cooling creates intermediate water masses, a characteristic feature of the temperate ocean. In areas with strong winter cooling, the warm surface layer that forms in the spring traps the bottom portion of the winter mixed layer. The trapped layer forms an intermediate water mass with temperature and salinity characteristics similar to the winter conditions and distinct from the summer surface layer and any layers below. If the intermediate water reaches the sea floor, it is known as a *bourrelet froid* ("cold cushion"; Mann and Lazier, 1996). These characteristics remain relatively unchanged during the summer and fall, although the water mass may be advected many kilometers during this time. When the surface waters cool the following winter, the intermediate layer is reexposed to the atmosphere. The long persistence

of winter signatures and their reappearance several years and many kilometers from their origin can be an important part of the oceans' climate on decadal and basin scales (McCartney, 1997; Sutton and Allen, 1997). Sutton and Allen (1997) charted the propagation of sea surface temperature anomalies around the North Atlantic many years after their creation. Although the anomalies appear at the surface, they travel at a slower rate than the surface waters, suggesting that they are surface manifestations of subsurface features. The time-scale of the propagation of these anamolies is similar to that of the NAO; thus, the intermediate waters may explain the persistance of the NAO signal (Sutton and Allen, 1997). Significant interannual variability in sea surface temperature along the Northwest Atlantic Shelf has been linked to the movements of subsurface waters that form in the Labrador and Slope Water Seas (Petrie and Drinkwater, 1993, ; Chapter 2).

Despite the importance of intermediate waters to climate, their influence on ecosystem processes has not been explored. Intermediate waters exert their strongest influence on near-surface properties at the end of winter; thus, biological phenomena occurring in the spring, such as the spring phytoplankton bloom, could be impacted by intermediate waters.

The physical and biological events that produce the spring bloom were first described by Gran and Braarud (1935); however, Sverdrup's critical depth theory (Sverdrup, 1953) is the classic quantitative description of the spring bloom. Sverdrup defines the critical depth z^* as the point where the integrated growth of the phyotplankton population balances the integrated mortality, and is formally expressed

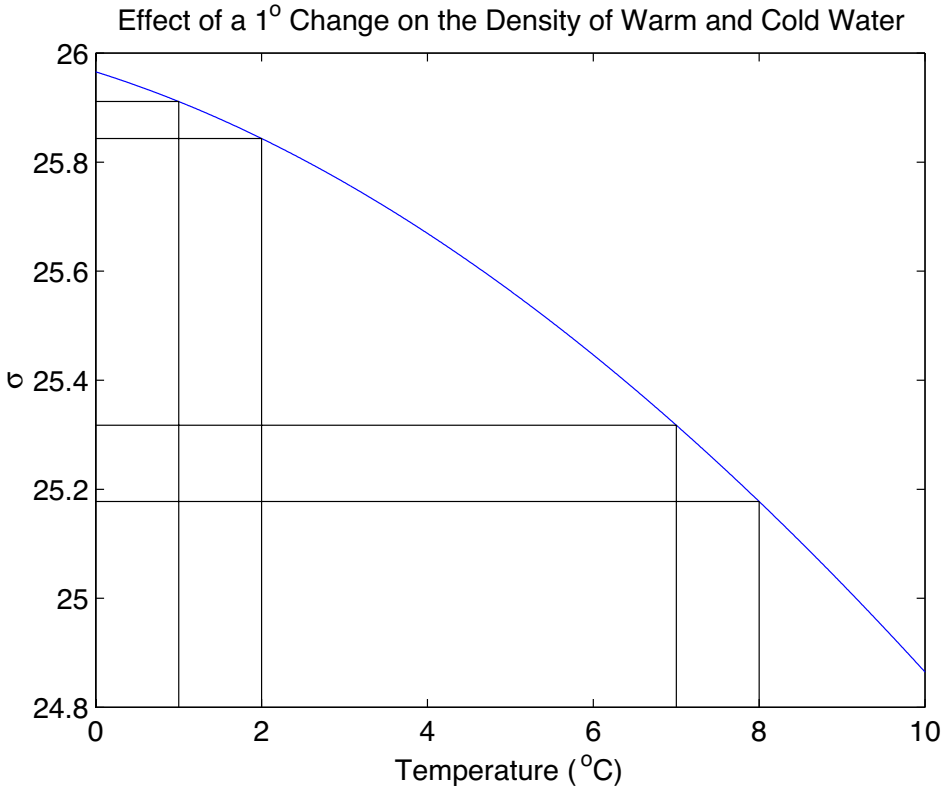

Figure 3.1: The density of sea water as a function of temperature according to the UNESCO equation of state. Changing the temperature by one degree has a greater effect on warmer water.

as:

$$\int_{-z^*}^{0} r(L(z,t))dz = \int_{-z^*}^{0} m dz. \tag{3.1}$$

where r is the growth rate which depends only on light (L), and m is the mortality rate. Assuming the population is evenly mixed above the pycnocline, when the pycnocline is deeper than z^*, the net growth rate of the population is negative. As stratification develops, the pycnocline shoals. Eventually, the pycnocline moves above z^* and a bloom begins.

Atmospheric effects, primarily wind mixing which influences the position of the

pycnocline relative to z^*, have received the most attention as sources of variability in spring bloom dynamics (Townsend et al., 1994). An assumption implicit in this view is that the initial state of the water column after winter—whether determined by variations in intermediate water types or winter weather—has little effect on the development of spring stratification. This would be the case if the density of sea water were a linear function of temperature. However, the relationship between temperature and density is non-linear (Figure 3.1). Raising the temperature of water decreases its density; for the same change in temperature, the change in density is greater for warmer water than for cooler water. Thus, two well-mixed water columns exposed to the same heating and mixing will stratify at different rates determined by their initial temperature, with the warmer water column stratifying more rapidly. The effect of initial temperature on stratification, which will be referred to as "nonlinear stratification," is based on well-established properties of water; however, the magnitude of nonlinear stratification and its influence on the spring bloom in the temperate ocean has not been investigated. This study uses a one-dimensional physical-biological model to address the potential effect of nonlinear stratification on the development of the spring bloom.

3.2 Methods

A series of numerical simulations were conducted using a simple phytoplankton model coupled to NubbleTS, a one-dimensional mixing model. Rather than attempt to reproduce the dynamics of a specific spring, the goal of this study was to

explore a range of physical and biological scenarios to identify the conditions under which nonlinear stratification is likely to have an impact on the development of the spring bloom.

3.2.1 The Physical Model: NubbleTS

NubbleTS is based on a mixing model, Nubble, which solves for the vertical distribution of density, horizontal velocity, turbulent kinetic energy, and mixing length, as well as diffusivities for mass and momentum using linear finite elements (Naimie, 1996; Lynch et al., 1995). The model uses the Mellor-Yamada level 2.5 turbulence closure scheme to compute the turbulent quantities and diffusivities for mass and momentum (Mellor and Yamada, 1982; Galperin et al., 1988; Blumberg et al., 1992). The model is forced at the surface by wind stress and heat flux.

Two key modifications were made to Nubble that allow NubbleTS to treat spring stratification in a more realistic manner. First, NubbleTS was modified to track the distribution of temperature and salinity and then compute density using the UNESCO equation of state (UNESCO, 1981). Second, the model was modified so that heat is added to the water column using a new scheme which permits incoming heat to penetrate into the water column. Shortwave radiation is the main source of incoming heat to the ocean, and it can penetrate many meters below the surface (Mann and Lazier, 1996); thus, heating only at the surface is physically incorrect and produces unrealistic temperature profiles. Heating due to shortwave radiation is represented in NubbleTS through a time-varying source

term, $S(t,z)$, added to the equation for the distribution of temperature:

$$\frac{\partial T}{\partial t} = \frac{\partial}{\partial z}(\kappa \frac{\partial T}{\partial z}) + q(t,z). \tag{3.2}$$

In idealized conditions, the energy reaching a specific depth declines exponentially from the surface at a constant attenuation rate. In reality, the attenuation rate varies with depth due to the distribution of pigments in the water; therefore, the energy q at depth z is determined by the radiation at the surface, q_0, and the radiation absorbed or reflected ($\widehat{\alpha}$), integrated from z to the surface:

$$q(t,z) = q_0(t) e^{\int_z^0 \widehat{\alpha}(s) ds}. \tag{3.3}$$

The value of $q_0(t)$ was chosen in the simulations so that the integral of q over the water column was equal to $Q(t)$, the desired net heat flux. Because heat loss occurs primarily in the top few centimeters through evaporation, infrared radiation, and conduction, the original surface boundary conditions were used whenever the prescribed heat flux was negative.

In addition to the energy absorbed directly by the water, radiation is absorbed by particles in the water, including phytoplankton. The optical qualities of the water can be modeled by partitioning the absorption into two components, one due to the non-biological properties of the water (including inorganic particles) and another due to phytoplankton (Kirk, 1994). The two components are related by a linear equation:

$$\widehat{\alpha}(z) = \alpha + \alpha_\lambda P(t,z) \tag{3.4}$$

where α is the absorption due to the non-biological properties, α_λ is the absorption by a milligram of chlorophyll, and P is the abundance of phytoplankton expressed as chlorophyll concentration. All simulations used a constant $\alpha_\lambda = 0.016$ m^2 mg Chl^{-1}, a typical value for phytoplankton in oceanic and coastal waters (Kirk, 1994).

3.2.2 The Biological Model

A photosynthesis model based on McGillicuddy et al. (1995) was used to simulate phytoplankton dynamics. The model is a simple reaction-diffusion equation:

$$\frac{\partial P}{\partial t} = (r(L) - m)P + \frac{\partial}{\partial t}(\kappa \frac{\partial P}{\partial z}) \tag{3.5}$$

where m is a constant loss rate and κ is the same vector of diffusion coefficients used in the equation for temperature (Equation 3.2). The term r is the growth rate, and it depends only on light L according to the formula:

$$r(L) = P_{\max}(1 - e^{-p_1 L(z,t)/P_{\max}}) \tag{3.6}$$

where $P_{\max}$ is the maximum photosynthetic rate and p_1 is the initial slope of the response of photosynthesis to light (Platt et al., 1980). As with heat, the vertical distribution of light, I decays with depth according to an exponential function:

$$I(z,t) = I_0(t) e^{\int_z^0 \widehat{\alpha}(s) ds} \tag{3.7}$$

where $I_0(t)$ is the incident radiation at the surface. The biological model was solved numerically using the same procedures employed in the physical model (Naimie, 1996). The model diliberately ignores the direct effect of temperature on phyto-

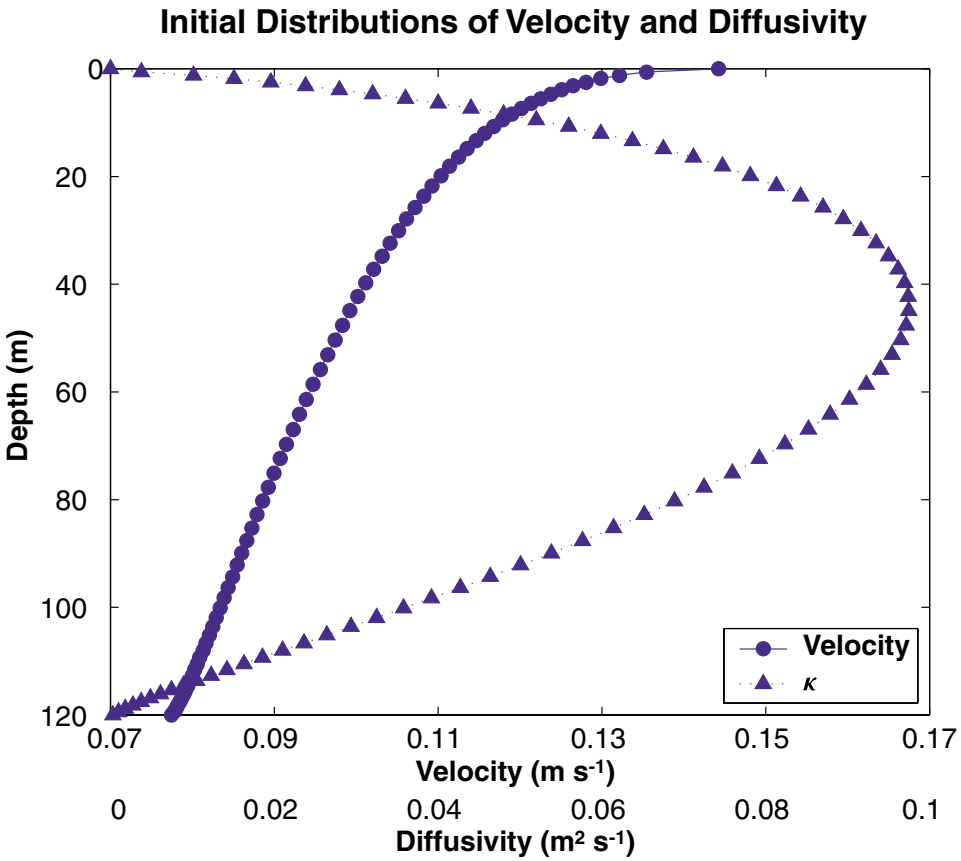

Figure 3.2: Vertical distribution of velocity and eddy diffusivity (κ) after the initialization period.

plankton growth in order to examine only the effect of temperature through nonlinear stratification.

3.2.3 Initialization

To facilitate the simulations, 6 initial condition files were created, each with a different temperature distribution. To create the initial condition files, the model was initialized with the velocity equal to zero, the turbulent quantities set to their minimum (nonzero) values, and a uniform temperature distribution with a unique initial

value. Six temperatures where chosen: 0, 1, 2, 3, 4, and 5° C. Using a time step of 120 seconds, the physical model was run for an initialization period of 4000 iterations with no heat flux. Over the first 1000 iterations, the wind stress was ramped linearly from zero to 0.08 pascal, a value typical of the Northwest Atlantic during early spring (Isemer and Hasse, 1987). Beyond the ramp-up period, the wind-stress value was held constant. The initialization period allowed the distribution of turbulence and momentum to equilibrate (Figure 3.2). All runs used a vertical mesh with 72 nodes and a maximum depth of 120 m. The distance between nodes was smallest near the surface and bottom.

3.2.4 The Simulations

The main goal of this study was to examine the potential for nonlinear stratification to account for interannual variability in the spring phytoplankton bloom. The simulations compared the development of stratification and the spring bloom across a range of surface forcing and parameter values centered on conditions in the Northwest Atlantic, a region where variations in intermediate waters are especially strong (Petrie and Drinkwater, 1993, ; Chapter 2) . Two sets of simulations, called "Physics" and "Biology", were conducted to explore the effects of the physical and biological forcings and parameters.

For each experimental treatment, 6 runs were performed, each starting from a unique initial condition file. The stratification and phytoplankton dynamics were simulated for 47 days starting from March 19 using a time step of 2 s. During this

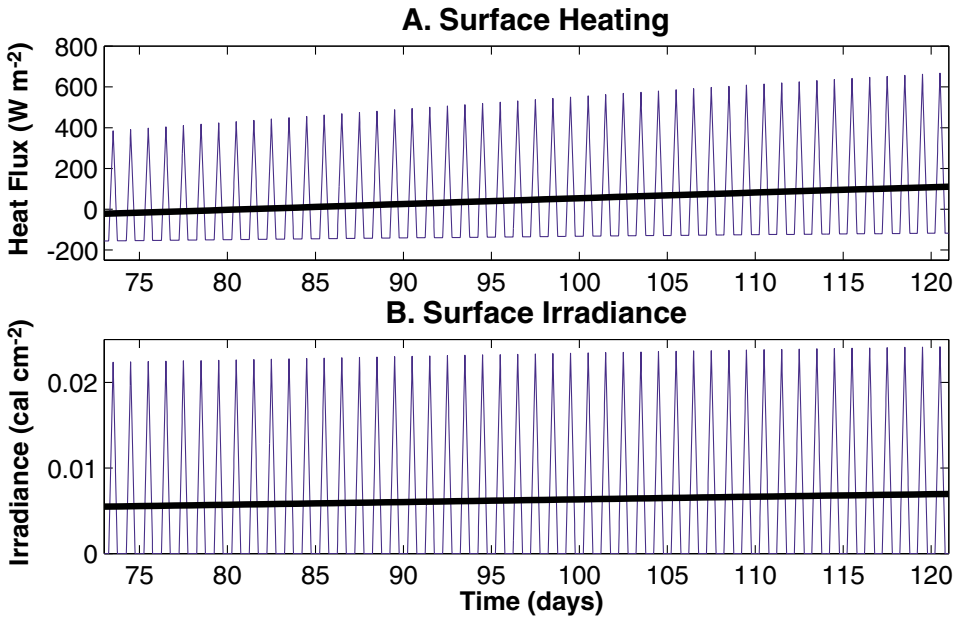

Figure 3.3: Forcing functions for (a) heat flux and (b) surface irradiance. The heavy line tracks the daily mean value.

time, the model was forced by a diurnal heating and cooling cycle (Figure 3.3 A) and a diurnal light cycle (Figure 3.3 B). The diurnal cycles were computed assuming that light or heat input increased linearly starting at sunrise, reached a maximum m for that day at noon, and then decreased linearly at sunset. The heat flux and light values for each night were held constant at l. Daylength was calculated according to Kirk (1994) for a latitude of 40° N. The daily minima and maxima varied sinusoidally throughout the year with the lowest values ($l_{\min}$ and $m_{\min}$) occurring at the winter solstice and the largest values ($l_{\max}$ and $m_{\max}$) occurring at the summer solstice. For heat flux, the solstice values were

$$l_{\min} = \text{-200 Wm}^{-2}, \quad m_{\min} = 50 \text{ Wm}^{-2}$$

$$l_{\max} = \text{-100 Wm}^{-2}, \quad m_{\max} = 800 \text{ Wm}^{-2}$$

which lead to net heat fluxes of 0 and 80 Wm^{-2} on days 82 and 110, consistent

with values for the Northwest Atlantic from the Bunker climatology (Isemer and Hasse, 1987) and similar to the values found by Mountain et al. (1996) for the Gulf of Maine.

Surface irradiance values (I_0) for the light function used in the photosynthesis model were computed using the same diurnally and seasonally varying function used to compute the net heat flux. The solstice values for the function were

$$l_{\min} = 0 \text{ cal cm}^{-2}, \quad m_{\min} = 0.0202 \text{ cal cm}^{-2}$$

$$l_{\max} = 0 \text{ cal cm}^{-2}, \quad m_{\max} = 0.0250 \text{ cal cm}^{-2}$$

The initial phytoplankton populations were vertically homogenous with the concentration equal to 0.2 mg Chl m^{-3}. The values of temperature, density, and phytoplankton concentration as well as the turbulent diffusivities at each node were recorded 5 times per day. Prior to analysis and visualization, the time series of concentrations were first integrated over the entire water column, and then the diurnal cycle was removed using a 5 point running-mean filter.

Physics Simulations

The Physics Simulations tested the effect of the most variable physical processes: the surface wind stress and the optical properties of the water column. These processes influence phytoplankton growth and the spring bloom by controlling the rate at which the pycnoclines shoals and when it crosses the critical depth. Five different wind-stress time series were used during the main simulations (Figure 3.4). The series were computed using hourly observations of wind speed taken from NOAA

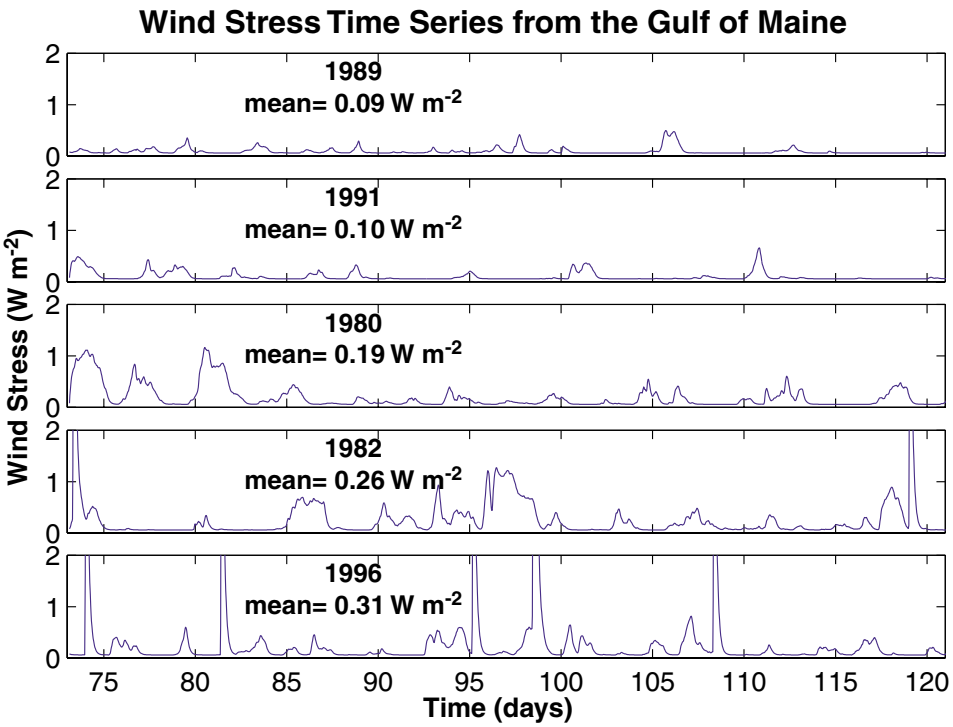

Figure 3.4: Time series of wind stress computed from wind speed measurements taken from NOAA Buoy 44005 in the Gulf of Maine. Data from the 5 springs with the most complete time series were used. The mean of each series during the simulation is printed below the year.

Buoy 44005[1] located in the Gulf of Maine at 42.9° N and 68.94° W . The five time series (1989, 1991, 1980, 1982, and 1996 in order of increasing mean wind speed) were selected to cover a range of mean wind speeds. The observations of wind speed (v) were converted to wind stress (τ) using the quadratic drag formula:

$$\tau = C_D(v)\rho_a v^2 \tag{3.8}$$

where

$$C_D = 0.0015(1 + e^{(12.5-v)/1.56})^{-1} + 0.00104 \tag{3.9}$$

[1]available from `http://seaboard.ndbc.noaa.gov`

and the density of air, ρ_a is equal to 1.2 kg m^{-3} (Gill, 1982). The wind-stress value at any iteration j during the simulation was determined by changing the previous value by a small fraction of the difference between the actual value and the previous value, e.g.

$$\tau_j = \tau_{j-1} + 0.0002(\tau_{\text{actual}} - \tau_{j-1}) \tag{3.10}$$

The actual values were calculated by linearly interpolating the buoy time series. This scheme allows the wind stress to increase smoothly from the value used during the initialization and also produces a slightly smoother time series. Additionally, the values of τ were forced to be ≥ 0.06 pascal. This minimum value provided a background level of mixing necessary to avoid numerical instability in the Mellor-Yamada scheme.

Four values of the attenuation coefficient α were tested using each of the five wind-stress series. The attenuation coefficients were 0.02, 0.04, 0.08, and 0.16 m^{-1}, and are representative of optical conditions found in oceanic and coastal waters (Kirk, 1994; Townsend et al., 1994). Increasing α decreases the total light in the system and reduces phytoplankton growth. In order to test only the physical effect of α, a different mortality rate m was used for each value of α (0.188, 0.171, 0.107, and 0.016 mg Chl m^{-3} day^{-2}, respectively). The mortality rates were chosen to produce a phytoplankton bloom near day 105 using the third wind-stress time series. The two parameters that determine phytoplankton growth were set to the same values used by McGillicuddy et al. (1995):

$$P_{\max} = 0.66 \text{ mg Chl m}^{-3} \text{ day}^{-1},\ p_1 = 0.0019 \text{ cal cm}^{-2}.$$

Table 3.1: Summary of the treatments in the two sets of simulations.

Simulation Name	Description
Physics	Combinations of the 5 wind series and α equal to 0.02, 0.04, 0.08, 0.16. A mortality rate was chosen for each α to produce a bloom near day 105 (0.188, 0.171, 0.107, and 0.016 respectively). $P_{\max}$ and p_1 were taken from McGillicuddy et al. (1995) (0.66 mg Chl m^{-3} day^{-1} and 0.0019 cal cm^{-2}, respectively.
Biology	Combinations of m and $P_{\max}$ equal to 0.5, 1, and 2 times their standard values (0.66 and 0.107 mg Chl m^{-3} day^{-1}, respectively). The 1980 wind-stress time series was used.

3.2.5 Biology Simulations

The Biology Simulations examined the influence of the two main biological parameters: the mortality rate m and the maximum photosynthetic rate $P_{\max}$. The physics settings for these runs were taken from the middle-range of the Physics Simulations: α =0.08 and wind stress from 1980 (Wind 3). The mortality and photosynthetic rates were either double, half, or the same as the rates used in the corresponding Physics treatment ($P_{\max}$ =0.66 and m=0.107 mg Chl m^{-3} day^{-1}). The values of these rates determine the critical depth, with increased growth or decreased mortality leading to deeper critical depths. Table 3.1 summarizes the treatments for both the Physics and Biology Simulations.

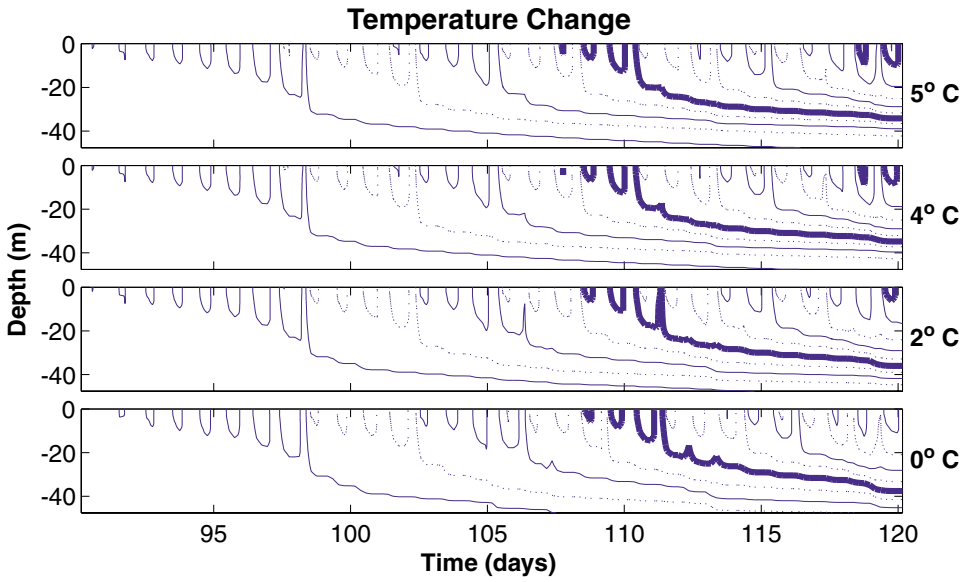

Figure 3.5: Contours of temperature relative to the initial temperature for the 0, 2, 4, and 5° C runs in Physics treatment with α =0.08 and using Wind 3. The contour interval is 0.1° and the minimum contour is 0.1°. The 0.5 and 1° contours are highlighted.

3.3 Results

The surface forcing used in the simulations caused all water columns to stratify; however, the experimental treatment and initial temperature had a significant influence on the development of stratification. The patterns in the temperature fields using the third wind-stress series (1980) with α equal to 0.08 exhibit the general patterns seen in the other treatments. A strong diurnal cycle was present for all initial temperatures with thermoclines shoaling during the day and sinking or disappearing completely at night (Figure 3.5); however, a permanent thermocline appeared by day 98. The thermoclines in the colder simulations were always deeper than those from warmer runs, although the difference was small. The effect of initial temperature is most obvious when a contour meets the surface. At the start of day 111, the

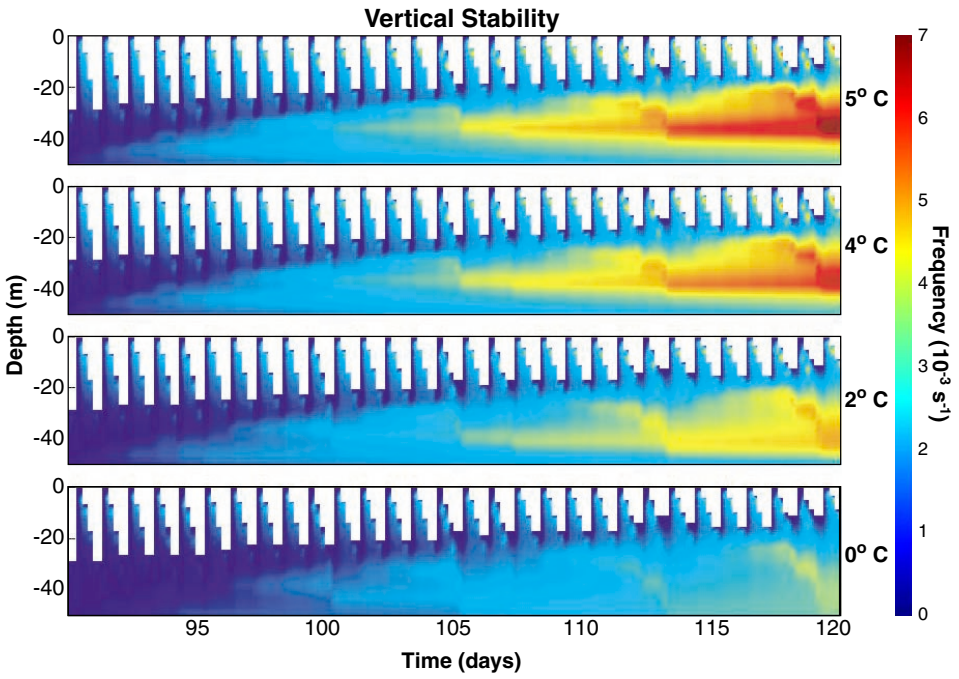

Figure 3.6: Distribution of the Brunt-Väisälä frequency which is a measure of a water column's ability to resist vertical mixing. White indicates an unstable water column.

0.5° contours (bold) from the 2° and 0° runs reach the surface , while the contours from the two warmest runs remain near 20 m.

Although the effect of nonlinear stratification is difficult to see when viewed as temperature change, nonlinear stratification has a significant effect on the stability of the water column. The static stability of a water column is determined by the vertical density gradient. Large density gradients such as those appearing around a strong thermocline provide a barrier to vertical mixing and water movement. A standard measure of water column stability is the Brunt-Väisälä frequency defined as the frequency that a parcel of water would move up and down if displaced from its equilibrium depth (Pond and Pickard, 1983; Mann and Lazier, 1996). Quantitatively,

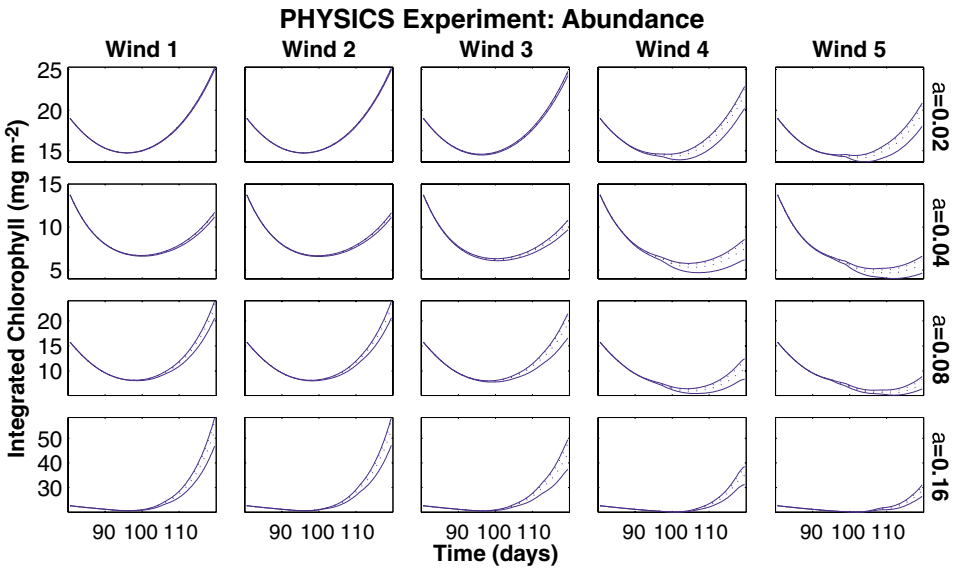

Figure 3.7: The development of populations starting in 0, 2, 4, and 5° C water for the Physics Simulations. The simulations were forced by the 5 wind-stress series (columns) and used 4 different values of α (rows). The abundance of the 0 and 5° C populations are plotted as solid lines, the 2 and 4° populations are plotted as dashed lines. In all observations the abundance increased with temperature.

the Brunt-Väisälä frequency is a function of the density gradient:

$$N = (\frac{g}{\rho}\frac{\partial \rho}{\partial z})^{-\frac{1}{2}} \tag{3.11}$$

with larger density gradients (more stable water columns) producing higher frequencies. Both the diurnal and permanent thermoclines were regions of high stability as indicated by the high Brunt-Väisälä frequencies (Figure 3.6). The stability of each water column increased throughout the simulation, but the increase was largest for the warmer water columns.

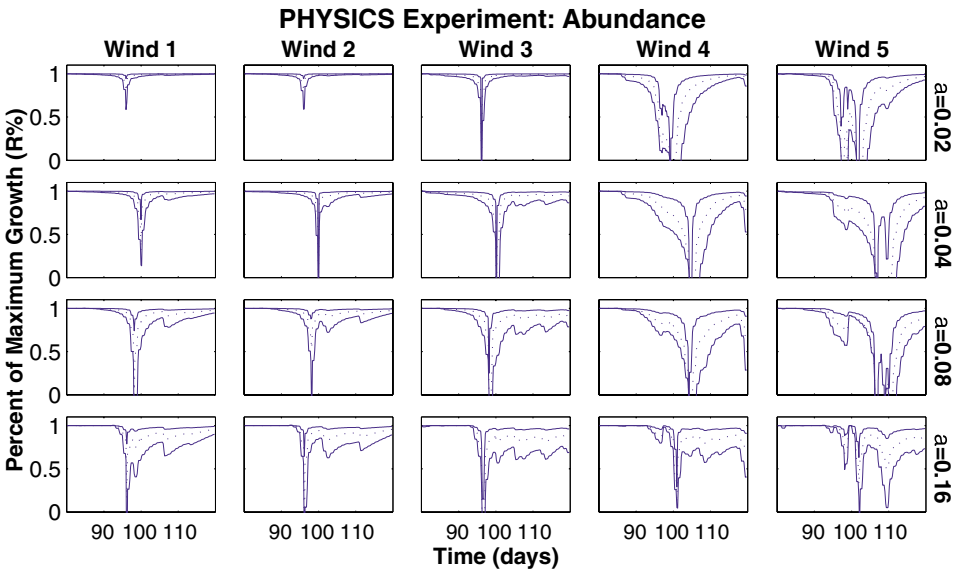

Figure 3.8: The growth rates of the 0, 2, and 4° populations for the Physics Simulations expressed as a percent of the maximum (5°) rate. The runs are arranged as in Figure 3.7. The growth rates of the 0 and 4° C populations are plotted as solid lines, the 2° population is plotted as a dashed line. In all observations the relative growth rate increased with temperature.

3.3.1 Physics Simulations

In all populations from the Physics Simulations, a period of rapidly increasing growth, the spring bloom, followed an initial decline in abundance (Figure 3.7); however, there was considerable variation in the population dynamics due to both wind forcing and optical properties. The three calmest years had large blooms which started around day 98, while the blooms were delayed several days and were weaker during the two windiest years. Within each year, the initial temperature had a noticeable effect on the populations. In all treatments, the largest populations were found in the warmest waters, but the difference between the coldest and warmest waters increased with the mean wind stress.

The influence of nonlinear stratification on phytoplankton dynamics is more apparent when viewed in terms of net growth rate (i.e. $r(L) - m$ in Equation 3.5). The growth rates were obtained by differencing the smoothed population time series and dividing by the population size and sampling interval. The growth rate for each initial temperature (R) were then normalized relative to the growth rate from the 5° population, using the formula:

$$R\% = 1 - \frac{R_{5^\circ} - R_j}{\max(|R_j|, |R_{5^\circ}|)}. \tag{3.12}$$

$R\%$ provides a uniform measure of the effect of nonlinear stratification on phytoplankton growth across all situations encountered. During typical conditions when the growth rates from populations starting in different initial temperatures are either all positive or all negative, the percent of the maximum growth rate ($R\%$) will be between 0 and 1. The reduction in growth rate is largest around the bloom period when growth rates shift from negative to positive (Figure 3.8). At the time of the bloom, the difference between R_{5° and the growth rate in cooler water is large relative to the maximum rate, and $R\%$ is negative. For years with little wind, the bloom appears as a sharp downward spike in the $R\%$ values, and there is only a slight reduction in growth rates after the bloom. Compared with calm years, the growth rates in windy years of the warm and cold populations separate several days before the bloom, and the difference persists longer after the bloom. Averaging the $R\%$ values over the last 30 days supports these conclusions: growth rates in the 4° populations were 95-99% of the 5° growth rates in the calmest years but only 80-90% in the windiest (Table 3.2). Independent of the treatment used, the growth

Table 3.2: Mean reduction in post-bloom growth rates relative to the 5° run ($R\%$) after day 90.

	$\alpha = 0.02$			$\alpha = 0.04$		
Wind Series	0°	2°	4°	0°	2°	4°
1	0.969	0.988	0.997	0.900	0.960	0.989
2	0.969	0.988	0.997	0.909	0.959	0.978
3	0.932	0.968	0.983	0.808	0.915	0.968
4	0.592	0.747	0.895	0.549	0.74	0.893
5	0.511	0.677	0.878	0.450	0.623	0.856
	$\alpha = 0.08$			$\alpha = 0.016$		
Wind Series	0°	2°	4°	0°	2°	4°
1	0.809	0.922	0.981	0.755	0.894	0.973
2	0.842	0.938	0.984	0.782	0.901	0.975
3	0.712	0.872	0.965	0.686	0.834	0.946
4	0.568	0.738	0.903	0.729	0.862	0.955
5	0.519	0.616	0.794	0.691	0.841	0.951

rates declined more rapidly for each 2° change at the coldest temperatures.

The attenuation coefficient also altered the effect that nonlinear stratification had on the spring bloom. Increasing α (and decreasing m) increased the difference in populations grown in the warmest and coldest waters. The relative growth rates show a similar pattern with initial temperature generally having a larger effect in waters with higher attenuation values (Figure 3.8). The two windiest years are the exception to this pattern. In these years, the relative growth rates declined when α was increased from 0.02 to 0.04, but the rates increased between 0.04 and 0.08 and between 0.08 and 0.16 (Table 3.2).

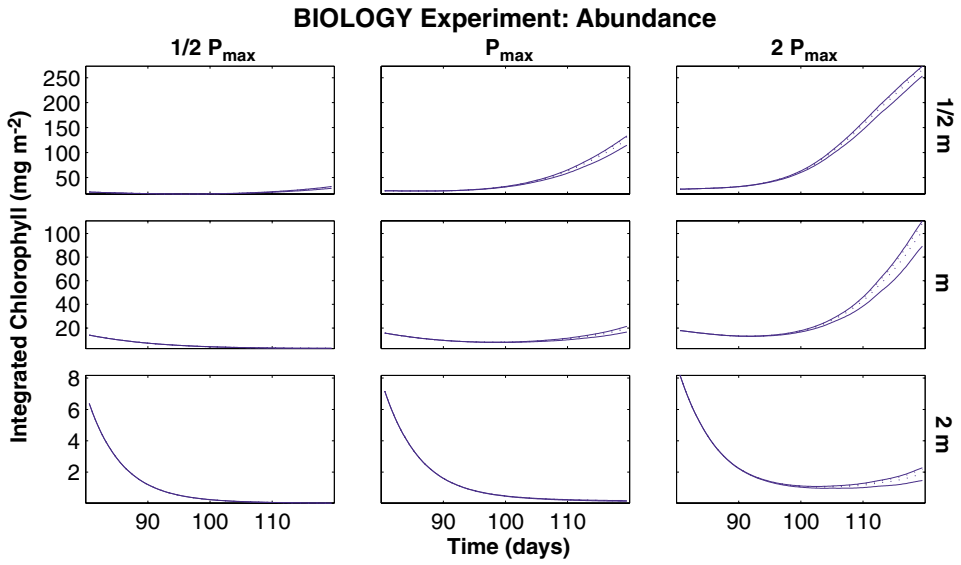

Figure 3.9: The development of populations starting in 0, 2, 4, and 5° C water for the Biology Simulations. The runs used combinations of $P_{\max}$ (columns) and m (rows) with their values either half , twice, or equal to the climatological values. The abundance of the 0 and 5° C populations are plotted as solid lines, the 2 and 4° populations are plotted as dashed lines. In all observations the abundance increased with temperature.

Biology Simulations

The population time series from the Biology Simulations (Figure 3.9) fall into three categories: those with negative growth throughout the run (low $P_{\max}$ and high mortality), those with positive growth throughout (high $P_{\max}$ and low mortality), and "normal" series with negative growth followed by a bloom ($P_{\max}$ and mortality reduced or increased by the same amount). The series with normal population dynamics occurred when $P_{\max}$ and m changed together (plots along the main diagonal in Figure 3.10). These treatment had relative growth patterns similar to those in the Physics Simulations, and the reduction in growth rates in cooler temperatures was nearly always greater in these treatments than in the others (Table 3.3). The only

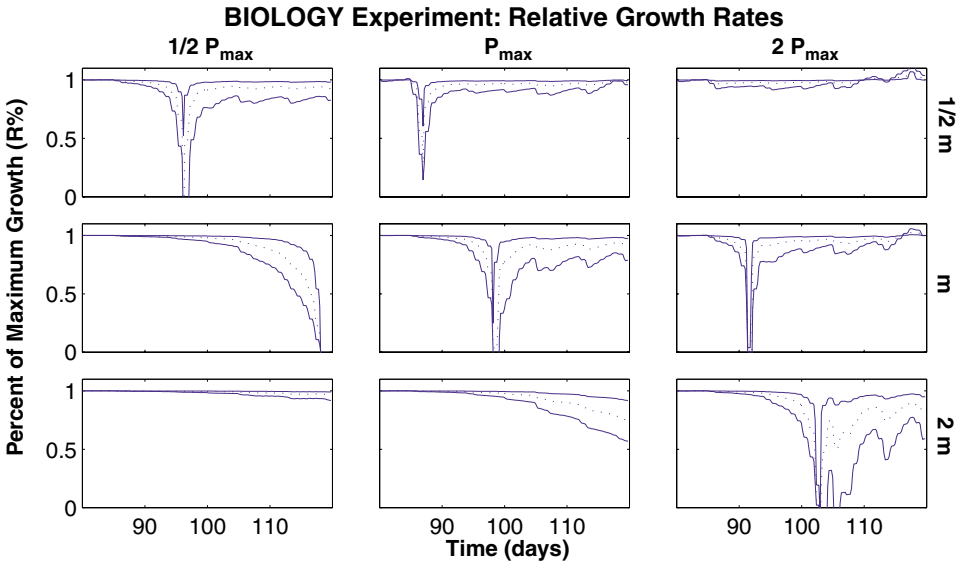

Figure 3.10: The growth rates of the 0, 2, and 4° populations for the Biology Simulations expressed as a percent of the maximum (5°) rate. The runs are arranged as in Figure 3.9. The growth rates of the 0 and 4° C populations are plotted as solid lines, the 2° population is plotted as a dashed line. For most observations, the relative growth rate increased with temperature.

exception is the treatment with m set to the climatological value and $P_{\max}$ reduced by one half. The populations under this treatment experienced a slight bloom at the end of the run that is not visible in Figure 3.9, and this treatment should be classified as normal.

The treatments with negative growth throughout (plots in lower-left portion of Figure 3.10) have growth-rate patterns similar to the pre-bloom period from treatments with normal dynamics. The mean reduction in the growth rate for the non-blooming treatments is high, relative to the normal treatments; however, this comparison does not reflect the true difference between these categories. If the runs were continued, the non-blooming treatments would exhibit normal dynamics, only spread over a longer time.

Table 3.3: Mean reduction in post-bloom growth rates relative to the 5° run ($R\%$) after day 90.

	$1/2P_{\max}$			$P_{\max}$			$2P_{\max}$		
m	0°	2°	4°	0°	2°	4°	0°	2°	4°
1/2	0.763	0.895	0.974	0.914	0.966	0.992	0.977	0.993	1.00
1	0.741	0.811	0.892	0.712	0.872	0.965	0.848	0.922	0.966
2	0.967	0.987	0.997	0.837	0.919	0.977	0.569	0.799	0.931

The three treatments with positive growth throughout exhibit a pattern not found in the previous simulations. At the end of these runs, the growth rates for the cold water are greater than those in the warm waters. This effect shows up as $R\%$ values greater than one, and results from self-shading—a density-dependent process where the phytoplankton concentrations in the surface waters significantly reduce the penetration of light through the water column and reduce the growth rate of the population.

3.4 Discussion

The investigation described above demonstrate that nonlinear stratification may be an important source of variability in the dynamics of the spring bloom. However, the magnitude of the effect depends critically on the biological rates and physical processes. Any process that decreases phytoplankton growth rates will magnify the effect of nonlinear stratification; thus, increasing the mortality rate, decreasing the photosynthetic rate, or slowing down the development of stratification will lead to a

greater difference between populations grown in warm versus cold conditions. These results can be understood in light of Sverdrup's critical depth theory (Sverdrup, 1953). The critical depth in the model is determined by the biological parameters and the distribution of light. The physical parameters and forcings and the initial temperature then determined how stratification develops.

The initial temperature had a subtle effect on the position of the thermocline. Assuming, as Sverdrup did, that mixing was constant above the thermocline, we would expect to see only a slight influence of initial temperature on the phytoplankton populations. However, mixing is not constant in the real world or in NUBBLETS. Because of the nonlinear relationship between temperature and density, small changes in temperature can have a large impact on density. Therefore, the water-column stability is a better indicator of the depth and strength of mixing than is the temperature change. At any point in time, even if the thermoclines are at nearly the same depth, the lower Brunt-Väisälä frequencies associated with colder water columns indicate that the corresponding populations are mixed more thoroughly(Figure 3.6).

Comparing two treatments with the same physics but with different critical depths, the effect of nonlinear stratification on the bloom is smaller in the treatment with the deeper critical depth. A deep critical depth means that the thermocline passes through this depth earlier in the year. Because the rate at which the thermocline shoals is greatest at the start of the simulation, the thermocline moves rapidly across the critical depth. Thus, under these conditions, a population's growth rate

shifts rapidly from negative to positive, allowing populations in cold water to catch up quickly to warmer populations. However, if the critical depth is shallow, the thermocline reaches this depth later in the year and lingers around it. Populations in these conditions have a prolonged period of near-zero growth that exaggerates the differences between warm and cold populations.

This explanation can account for the differences seen in the simulations above. Increasing the wind stress slows stratification and increases the separation in time between when warm and cold water columns reach the critical depth. The effect of changing α is more difficult to interpret. Increasing α keeps more of the incoming heat near the surface; thus, the water warms faster and a shallower thermocline develops. Increasing either of the growth terms or decreasing the loss term moves the critical depth deeper, diminishing the impact of nonlinear stratification.

3.4.1 Modelling Issues

This study has established that initial water column temperature may be an important source of interannual variability in the spring bloom. However, it is impossible to include all physical and biological processes in a single model, so it is necessary to consider the impact of the model assumptions on the results.

The biological model's most obvious shortcoming is that the growth rate is determined only by light. The importance of nutrient limitation as a controlling factor for phytoplankton populations is well established. Since reduced vertical structure in winter is a prerequisite for a spring bloom, regions where a bloom occurs will

also have increased concentrations of nutrients in the surface waters due to the winter mixing. For this reason, nutrient limitation likely plays a small role during the spring bloom period. After the bloom period, nutrient limitation becomes more important, and the decreased stability of cold water columns may allow a greater flux of nutrients into the mixed layer, reducing the effect of nonlinear stratification in the late spring and summer.

This study addressed the influence of temperature on stratification, but did not examine the direct effect that temperature has on phytoplankton biology. Photosynthesis rates rates can increase with higher temperatures (reviewed in Kirk (1994)), and the effect is due mostly to increases in saturating light levels–analogous to raising $P_{\max}$. This process would enhance the differences between the population dynamics in warm and cold water, although herbivore growth and grazing rates are also temperature dependent and may compensate for any increase in phytoplankton growth.

A standard assumption made by NUBBLETS and most circulation models (Blumberg and Mellor, 1987; Haidvogel et al., 1991; Lynch and Werner, 1991) is that the water column is in hydrostatic equilibrium. At the scales considered in most oceanographic studies, this assumption is valid; however, the assumption precludes several processes that may be important in the development of spring stratification. In particular, the hydrostatic assumption eliminates internal and surface gravity waves. These processes may be an important source of vertical mixing; however, there is no reason to expect that their effects should counteract nonlinear stratification.

Table 3.4: Mean reduction in post-bloom growth rates after day 90 for the treatments using Wind 2-4 and with α =0.08 from the Physics Simulations. The reduction is relative to the 5° run from Wind 2.

	Wind File		
Temp.	2	3	4
5°	1.000	0.888	0.244
4°	0.984	0.862	0.217
3°	0.964	0.829	0.188
2°	0.938	0.786	0.168
1°	0.900	0.731	0.141
0°	0.842	0.646	0.105

3.4.2 Nonlinear Stratification and Real Ecosystems

Results from these simulations suggest that nonlinear stratification could be an important process influencing the dynamics of the spring bloom, but it is necessary to put the results into the context of other sources of variability in the spring bloom. Wind forcing has received the most attention as a source of variability in the spring bloom (Dickson et al., 1988). Given the influence of wind mixing on the timing of the spring bloom, it is useful to compare the reduction in growth caused by colder conditions to the changes due to wind variations. Wind series 2, 3, and 4 encompass a range of wind forcing. Using the populations from the Physics Simulations with α =0.08, it is possible to compare the effect of nonlinear stratification to that of the wind. To accomplish this, the reduction in growth rate was computed as a percentage of the rate from the Wind 2, 5° treatment (Table 3.4); i.e., the R%

Table 3.5: Percent of the growth-rate reduction from Table 3.4 due to the temperature change.

	Wind File		
Temp.	2	3	4
5°	0	0	0
4°	1.000	0.188	0.035
3°	1.000	0.345	0.069
2°	1.000	0.477	0.091
1°	1.000	0.584	0.120
0°	1.000	0.684	0.155

values relative to this run rather than the 5° run for each wind treatment.

Taking the difference in the percent reduction between each run and the corresponding 5° run and dividing by the total change (1 minus the values in Table 3.4) gives the proportion of the change in the growth rate due to the temperature change (Table 3.5). There is only a slight difference between the second and third wind time series, so a large portion of the difference between these treatments was due to the temperature change, 33% for a 2° change, 47% for a 3° change. The mean wind stress in Wind 4 is more than double that of Wind 2, and the calculations suggest that a smaller proportion of the growth rate reduction was due to temperature. However, the blooms in the Wind 4 treatments were delayed considerably, so the post-bloom period, when nonlinear stratification has its strongest effect, was not simulated. Therefore, the values in Tables (3.4 and 3.5) underestimate the effect of temperature.

Comparing one year to another, the differences in the wind forcing and light field will be the main sources of variability in the spring bloom; however, if anomalous temperature conditions persist for several years, the variability in wind and light will likely average out, leaving only the effects of nonlinear stratification. As discussed in Chapter 2, the waters along the Northwest Atlantic Shelf fluctuate between warm and cold states, with the system often remaining in the same state for several years. Sutton and Allen (1997) followed sea surface temperature anomalies circulating around the North Atlantic. These anomalies persisted for many years, providing another situation where nonlinear stratification may be a factor. These patterns and the decadal changes in the Gulf of Maine are situations where nonlinear stratification could play an important role in the long-term trends in spring bloom patterns. The large spatial extent of the sea surface temperature anomalies described by Sutton and Allen (1997) and of the Coupled Slope Water System in the Northwest Atlantic (Chapter 2) will also damp out atmospheric variability and enhance the effect of nonlinear stratification.

3.5 Conclusion

The results presented above suggest that nonlinear stratification may be an important mechanism accounting for variability in the spring bloom, especially on a decadal scale. Observations from real oceans will be required to conclusively establish the importance of nonlinear stratification, and this study provides some guidance for identifying regions where nonlinear stratification may play a significant

role. The effect of nonlinear stratification on the spring bloom is small relative to the magnitude of other processes leading to variations in the bloom; however, it is a persistent process, and its influence may be particularly strong on large spatial or temporal scales.

3.6 References

Blumberg, A. F., Galperin, B., and O'Connor, D. J. (1992). Modeling the vertical structure of open-channel flows. *J. Hydraulic Engin.*, 11:1119–1134.

Blumberg, A. F. and Mellor, G. L. (1987). A description of a three-dimensional coastal ocean circulation model. In Heaps, N., editor, *Three-dimensional coastal ocean models*. American Geophysical Union.

Curry, R. G., McCartney, M. S., and Joyce, T. M. (1998). Oceanic transport of subpolar climate signals to mid-depth subtropical waters. *Nature*, 388:575–577.

Dickson, R. (1997). From the Labrador Sea to global change. *Nature*, 386:649–650.

Dickson, R., Lazier, J., Meincke, J., Rhines, P., and Swift, J. (1996). Long-term coordinated changes in the convective activity of the North Atlantic. *Prog. Oceanog.*, 38:241–295.

Dickson, R. R., Kelly, P. M., Colebrook, J. M., Wooster, W. S., and Cushing, D. H. (1988). North winds and production in the eastern North Atlantic. *Journal of Plankton Research*, 10:151–169.

Galperin, B., Kantha, L. H., Hassid, S., and Rosati, A. (1988). A quasi-equilibrium turbulent energy model for geophysical flows. *J. Atmos. Sci.*, 45:55–62.

Gill, A. E. (1982). *Atomsphere-ocean dynamics*, volume 30 of *International Geophysics Series*. Academic Press.

Gran, H. H. and Braarud, T. (1935). A quantitative study of the phytoplankton on the Bay of Fundy and the Gulf of Maine (including obsevations on hydrography, chemistry and turbidity). *Journal of the Biological Board of Canada*, 1:279–433.

Haidvogel, D. B., Wilkin, J. L., and Young, R. (1991). A semi-spectral primitive equation ocean circulation model using vertical sigma and orthogonal curvilinear horizontal coordinates. *J. Comput. Phys.*, 94:151–185.

Isemer, H. J. and Hasse, L. (1987). *The Bunker Climate Atlas of the North Atlantic Ocean, Vol 2: Air-sea Interactions*. Springer-Verlag.

Kirk, J. T. O. (1994). *Light and Photosynthesis in Aquatic Ecosystems*. Cambridge University Press.

Lynch, D. R., Ip, J. T. C., Naimie, C. E., and Werner, F. E. (1995). Convergence studies of tidally-rectified circulation on Georges Bank. In Lynch, D. R. and Davies, A. M., editors, *Quantitative Skill Assessment for Coastal Ocean Models*, number 48 in Coastal and Estuarine Series, pages 153–174. American Geophysical Union.

Lynch, D. R. and Werner, F. E. (1991). Three-dimensional hydrodynamics on finite elements, part ii: Nonlinear time-stepping model. *Int. J. Numerical Methods in Fluids*, 12:851–875.

Mann, K. and Lazier, J. (1996). *Dynamics of Marine Ecosystems: Biological-Physical Interactions in the Oceans*. Blackwell Science.

McCartney, M. S. (1997). Is the ocean at the helm? *Nature*, 388:521–522.

McGillicuddy, D. J., McCarthy, J. J., and Robinson, A. R. (1995). Coupled physical and biological modeling of the spring bloom in the North Atlantic (I): model formulation and one-dimensional bloom processes. *Deep-Sea Res. I*, 42:1313–1357.

Mellor, G. L. and Yamada, T. (1982). Development of a turbulence closure model for geophysical fluid problems. *Rev. Geophys. and Space Phys.*, 20:851–875.

Mountain, D., Strout, G. A., and Beardsley, R. C. (1996). Surface heat flux in the Gulf of Maine. *Deep Sea Res. II*, 43:1533–1546.

Naimie, C. E. (1996). A turbulent boundary layer model for the linearized shallow water equations: Nubble User's Manual (Release 1.1). Technical Report NML-96-1, Thayer School of Engineering, Dartmouth College.

Petrie, B. D. and Drinkwater, K. (1993). Temperature and salinity variability on the Scotian Shelf and in the Gulf of Maine 1945-1990. *J. Geophys. Res.*, 98:20079–20089.

Platt, T., Gallegos, C. L., and Harrison, W. G. (1980). Photoinhibition of photosynthesis in natural assemblages of marine phytoplankton. *J. Mar. Res.*, 38:687–701.

Pond, S. and Pickard, G. L. (1983). *Introductory Dynamical Oceanography*. Pergamon Press.

Sutton, R. T. and Allen, M. R. (1997). Decadal predictability of North Atlantic sea surface temperature and climate. *Nature*, 388:563–567.

Sverdrup, H. U. (1953). On conditions for the vernal blooming of phytoplankton. *Journal du Conseil Permanent International pour l'Exploration de la Mer*, 18:287–295.

Townsend, D. W., Cammen, L. M., Holligan, P. M., Cambell, D. E., and Pettigrew, N. R. (1994). Causes and consequences of variability in the timing of spring phytoplankton blooms. *Deep Sea Res. I*, 41:747–765.

UNESCO (1981). Tenth report of the joint panel on oceanographic tables and standards. Technical Report 36, UNESCO.

Chapter 4

Computing Ocean Circulation on Clusters of Workstations

4.1 Introduction

Our understanding of the effect of climate variability on populations is based primarily on correlational studies similar to the one described in Chapter 2. Studies of this kind are useful for associating population fluctuations with physical changes, but they can only suggest mechanisms that might account for the correlations. Testing hypotheses on the scales required by climate studies can only be done through simulation. The large domains and long time-scales required by these studies push the limits of most computer workstations; thus, parallel computers, either commercial supercomputers or clusters of workstations, that can reduce simulation time or allow for increased problem size by dividing the computational load among several computers, will be an important technology for studying population-climate interactions.

Parallelizing a model has traditionally meant running it on an expensive supercomputer. The processors on these systems are linked by a shared-memory system or a special purpose, high-speed network. However, the software required to link low-cost clusters assembled from standard components has been around for some time (Sunderam et al., 1994; Gropp et al., 1996). The last few years have witnessed a dramatic increase in the number of personal computers and the speed of these systems. The high ratio of performance to cost of today's personal computers and workstations means that many research groups can afford to build a dedicated cluster with capabilities rivalling the supercomputers of only a few years ago. The potential of these systems is great enough that some of the supercomputing needs of national labs such as NASA's Goddard Space Flight Center and Sandia National Laboratory are being filled by massively parallel systems built from commodity hardware (Bollinger, 1999; Brightwell et al., 2000). Ocean models will need to exploit the possibilities of these low-cost, high-performance systems, and any program that can achieve good performance on these systems should see equivalent or better performance on supercomputers.

This paper describes the development of MPQUODDY, the parallel implementation of a finite-element model for computing ocean circulation. The development of MPQUODDY illustrates the basic concepts behind parallelizing an ocean circulation model and the considerations necessary to achieve good parallel performance on cluster systems. Like most ideas encountered in computing, these concepts are not specific to ocean models, but are easily generalized to other finite-difference and

finite-element models.

4.2 Ideas, Methods, and Model Development

The equations of motion describe how the state of the ocean changes with time based on its current distribution of mass (temperature and salinity) and momentum and any external forces such as surface heating or wind. To solve these equations on a computer, it is necessary to approximate the continuous fields of ocean properties such as temperature or velocity by a finite number of points. These points, also called *nodes*, are linked with neighboring points to form a *mesh*. Meshes come in two types, structured and unstructured. The distance between the points in a structured mesh is either constant, forming an evenly spaced grid, or determined by a simple function, forming a graded or curvilinear mesh. Structured meshes are the standard discretizations used by finite difference models, and are typically composed of rectangles. The spacing between nodes in an unstructured mesh is not regular; thus, the use of unstructured meshes allows the model to better represent irregular domains such as coastlines and allows increased resolution in areas where the modeled fields change rapidly. Unstructured meshes are used mainly by finite element models and are typically composed of triangles.

A generic mesh, either structured or unstructured, is a set of non-overlapping polygons called elements, each composed of a fixed number of vertices called nodes. For a computer program to perform calculations defined on a mesh, the program needs to know where the nodes are and how they are connected. The node positions

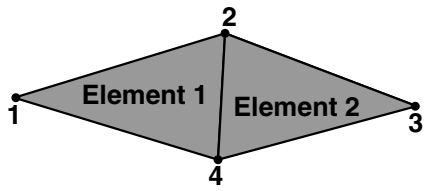

Figure 4.1: A simple unstructured mesh composed of two triangular elements.

and connections in a structured mesh can be easily determined from the simple function defining the mesh; however, programs using unstructured meshes must store the mesh information. There are two common ways to describe an unstructured mesh: element lists and adjacency matrices. A mesh described by an element list uses two data structures representing the set Nod containing the location of the nodes and the set called Ele that specifies which nodes are used to make up each element. Using this notation, a mesh is defined formally as

$$Mesh = (Nod, Ele). \tag{4.1}$$

If the mesh is made of triangles, each entry in Ele will contain three nodes from Nod that make up an element. For the two-element mesh in Figure 4.1, the elements are defined:

	Node		
Element	1	2	3
1	1	2	4
2	2	3	4

(4.2)

An adjacency matrix is an n-by-n matrix of ones and zeros, where n is the number of nodes in the mesh. Each entry (i, j) in the matrix will be 1 if there is a connection between nodes i and j, and zero if there is no connection. For the mesh in Figure

4.1, the adjacency matrix is

$$A = \begin{bmatrix} 0 & 1 & 0 & 1 \\ 1 & 0 & 1 & 1 \\ 0 & 1 & 0 & 1 \\ 1 & 1 & 1 & 0 \end{bmatrix}. \tag{4.3}$$

Adjacency matrices are always symmetric and will generally be sparse (have many more zeros than ones). The main difference between these two descriptions of a mesh is that element lists define the elements explicitly.

4.2.1 The Basic Model

MPQUODDY is the parallel analog of QUODDY, a finite-element circulation model developed by a community of modelers lead by Dan Lynch (Lynch and Werner, 1991; Lynch et al., 1996). The QUODDY algorithm uses finite-elements to solve for the three-dimensional distribution of mass and momentum. QUODDY's use of finite elements and unstructured meshes sets it apart from most other ocean models (Haidvogel et al., 2000), and it has been used chiefly for simulations of the circulation in shelf regions (Naimie, 1996; Loder et al., 2001, e.g.).

QUODDY solves a special form of the equations of motion known as the shallow water equations (Lynch and Werner, 1991). The numerical scheme divides the solution at each time step into two pieces. First the sea-surface elevation is obtained from the wave equation. This is accomplished by solving a finite-element problem over a large mesh representing the horizontal domain. The finite-element formulation leads to a large, spares linear system; however, the matrix, which has the same structure as the mesh's adjacency matrix but with a nonzero diagonal,

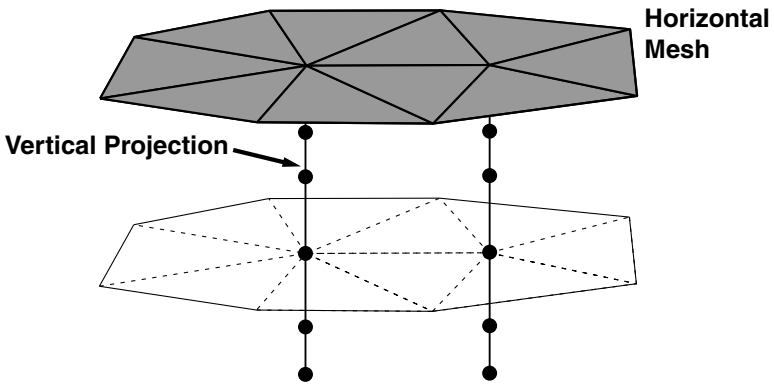

Figure 4.2: A small horizontal mesh showing the vertical projections used by QUODDY.

depends only on the geometry of the domain. Once the sea-surface elevation is found, the distribution of mass, momentum, and turbulent quantities can be computed by solving one-dimensional finite element problems on vertical projections under each horizontal node (Figure 4.2). Thus, the solution is partitioned into one large two-dimensional problem and many small one-dimensional problems, and this partitioning determines how QUODDY is implemented in parallel.

4.2.2 Parallel Programming Considerations

The goal of parallel processing is to divide the computational work among several processors. Ideally, if one has P computer processors available, then it should be possible to run the parallel version of an algorithm P-times faster than on a single processor. However, perfect parallel performance is not possible for most algorithms. Two effects, communication time and load imbalance, will reduce the performance of a parallel algorithm, and the parallel performance of an algorithm depends on

how well these effects are minimized.

If the subproblems being run on each processor are not independent of one another, the processors will have to share data by communicating. If the processors are located on the same computer, they can communicate over the system's shared memory; otherwise, communication must take place over a network. Communication over shared memory is considerably faster than over a network, but both schemes must spend time managing the exchange of data which reduces the performance. As a problem is divided among more and more processors, the amount of data that must be sent between the processors increases; thus, as P increases, the speed of the algorithm will be increasingly worse than P-times the speed of the serial algorithm.

If the amount of work assigned to each processor is not equal, the processor with the smallest job will race ahead over the others. However, when this processor reaches a section of code requiring data from another processor, it will be forced to sit idle, waiting for the other processor to catch up. Idle time results from a load imbalance and reduces the performance of the algorithm.

4.2.3 Parallelization: Domain decomposition

In order to run in parallel, an algorithm must be divided into pieces that can be given to multiple processors. The finite difference and finite element techniques solve partial differential equations by discretizing the computational domain into many small pieces. The numerical analog to the PDE is then solved for each of these small pieces. A natural way to parallelize algorithms of this type is to divide

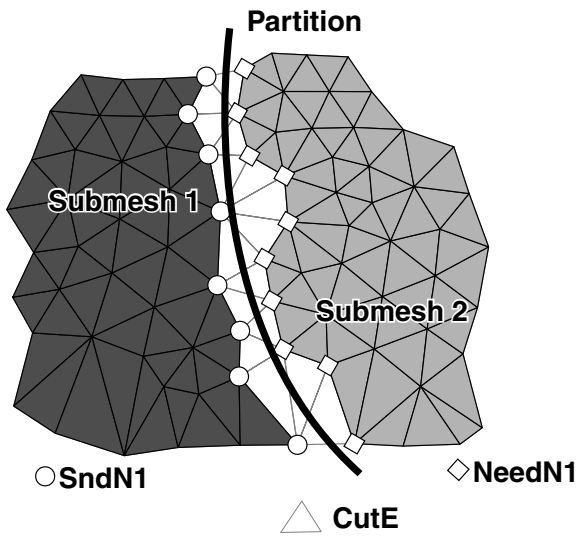

Figure 4.3: A mesh divided into two submeshes by a single partition (dark line). The elements that the partition passes through belong to the set $CutE$ (white). The shaded elements are the local elements ($LocE$) for each submesh. The nodes marked with circles must be sent from submesh 1 ($SendN_1$) and are needed by submesh 2 ($NeedN_2$). The nodes needed by submesh 1 are marked by squares ($NeedN_1$). These nodes are sent from submesh 2 ($SendN_1$). The remaining nodes are interior to each mesh ($IntN$).

the mesh into several pieces; a process known as domain decomposition. Because QUODDY separates the computation into horizontal and vertical parts, decomposing the horizontal mesh is a straightforward way to parallelize this model.

Decomposing an unstructured mesh is conceptually easy, but finding a decomposition that can be run efficiently in parallel is a computationally hard problem. Specifically, a good decomposition will minimize the load imbalance and communications by creating subdomains of the same size and reducing the amount of data that must be shared. The definition of a good domain decomposition will be made more explicit below, but only after developing some notation. The formal nota-

tion will also facilitate the identification of the data that must be shared between processors.

A mesh is decomposed by a series of partitions—curves that begin and end outside the domain boundary and that do not coincide with any nodes (dark line in Figure 4.3). Defining the elements using an element list, a partition (also called an *edge separator;* Gilbert et al., 1998) will pass through a subset of Ele that will be labeled $CutE$. In the case of a single partition, removing the elements in $CutE$ will divide the mesh into two distinct submeshes, $(LocN_1, LocE_1)$ and $(LocN_2, LocE_2)$. We can redefine the original mesh as

$$Mesh = (LocN_1 \cup LocN_2,\ LocE_1 \cup LocE_2 \cup CutE) \tag{4.4}$$

Note that the nodes in $LocN_1$ are distinct from those in $LocN_2$. The $LocE_j$'s are also distinct from each other, and are each composed solely of from nodes in the corresponding sets. The third set, $CutE$, refers to nodes in both sets. The decomposition can also be thought of as dividing the mesh into two sub meshes, each composed of a node-element combination:

$$\begin{aligned} Mesh &= Mesh_1 \cup Mesh_2 \cup (CutN, CutE) && (4.5) \\ &= (LocN_1, LocE_1) \cup (LocN_2, LocE_2) \cup (CutN, CutE). && (4.6) \end{aligned}$$

This view requires a third submesh containing $CutE$ and the nodes in the cut elements, $CutN$. Because $CutN$ is made up from nodes in the two $LocN$, including it in the union of nodes in Equation 4.4 would be redundant. Using more partitions will cut the mesh into more submeshes, although the actual number of submeshes

produced will depend on the orientation of the partitions.

The point of decomposing a mesh is to divide the computation among several processors. Any calculations involving only elements in submesh j ($LocN_j$ and $LocE_j$) can be performed independently of the information on the other submeshes. Calculations involving $CutE$ will require information from multiple submeshes. The formal notation developed above simplifies the classification of the nodes.

Taking the point of view of process 1 in Figure 4.3, $CutN$ can be divided into two sets: the "send nodes" ($SendN_1$) containing nodes from $LocN_1$, and the "needed nodes" ($NeedN_1$, also known as "ghost nodes") containing nodes from $LocN_2$. Conceptually, the nodes in $SendN_1$ reside on processor 1, but their data must be sent periodically to processor 2, while $NeedN_1$ are the nodes containing the data processor 1 must receive. We can define an additional set of nodes called "interior nodes" ($IntN_j$) which are used only by the local processor. Formally, $IntN_j$ is formed by removing the $SendN_j$ from $LocN_j$. Thus, a processor's local nodes ($LocN$) are divided into two sets: the interior nodes, $IntN$, and the $SendN$ that occur on the edge of the cut and must be sent to another processor (Table 4.1).

The main difference between a serial model and its domain decomposition-based parallel analog is that the parallel version requires periodic communication of the data in the $NeedN$. Relative to the speed of computation, the rate at which processors can share data is quite slow, even on shared-memory systems. This suggests that we should try to find domain decompositions that minimize the number of needed nodes. Additionally, the number of nodes in each submesh should be as

Table 4.1: Definition of the sets to which the nodes are assigned.

$LocN_j$	=	"Local Nodes"—nodes for which processor j is responsible
$IntN_j$	=	"Interior Nodes"—nodes used only by processor j
$SendN_j$	=	"Send Nodes"—nodes that are required by another processor
$NeedN_j$	=	"Needed Nodes"—nodes processor j requires, but are not in $LocN_j$

close as possible to minimize load imbalance. Unfortunately, finding the partitions that produce an optimal domain decomposition of an unstructured mesh is an NP-hard problem (Gilbert et al., 1998). That a problem is "NP-hard" means that it belongs to a class of algorithms for which no "fast" (i.e. polynomial-time) algorithm has been found nor is likely to exist (Cormen et al., 1990). However, several fast algorithms do exist that will produce decompositions that are close to optimal (Hendrickson and Leland, 1995; Gilbert et al., 1998). The decompositions used in this study were constructed with the MESHPART toolbox (Gilbert et al., 1998) which partitions a mesh using geometric separators (Miller et al., 1998). The decomposition routine in MESHPART recursively cuts the mesh; thus, the number of submeshes is always a power of two.

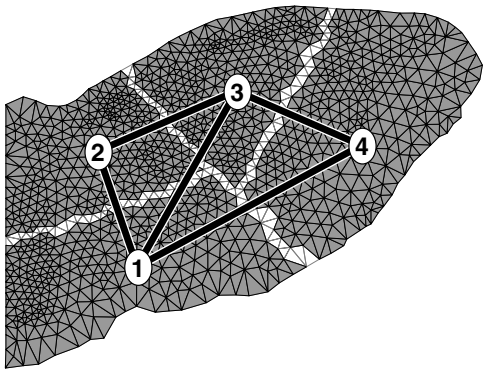

Figure 4.4: A mesh divided into four submeshes. The heavy lines link the processors that must communicate between each other.

4.2.4 Modifications to QUODDY

The task of parallelization is largely one of communication and data management. Communication is handled by calls to a communication library which hides the details of the communication hardware from the programmer. For distributed computing, the most popular library is MPI (Message Passing Interface; Snir et al., 1996). The main data management tasks are to organize the communications, provide routines to perform the communications, and identify where communication must occur.

The submeshes produced during the domain decomposition have the same structure as the original mesh; thus, MPQUODDY required only a few modifications to the original algorithm. Specifically, MPQUODDY needs to organize the nodes according to the sets in Table 4.1, determine the data that must be sent and received and where it is going to or coming from, and then a routine must be developed to handle the communications. To inform MPQUODDY of the node-classes, the nodes

and elements are sorted after decomposition into the sets defined above and stored in a file which MPQUODDY reads. After reading this file, each processor knows which nodes it needs but not which processors own these nodes. To organize the communications, each processor sends the identity of its needed nodes to all of the processors. Each processor then compares the list of all needed nodes to its send nodes. The processors store the identities of the processors with whom they must communicate and the nodes that must be sent to each of them. Then, the processors announce to the whole group the nodes they will send, and from this list, each determines which processors have its needed nodes.

The final initialization step is to determine the order in which the communications must occur. The simplest and often most efficient mode of communication in MPI (and other similar libraries) is the point-to-point scheme. A processor sends data to another using point-to-point communications by executing a call to `MPI_Send` specifying the data to be sent and the processor to which it should be sent. The communication occurs when the receiving processor executes a call to `MPI_Recv`. The key disadvantage to the point-to-point scheme is the possibility of *deadlock*. As an example, consider a mesh split into four pieces (Figure 4.4). If each processor tried to share data with the processor labeled with the number one greater than its own (i.e. 1 with 2, 2 with 3, 3 with 4, and 4 with 1), then every processor will be attempting to communicate with a processor that is not prepared to communicate with it. The program will not proceed beyond this point. To avoid deadlock, MPQUODDY divides the processors in half and each processor first communicates

with the processors in the opposite half. The communications within each half are organized in the same way, and the procedure is repeated until no more processors remain. This communication scheme avoids deadlock, but may not be the most efficient. Since the mesh used in MPQUODDY does not change during the simulation, the communications are initialized only once.

Two subroutines were created to handle the actual communications. The subroutine `basic_comm` takes an array of data defined on the nodes and performs the communications necessary to update the needed nodes on each processor. The subroutine `twoD_comm` performs the same function on two-dimensional arrays (horizontal-by-vertical). These routines, as well as the routines to read in the domain decomposition and organize communications, are packaged in a library called `commlibMP`.

The data in the needed nodes are used only under two circumstances: when the array is accessed in a loop through the element array, and when multiplying by the wave-equation matrix. Therefore, identifying where to place the calls to the communication routines is simply a matter of searching the code for these circumstances. Element loops have the form

```
for l=1:ne
   for k=1:3
      j=ele(l,k);
      Something involving array(j)
   end
end
```

Because they must loop over all elements, the processors must access the needed nodes in the array. Thus, a `basic_comm` must be performed on the array before the loop.

In both serial and parallel versions of QUODDY, the wave-equation matrix depends only on the geometry of the mesh, so it does not change during the simulation. In the serial version, the matrix is factored once, and the wave equation is solved in each iteration by a forward and back substitution using the factors. Both forward and back substitution are inherently serial procedures and are difficult to do efficiently in parallel (Golub and Ortega, 1993), especially if domain decomposition is used. Instead of solving the matrix problem directly, MPQUODDY uses a standard iterative method known as conjugate gradients (Golub and Van Loan, 1996). The conjugate gradient algorithm involves repeated matrix-vector multiplications, and although the multiplication is simple in parallel, the needed nodes of the vector must be updated before each multiplication. The number of multiplications required before the algorithm converges to the answer can be reduced by preconditioning the matrix. The wave-equation matrix is diagonally dominant, and MPQUODDY uses diagonal scaling as a simple preconditioner.

4.2.5 Performance Experiments

A series of performance experiments was conducted to test the efficiency of MPQUODDY and to identify improvements that should be made. The experiments were designed to mimic the simulations for which QUODDY has typically been used. Specifically, the simulations compute the circulation caused by the M2 component of the semidiurnal tides in three shelf areas: Georges Bank (BANK150), the Gulf of Maine (G2S), and the coast of North Carolina (NCHIRES; Figure 4.5). The first two meshes

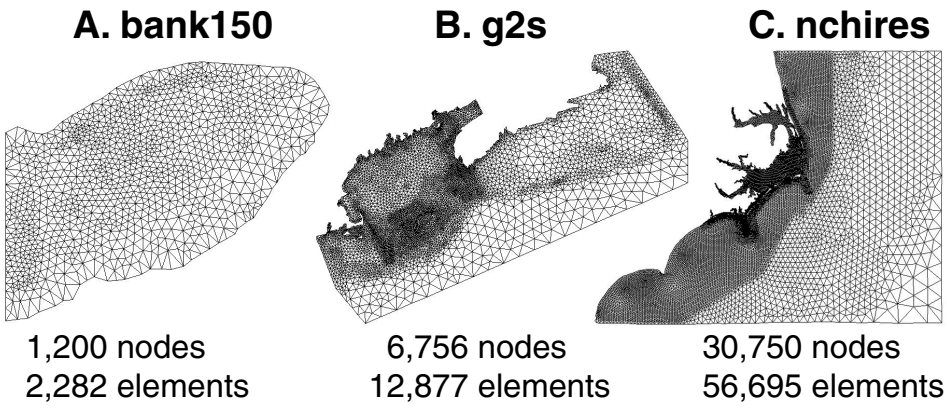

Figure 4.5: The three meshes used in the timing experiments.

have only a few thousand nodes (1,200 and 6,756, respectively) and are a typical size for QUODDY simulations. The North Carolina mesh has over 30,000 nodes and is large enough to tax the resources of many desktop workstations. Each mesh was decomposed using MESHPART into 2, 4, 8, 16, and 32 submeshes. All simulations used 21 nodes in the vertical projections, with increased resolution near the surface and bottom.

The timing experiments were conducted on the AC^3 Velocity cluster at the Cornell Theory Center. Velocity has 64 compute nodes that each have four Pentium III Xeon processors running at 500 MHz and 4 gigabytes of RAM. The nodes communicate over a Giganet switch. The performance of MPQUODDY was tested on 1, 2, 4, 8, and 16 nodes. These nodes introduce an additional level of complexity, since a job requiring P processors can be run on P, $P/2$, or $P/4$ nodes, i.e. 1, 2, or 4 processors per node. For each set of cluster nodes, three runs of each mesh were made: one using only one processor on each node, another using two, and a third

using all for processors. The code was compiled using the Microsoft Visual C++ compiler with the "max speed" optimization option set and with the inlining option set to "any suitable." Velocity differs only in size from the clusters that a research group could build.

Calls to timing subroutines were placed around six sections of code inside the main timing loop. The first section, called PRE, contains calls to the routines computing the horizontal pressure gradients. The second section is the subroutine `Elevation` which solves the wave equation. The third section is the subroutine `Vertical` which computes the three-dimensional distribution of velocity, temperature, salinity, and the turbulent quantities. The fourth and fifth sections contain calls to the communications routines `basic_comm` and `twoD_comm`. The last section, called POST, performs housekeeping—updating and copying arrays before the next loop. The time spent in the sections during each iteration was stored in an array and then written to a file by each processor after 200 iterations. The timing data was analyzed by taking the mean time for each section and each processor.

4.3 Results

The mean time for an iteration using the BANK150 mesh declined when 2 or 4 processors were used (Figure 4.6 A); however, the time actually increased for 16 and 32 processors. The times depended weakly on the number of processors per node. A better indicator of the performance of a parallel program is how close it comes to the ideal case of a factor of P increase in speed when P processors are used. This

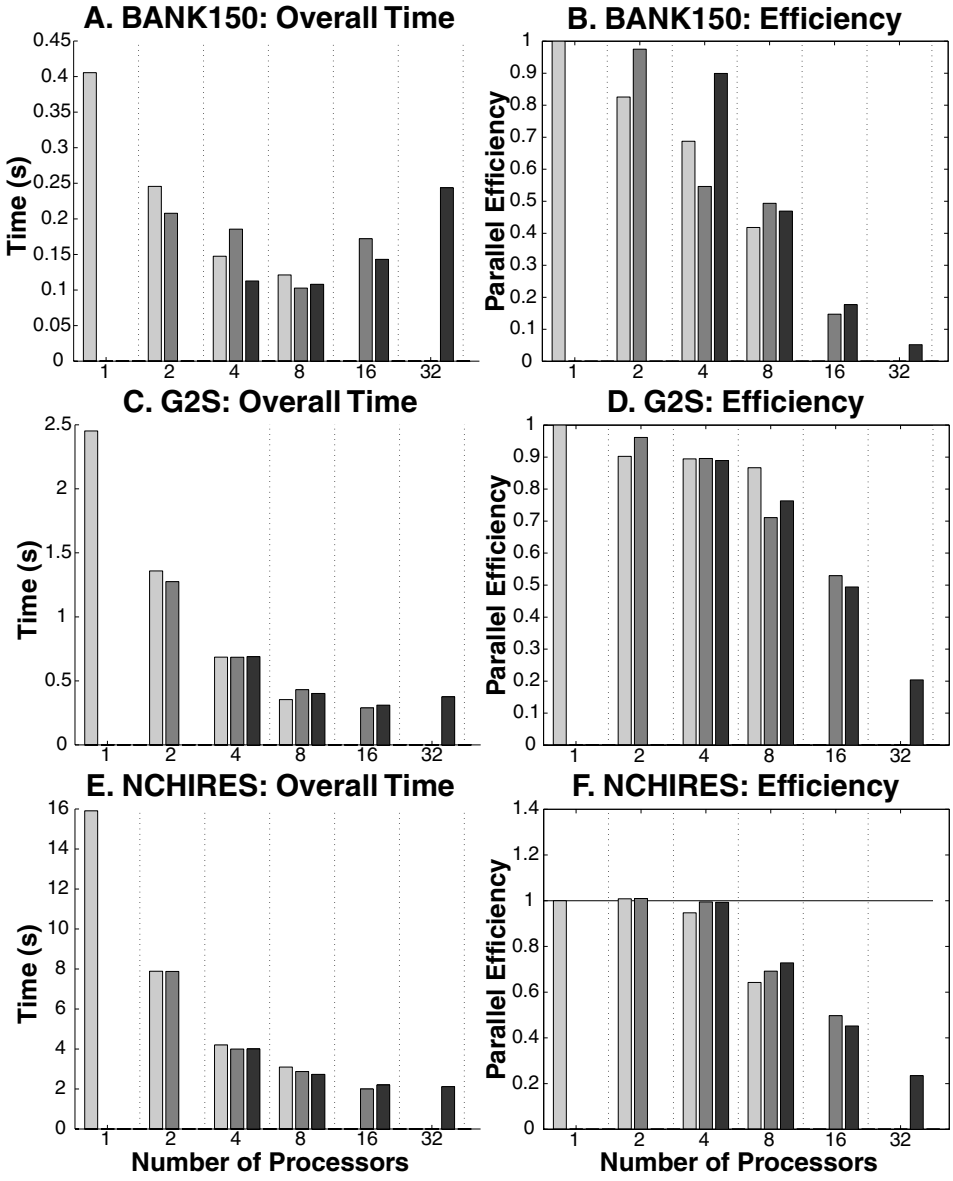

Figure 4.6: Performance of MPQUODDY on the BANK150 (A and B), G2S (C and D), and NCHIRES (E and F) mesh measured as time for a complete iteration and parallel efficiency. The shading indicates the number of processors per node: light = 1, medium = 2, dark = 4.

concept, known as speed-up, is defined as

$$\text{Speed-Up} = \frac{\text{Time on 1 Processor}}{(\text{Time on } P \text{ Processors})}. \tag{4.7}$$

A related measure is the parallel efficiency, defined as the speed-up divided by the number of processors. For the BANK150 mesh, the performance of MPQUODDY on two processors is nearly perfect (it runs almost twice as fast and has an efficiency close to one), especially if the processors are on the same node (Figure 4.6 B).

As expected, the parallel performance of MPQUODDY improved when run on the larger meshes (Figures 4.6 C-F). On both the G2S and NCHIRES meshes, the total time continued to decline as more processors were used, except for the 32 processor run. The number of processors per node had even less of an effect on these meshes than on BANK150. The parallel efficiency of the NCHIRES runs were greater than those using the G2S mesh for 2 and 4 processors. With 2 processors, the NCHIRES runs had efficiencies greater than one and ran more than twice as fast as the single processor version. This phenomenon is known as "superlinear speed-up" and occurs when the decrease in problem size when running in parallel allows more efficient use of the processors' local memory. On 8 processors, the G2S example was more efficient than NCHIRES, but they were comparable on 16 and 32 processors.

When run in serial on the G2S mesh, MPQUODDY spends about half of each iteration in the `Vertical` subroutine (Figure 4.7). Together, the pre and post-processing sections account for another 45% of the time, while the time spent in `Elevation` is almost negligible. However, as the number of processors increases,

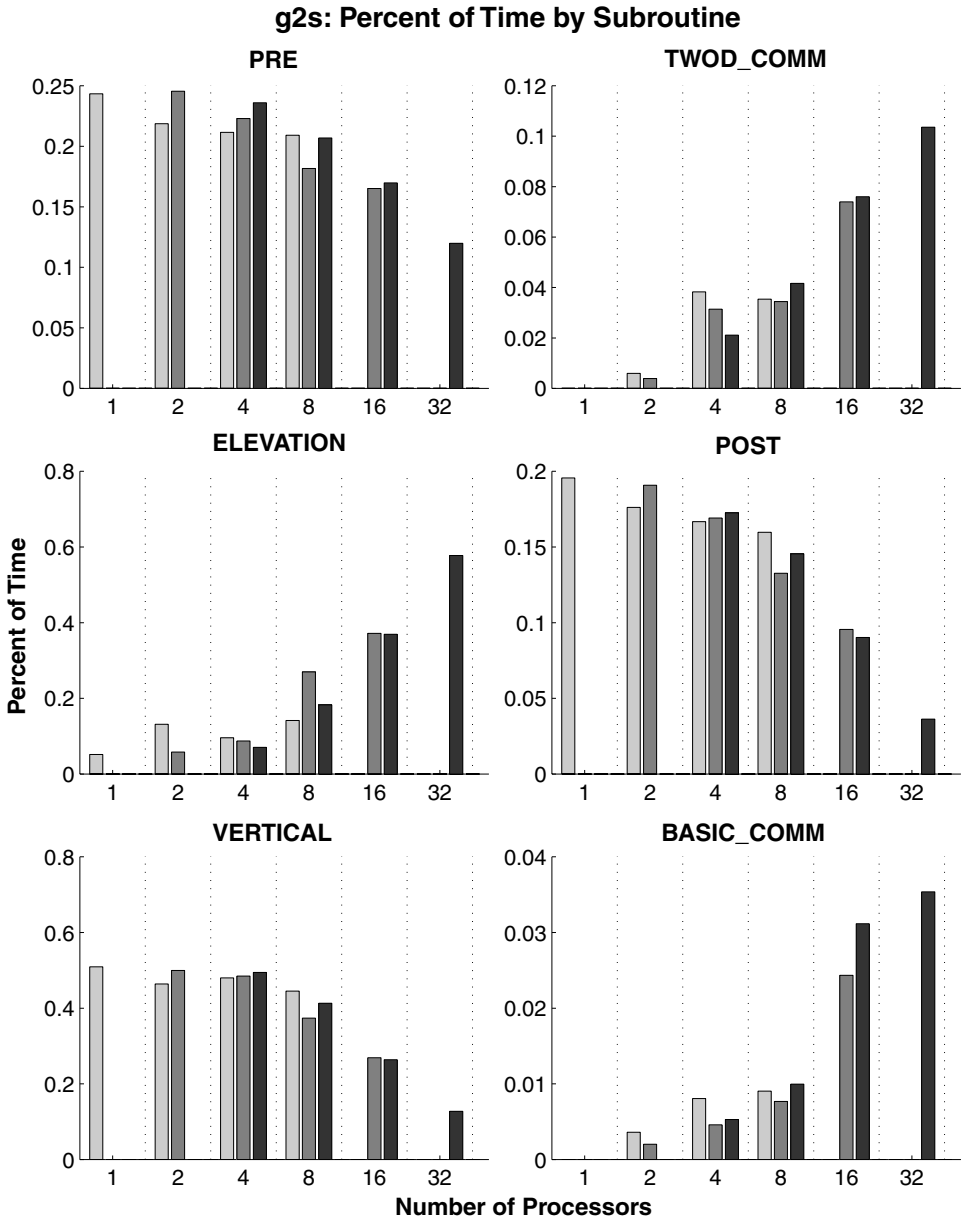

Figure 4.7: The percent of the time spent in the six timing sections during the G2S runs. The shading indicates the number of processors per node: light = 1, medium = 2, dark = 4.

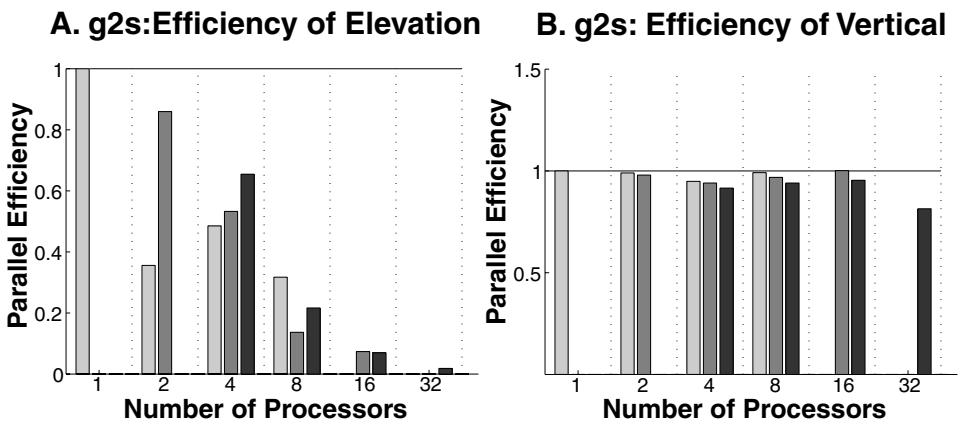

Figure 4.8: The efficiency of subroutines `Elevation` (A) and `Vertical` (B) during the G2S runs. The shading indicates the number of processors per node: light = 1, medium = 2, dark = 4.

a larger percentage of the time is spent in `Elevation`, and this routine eventually overwhelms the rest of the computation. The parallel efficiency of the `Vertical` subroutine is always close to one, while the efficiency of `Elevation`, which contains the majority of communication, declines dramatically (Figure 4.8). The patterns for the NCHIRES mesh are similar. On the NCHIRES mesh, `Elevation` accounts for nearly a third of the processing time, comparable to the time spent in `Vertical` (Figure 4.9). Unlike the G2S example, the proportion of time spent in `Elevation` declines for 2 and 4 processors, but the trend reverses for more than 8 processors. This pattern is more evident in the plots of parallel efficiency (Figure 4.10) which indicate super-linear speed-up for `Elevation` on 2 and 4 processors.

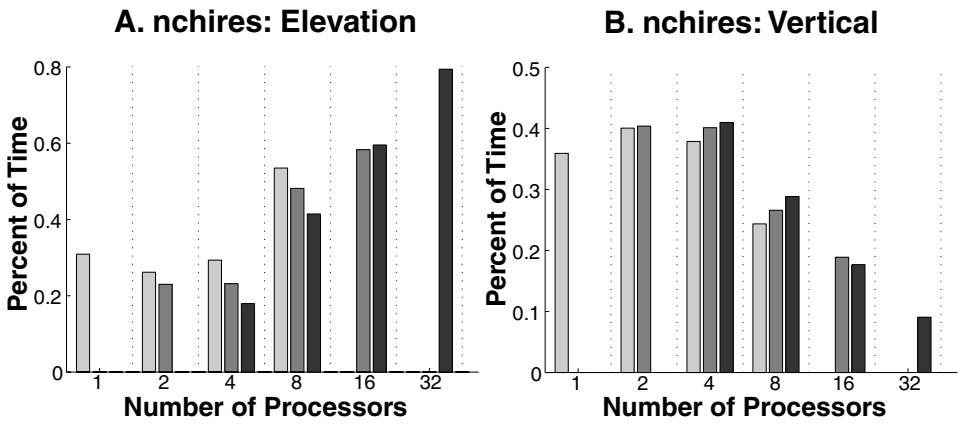

Figure 4.9: The percent of time spent in subroutines `Elevation` (A) and `Vertical` (B) during the NCHIRES runs. The shading indicates the number of processors per node: light = 1, medium = 2, dark = 4.

4.4 Discussion

The performance of MPQUODDY was quite good when run on 4 or fewer processors, and some speed up was still evident using up to 16 processors on the two largest problems. The increase in performance with problem size is a standard result in parallel computing (Golub and Ortega, 1993), and results from the smaller ratio of communication-to-computation inherent in larger problems. However, there was only a slight increase in the performance between NCHIRES and G2S, even though NCHIRES has nearly five times the number of nodes as G2S.

A first attempt was made to improve the performance of MPQUODDY, especially on large numbers of processors. The presence of four processors on each Velocity node creates two levels of communication, and communication between processors on a node should be faster than that between processors on separate nodes. After looking carefully at how the submeshes were assigned to the processors, it was

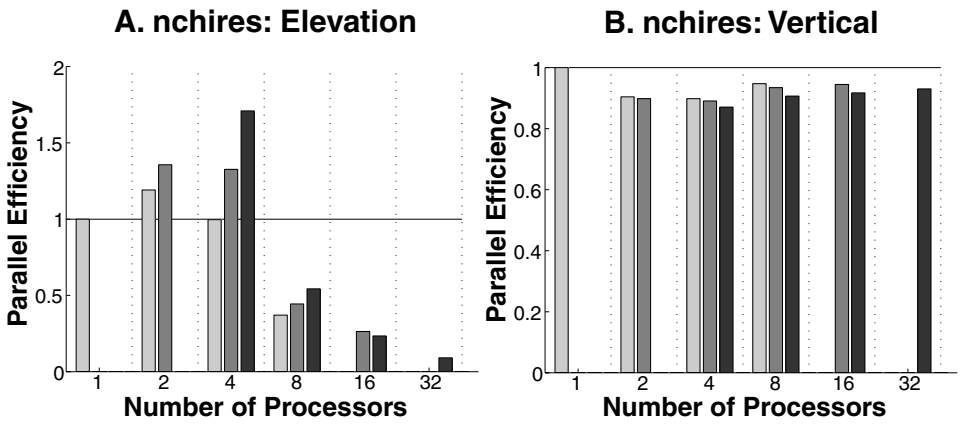

Figure 4.10: The efficiency of subroutines `Elevation` (A) and `Vertical` (B) during the NCHIRES runs. The shading indicates the number of processors per node: light = 1, medium = 2, dark = 4.

noticed that the submeshes were "dealt" to each node as if the nodes were playing a game of cards, with the submeshes serving as the cards. For the decomposition shown in Figure 4.4, this would mean that submeshes 1 and 3 would occur on the same node even though they must share only a small amount of data. Thus, Velocity's default procedure for assigning jobs interacts negatively with the way that MESHPART numbers the decomposition. To correct this, a simple program called `Machine_Divide` was created to alter the file that determines how the jobs are assigned to the nodes. The new assignment procedure improved the efficiency of MPQUODDY using 8 and 16 processors on G2S and NCHIRES, especially when all processors on the nodes were used (Figure 4.11). However, the improvement was greatest for G2S.

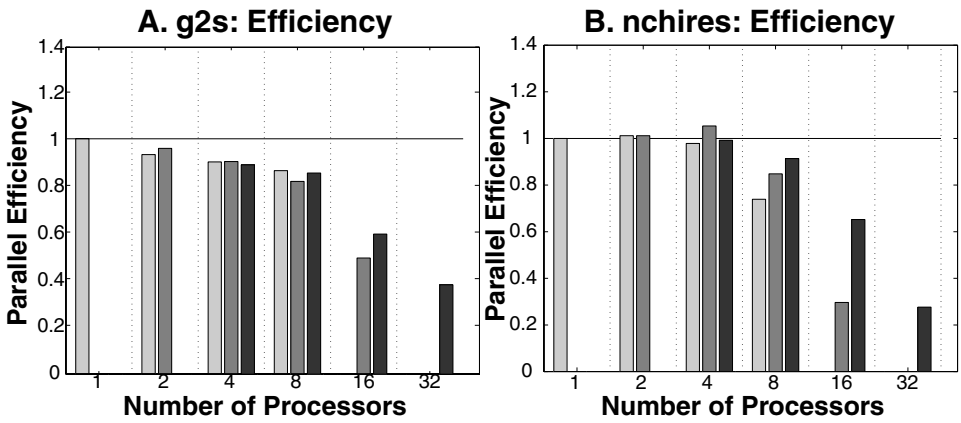

Figure 4.11: The efficiency of runs using the G2S (A) and NCHIRES (B) meshes with processors assigned by `Machine_Divide`. The shading indicates the number of processors per node: light = 1, medium = 2, dark = 4.

4.4.1 Future Improvements

The surprisingly poor performance of MPQUODDY using the NCHIRES mesh provides an excellent opportunity to identify improvements that should be made.. The `Elevation` subroutine is the main factor limiting the parallel performance of MPQUODDY, especially on the NCHIRES mesh. Within `Elevation`, the bulk of the time is spent solving the linear system in the conjugate gradients subroutine. For the BANK150 and G2S meshes, the conjugate gradients solver takes ∼15 iterations to find the solution; however, the solver takes over 200 iterations on the NCHIRES mesh. The convergence rate of the conjugate gradient algorithm is closely tied to the condition number of the matrix (Golub and Van Loan, 1996). The condition number is a measure of how similar a matrix is to the identity matrix. A large condition number indicates that a matrix is very different from the identity matrix and implies that the solution of any problems involving this matrix will have limited

Table 4.2: Condition numbers for the matrices from the three meshes. The condition numbers after diagonal scaling are also given. The condition numbers are relative to the 1-norm and were computed using Matlab's `condest` function.

	Condition number	
Mesh	Normal	with Diagonal Scaling
BANK150	2.2×10^8	7.1×10^7
G2S	2.7×10^9	6.0×10^8
NCHIRES	4.5×10^9	2.1×10^9

accuracy. Pre-conditioning speeds up conjugate gradients by reducing the condition number of the matrix. The condition number of a matrix from a finite-element problem is determined primarily by the resolution of the mesh, with the condition number increasing as the square of the resolution (Johnson, 1987). For the three meshes used in this study, the condition number increased with the size of the mesh (Table 4.2). The diagonal scaling preconditioner used by MPQUODDY reduced the condition number in all cases, although the actual reduction varied considerably. Diagonal scaling reduced the condition number of the G2S matrix by a factor of five, while it reduced the condition number of the NCHIRES matrix by barely a factor of two. This suggests that the performance of MPQUODDY, even in serial, could be improved by finding a better preconditioner. Several classes of preconditioner such as the Schwarz methods, iterative substructuring, and the multigrid method are based on domain decomposition and may be especially relevant for MPQUODDY (Greenbaum, 1997).

Although the scalability of MPQUODDY on the largest mesh was disappoint-

ing given the performance on the medium-sized G2S mesh, the performance of MPQUODDY is comparable to other parallel circulation models (Bleck et al., 1995; Öksüzoğlu and van Hees, 1998; Boukas et al., 1999). Among these models, the Princeton Ocean Model (POM; Blumberg and Mellor, 1987) is the most similar to QUODDY; the key difference is POM's use of finite differences rather than finite elements. Unlike QUODDY's unstructured meshes, the structured grids used by POM can be decomposed optimally; however, the parallel efficiency of POM using 8 and 16 processors on a very large mesh (43,200 nodes) was slightly worse than that for MPQUODDY on G2S and NCHIRES (Boukas et al., 1999).

4.5 Conclusion

Although there is still room for improvement, MPQUODDY provides a fast alternative to serial circulation models. Even a modest system of only a few PCs linked together over a standard network could run MPQUODDY several times faster than on a single computer, and the performance will be even better on commercial systems. This combination of software and hardware will allow future work to explore the impact of climate variability on ocean circulation and the effect of climate-induced circulation changes on marine populations.

4.6 References

Bleck, R., Dean, S., O'Keefe, M., and Sawdey, A. (1995). A comparison of data parallel and message passing versions of the miami isopycnic coordinate model (micom). *Parallel Computing*, 21:1695–1720.

Blumberg, A. F. and Mellor, G. L. (1987). A description of a three-dimensional coastal ocean circulation model. In Heaps, N., editor, *Three-dimensional coastal ocean models*. American Geophysical Union, New York.

Bollinger, T. (1999). Linux in practics: an overview of applications. *IEEE Software*, 16:875–906.

Boukas, L. A., Mimikou, N. T., Missirlis, N. M., Mellor, G. L., Lascaratos, A., and Korres, G. (1999). The parallelization of the Princeton Ocean Model. In *Euro-Par '99 Parallel Processing*, volume 1685 of *Lecture Notes in Computer Science*, pages 1395–1402. Springer, Berlin.

Brightwell, R., Fisk, L. A., Greenberg, D. S., Hudson, T., Levenhagen, M., Maccabe, A. B., and Riesen, R. (2000). Massively parallel computing using commodity components. *Parallel Computing*, 26:243–266.

Cormen, T. H., Leiserson, C. E., and Rivest, R. L. (1990). *Introduction to Algorithms*. MIT Press, Cambridge, MA.

Gilbert, J. R., Miller, G. L., and Teng, S.-H. (1998). Geometric mesh partitioning: implementation and experiments. *SIAM Journal of Scientific Computing*, 19:2091–2110.

Golub, G. H. and Ortega, J. M. (1993). *Scientific Computing: An Introduction with Parallel Computing*. Academic Press, San Diego, CA.

Golub, G. H. and Van Loan, C. F. (1996). *Johns Hopkins University Press*. Academic Press, Baltimore, ML.

Greenbaum, A. (1997). *Iterative Methods for Solving Linear Systems*. Society for Industrial and Applied Mathematics, Philadelphia, PA.

Gropp, W., Lusk, E., Doss, N., and Skjellum, A. (1996). A high-performance, portable implementation of the MPI message passing interface standard. *Parallel Computing*, 22:789–828.

Haidvogel, D. B., Blanton, J., Kindle, J. C., and Lynch, D. R. (2000). Coastal ocean modeling: processes and real-time systems. *Oceanography*, 13:35–46.

Hendrickson, B. and Leland, R. (1995). An imporved spectral graph partitioning algorithm for mapping parallel computations. *SIAM Journal of Scientific Computing*, 16:452–469.

Johnson, C. (1987). *Numerical Solution of Partial Differential Equations by the finite element method*. Cambridge University Press, Cambridge, UK.

Loder, J. W., Shore, J. A., Hannah, C. G., and Petrie, B. D. (2001). Decadal-scale hydrographic and circulation variability in the Scotia-Maine region. *Deep-Sea Research II*, 48:3–36.

Lynch, D. R., Ip, J. T. C., Naimie, C. E., and Werner, F. E. (1996). Comprehensive coastal circulation model with application to the Gulf of Maine. *Continental Shelf Research*, 16:875–906.

Lynch, D. R. and Werner, F. E. (1991). Three-dimensional hydrodynamics on finite elements. Part II: non-linear time-stepping model. *International Journal for Numerical Methods in Fluids*, 12:507–533.

Miller, G. L., Teg, S.-H., Thurston, W., and Vavasis, S. A. (1998). Geometric separators for finite-element meshes. *SIAM Journal of Scientific Computing*, 19:364–386.

Naimie, C. E. (1996). Georges Bank residual circulation during weak and strong stratification periods: prognostic numerical model results. *Journal of Geophysical Research*, 101:6469–6486.

Öksüzoğlu, H. and van Hees, A. G. M. (1998). A barotropic global ocean model and its parallel implementation on unstructured grids. In *High-performance computing and networking*, volume 1401 of *Lecture Notes in Computer Science*, pages 125–132. Springer, Berlin.

Snir, M., Otto, S. W., Huss-Lederman, S., Walker, D. W., and Dongarra, J. (1996). *MPI The Complete Reference*. MIT Press, Cambridge, MA.

Sunderam, V. S., Geist, G. A., Dongarra, J., and Manchek, R. (1994). The PVM concurrent computing system: evolution, experience, and trends. *Parallel Computing*, 20:531–545.